

Magic of Fluctuations

From Fluctuations in Quantum Information to Magic Resources

Ahmadi, A.

DOI

[10.4233/uuid:f4be0218-4ef6-48d0-906f-5077741a034d](https://doi.org/10.4233/uuid:f4be0218-4ef6-48d0-906f-5077741a034d)

Publication date

2025

Document Version

Final published version

Citation (APA)

Ahmadi, A. (2025). *Magic of Fluctuations: From Fluctuations in Quantum Information to Magic Resources*. [Dissertation (TU Delft), Delft University of Technology]. <https://doi.org/10.4233/uuid:f4be0218-4ef6-48d0-906f-5077741a034d>

Important note

To cite this publication, please use the final published version (if applicable). Please check the document version above.

Copyright

Other than for strictly personal use, it is not permitted to download, forward or distribute the text or part of it, without the consent of the author(s) and/or copyright holder(s), unless the work is under an open content license such as Creative Commons.

Takedown policy

Please contact us and provide details if you believe this document breaches copyrights. We will remove access to the work immediately and investigate your claim.

MAGIC OF FLUCTUATIONS

FROM FLUCTUATIONS IN QUANTUM INFORMATION TO MAGIC
RESOURCES

MAGIC OF FLUCTUATIONS

FROM FLUCTUATIONS IN QUANTUM INFORMATION TO MAGIC
RESOURCES

Dissertation

for the purpose of obtaining the degree of doctor
at Delft University of Technology,
by the authority of the Rector Magnificus Prof. dr. ir. T.H.J.J. van der Hagen,
chair of the Board for Doctorates,
to be defended publicly on
3rd of March 2025 at 17:30 o'clock

by

Arash AHMADI

Master of Science in Physics,
Institute for Advanced Studies in Basic Sciences, Zanjan, Iran,
born in Hamedan, Iran.

This dissertation has been approved by the promoters and supervisors.

promotor: Prof. dr. S. Groeblacher

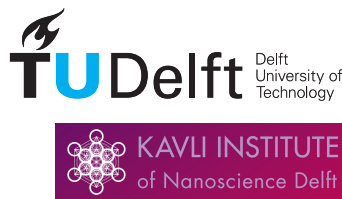
copromotor: Dr. E. Greplová

Composition of the doctoral committee:

Rector Magnificus,	voorzitter
Prof. dr. S. Groeblacher,	Technische Universiteit Delft
Dr. E. Greplová,	Technische Universiteit Delft

Independent members:

Prof. dr. L. DiCarlo	Technische Universiteit Delft
Prof. dr. V. Dunjko	Universiteit Leiden
Dr. J. Tura Brugués	Universiteit Leiden
Dr. M. Doosti	University of Edinburgh, UK
Prof. dr. Y. M. Blanter	Technische Universiteit Delft, reserve member



Keywords: Magic Resource, Non-stabilizerness, Information Scrambling, Variational Quantum States, Quantum Information

Printed by: Gildeprint, the Netherlands

Front & Back: Artistic decapitation of quantum magic and fluctuations, conceived by Arash Ahmadi and GPT-4o.

Copyright © 2025 by A. Ahmadi

ISBN 978-94-6518-020-5

An electronic version of this dissertation is available at
<http://repository.tudelft.nl/>.

CONTENTS

Summary	vii
Samenvatting	ix
Preface	xi
1 Introduction	1
1.1 Quantum Mechanics	2
1.2 Quantum Computing	2
1.3 Non-stabilizerness or Magic	5
1.4 Information Scrambling	6
1.5 Variational Quantum States	8
1.6 Outline of the Chapters of this Thesis	10
1.7 Author's contributions	10
2 Quantifying non-stabilizerness via information scrambling	17
2.1 Introduction	18
2.2 Methods	19
2.2.1 Magic	19
2.2.2 Information scrambling	20
2.3 Results	22
2.3.1 Mana and OTOC	22
2.3.2 The Stabilizer Renyi entropy and OTOC	22
2.3.3 The magic generated by time evolution of a Hamiltonian	23
2.4 Conclusion and Discussion	25
2.5 Acknowledgments	26
2.6 Appendix-1: Mana	27
2.7 Appendix-2: Clifford and non-Clifford gates definitions.	27
2.7.1 Clifford gates.	28
2.7.2 Non-Clifford gates	28
2.8 Appendix-3: Proof of Lemma 1	28
2.9 Appendix-4: Propagation of error	30
3 Mutual information fluctuations and non-stabilizerness in random circuits	37
3.1 Introduction	38
3.2 Random circuits and mutual information.	39
3.2.1 Definitions and notation.	39
3.2.2 Relation of mutual information fluctuations and magic	40
3.2.3 Analytical relation of N_T and $\ln(\delta_{I^{(2)}})$	40

3.3	Effect of magic on measurement-induced phase transition	41
3.4	Discussion and Conclusions	45
3.5	Author contributions	45
3.6	Data availability.	46
3.7	Acknowledgements	46
3.8	Appendix-1:Fourth moment of spin measurements.	47
3.9	Appendix-2:Analytical treatment of entropy fluctuations	47
3.9.1	Moments of the unitary and Clifford groups	48
3.9.2	Main theorem	49
4	Quantum resources of quantum and classical variational methods	65
4.1	Introduction	66
4.2	Methods	67
4.2.1	Transverse-Field Ising Model.	67
4.2.2	Parameterized Quantum States	68
4.2.3	Non-stabilizerness.	73
4.3	Results	73
4.3.1	Quantum and Classical Model Accuracy	73
4.3.2	Non-stabilizerness and Symmetry	74
4.3.3	Fluctuations in Quantum and Classical Solutions	76
4.4	Discussion and Conclusions	77
4.5	Data and Code Availability	78
4.6	Author Contributions	78
4.7	Acknowledgments	79
4.8	Appendix-1:NQS architecture.	79
4.9	Appendix-2:VQE architecture	80
5	Conclusion	91
	Acknowledgements	95
	Curriculum Vitæ	97
	List of Publications	99

SUMMARY

The recent progress in quantum technologies shines a bright light on the future of quantum computation. However, resource estimation for quantum computations remains a key challenge. The resource I study in this thesis is known as *Magic* or *Non-stabilizerness* and it represents the key requirement for quantum computational advantage in computation. Recent studies in quantum information suggested wide classes of quantifiers for non-stabilizerness.

In this thesis, I develop novel techniques for quantifying non-stabilizerness with the tools from quantum information theory. I am specifically interested in making quantum resource estimation computationally as efficient as possible so that quantum resource estimation can become a routine step in both numerical and experimental exploration of quantum computing.

I show that by measuring the spreading of the local information in the quantum system, we can quantify non-stabilizerness. The measures of such information-spreading can be classified into two categories, *entropic-based measures*, such as mutual information, and *correlator-based measures* such as Out-of-Time Ordered Correlators. I investigated both classes of measures and I related them both numerically and analytically to the estimation of non-stabilizerness.

Finally, I relate non-stabilizerness quantification to classical variational methods. Classical methods designed to approximate quantum states are by construction not restricted by non-stabilizerness. The question therefore remained how well these techniques can capture quantum resources. I provide a systematic benchmark for both classical and quantum approximate methods of expressing quantum states and their trade-off between non-stabilizerness expressivity and ground-state energy accuracy. We observed that having better energy accuracy is necessary but insufficient to have better accuracy in non-stabilizerness.

This Thesis forms a bridge between quantum information resource theory and condensed matter physics and offers a stepping stone towards further exchange between these two fields.

SAMENVATTING

De recente vooruitgang in kwantumtechnologieën werpt een helder licht op de toekomst van kwantumcomputing. Het schatten van bronnen voor kwantumcomputing, zogeheten 'quantum resources', blijft echter een belangrijke uitdaging. De bron, ofwel 'resource' die ik in dit proefschrift bestudeer, staat bekend als Magic of Non-stabilizerness en deze vertegenwoordigt de belangrijkste vereiste voor kwantumcomputationeel voordeel in computatie. Recente studies in kwantuminformatie suggereerden brede klassen van kwantoren voor non-stabilizerness.

In dit proefschrift ontwikkel ik nieuwe technieken voor het kwantificeren van non-stabilizerness met de tools uit de kwantuminformatietheorie. Ik ben specifiek geïnteresseerd in het computationeel gezien zo efficiënt mogelijk maken van de kwantumbronnen schatting, zodanig dat deze schatting een routinestap kan worden in zowel numerieke als experimentele verkenning van kwantumcomputing.

Ik laat zien dat we non-stabilizerness kunnen kwantificeren door de verspreiding van de lokale informatie in het kwantumsysteem te meten. De metingen van dergelijke informatieverspreiding kunnen worden ingedeeld in twee categorieën: entropische metingen, zoals wederzijdse informatie, en correlatorgebaseerde metingen zoals Out-of-Time Ordered Correlators. Ik heb beide klassen van metingen onderzocht en ze numeriek en analytisch gerelateerd aan de schatting van non-stabilizerness.

Tot slot relateer ik de non-stabilizerness-kwantificering aan klassieke variationele methoden. Klassieke methoden die zijn ontworpen om kwantumtoestanden te benaderen, worden per definitie niet beperkt door non-stabilizerness. De vraag bleef daarom hoe goed deze technieken kwantumbronnen kunnen vastleggen. Ik bied een systematische maatstaf voor zowel klassieke als kwantum benaderingsmethoden om kwantumtoestanden uit te drukken en hun afweging tussen non-stabilizerness-expressiviteit en nauwkeurigheid van grondtoestand energie. We hebben waargenomen dat een betere energienauwkeurigheid noodzakelijk is, maar niet voldoende om een betere nauwkeurigheid te hebben in non-stabilizerness.

Dit proefschrift vormt een brug tussen de theorie van kwantuminformatiebronnen en de natuurkunde van gecondenseerde materie en biedt een opstap naar verdere uitwisseling tussen deze twee vakgebieden.

PREFACE

The sky is blue...

Sitting in the garden. Surrounded by flowers and herbs... I think twice: how and what to write my thesis. To let you know, I am in north Italy, in a village in the Alps mountains.

Still, my mind is engaged... I have come to a house that has an incredible fountain in a room down the stairs and an amazing cave upstairs...

I say to myself: what a wonderful life... that's why I would like to dedicate this thesis to the first cave dweller who could help to survive human beings.

Little by little, I am convinced to write somehow.... to share my little knowledge with you, with the world...

*Arash Ahmadi
Delft, January 2025*

1

INTRODUCTION

In the introduction chapter, I will briefly describe historical notes on quantum mechanics and quantum computing. I will also develop a brief introduction to the basics of quantum computing. I will follow these up with discussions of the resource theory of quantum computation and, in the next section, a brief overview of information scrambling. I conclude with a brief description of the classical variational approximation of quantum states. Throughout this thesis, I will develop a unified framework that connects these diverse concepts and gives a new perspective on the role of non-stabilizerness in contemporary quantum research.

1.1. QUANTUM MECHANICS

Quantum mechanics was introduced as a new theory for the description of the physical laws of the universe in the early 20th century. Since then many new concepts developed that are contrary to our daily experience of the physical world. Examples of these non-trivial concepts include the probabilistic nature of quantum mechanics, the superposition of the quantum states, the emergence of entanglement in quantum systems, and others.

With the help of the laws of quantum physics, we could achieve milestones in technology. With the introduction of semiconductors, we could change the face of the world with electronics. We could enhance the healthcare system by studying quantum mechanical effects in Chemistry, which led to discoveries of new medications. We also introduced new imaging techniques in healthcare, such as magnetic resonance imaging (MRI), which works with the laws of quantum physics.

All these technologies that emerged from the introduction of quantum mechanics belong to an era called the first quantum revolution. However, now we are in an era called the second revolution. Now we are introducing technologies that directly work with the laws of quantum physics. Examples of quantum technologies are Quantum Computation, Quantum Communication, Quantum Sensing and Quantum Simulation.

1.2. QUANTUM COMPUTING

The initial idea of quantum computing came from Richard Feynman [1] when he suggested using a computer that works based on the laws of quantum physics to study quantum physics. Nowadays, the building blocks of the quantum computers are qubits. A qubit is a two-level quantum system. Due to the superposition principle of quantum mechanics, a qubit can be in an arbitrary superposition $|\psi\rangle$ of any two states of $|0\rangle$ and $|1\rangle$

$$|\psi\rangle = \alpha|0\rangle + \beta|1\rangle, \quad (1.1)$$

where $|\alpha|^2 + |\beta|^2 = 1$, $\{\alpha, \beta\} \in \mathbb{C}$ and $|\alpha|^2$ and $|\beta|^2$ are the probability of measuring $|0\rangle$ and $|1\rangle$ respectively and $|\psi\rangle \in \mathcal{H}$ where \mathcal{H} is known as Hilbert space. By increasing the number of qubits, we get exponentially larger in the number of amplitudes, α s and β s, such that for N -qubit system, the size of the Hilbert space grows as 2^N . So as the system size grows, it becomes more challenging to interpret it classically.

The time evolution of a quantum system is described by the Schrodinger equation. As Schrodinger stated in 1926 [2] any non-relativistic quantum time evolution process evolves by

$$i\hbar \frac{\partial}{\partial t} |\psi\rangle = H|\psi\rangle, \quad (1.2)$$

where H is the Hamiltonian of the system and $|\psi\rangle$ is the state. The Hamiltonian, H needs to be a Hermitian operator.

For any Hermitian H , we can rewrite Eq. 1.2 as [3]

$$|\psi(t)\rangle = U(t, t_0) |\psi(t_0)\rangle, \quad (1.3)$$

where U is a unitary operator defined as $UU^\dagger = I$.

In digital quantum computation, we discretize the unitary operator U in a set of gates, similar to classical computation. There are many possible quantum gates. Here, I will introduce the set of gates that are used in this thesis.

Identity. Identity is a single-qubit gate denoted by I , and it leaves the state unchanged

$$I = \begin{pmatrix} 1 & 0 \\ 0 & 1 \end{pmatrix}, \quad I|0\rangle = |0\rangle, \quad I|1\rangle = |1\rangle. \quad (1.4)$$

Pauli Gates. Pauli gates are set of single-qubit gates denoted by X , Y , and Z and their matrix form and their action on the basis $|0\rangle$ and $|1\rangle$ defined as,

$$X = \begin{pmatrix} 0 & 1 \\ 1 & 0 \end{pmatrix}, \quad X|0\rangle = |1\rangle, \quad X|1\rangle = |0\rangle, \quad (1.5)$$

$$Y = \begin{pmatrix} 0 & -i \\ i & 0 \end{pmatrix}, \quad Y|0\rangle = i|1\rangle, \quad Y|1\rangle = -i|0\rangle, \quad (1.6)$$

$$Z = \begin{pmatrix} 1 & 0 \\ 0 & -1 \end{pmatrix}, \quad Z|0\rangle = |0\rangle, \quad Z|1\rangle = -|1\rangle. \quad (1.7)$$

The set of Pauli gates and Identity forms the first level, \mathcal{C}_1 , of the Clifford hierarchy [4].

Hadamard. Hadamard gate is also a single-qubit gate, denoted by H , and it is responsible for producing superposition on the quantum state. Its matrix form and its action on the basis $|0\rangle$ and $|1\rangle$ defined as,

$$H = \frac{1}{\sqrt{2}} \begin{pmatrix} 1 & 1 \\ 1 & -1 \end{pmatrix}, \quad H|0\rangle = \frac{|0\rangle + |1\rangle}{\sqrt{2}}, \quad H|1\rangle = \frac{|0\rangle - |1\rangle}{\sqrt{2}}. \quad (1.8)$$

Phase. Phase gate is also a single-qubit gate, shown by S , and it gives the qubit a $\pi/2$ phase. Its matrix form and its action on the basis $|0\rangle$ and $|1\rangle$ defined as,

$$S = \begin{pmatrix} 1 & 0 \\ 0 & i \end{pmatrix}, \quad S|0\rangle = |0\rangle, \quad S|1\rangle = i|1\rangle. \quad (1.9)$$

Controlled-NOT. Controlled-NOT is a double-qubit gate, shown by CNOT, and it is responsible for producing entanglement in the state.

$$\text{CNOT} = \begin{pmatrix} 1 & 0 & 0 & 0 \\ 0 & 1 & 0 & 0 \\ 0 & 0 & 0 & 1 \\ 0 & 0 & 1 & 0 \end{pmatrix}, \quad \text{CNOT}|00\rangle = |00\rangle, \quad \text{CNOT}|01\rangle = |01\rangle, \quad (1.10)$$

$$\text{CNOT}|10\rangle = |11\rangle, \quad \text{CNOT}|11\rangle = |10\rangle.$$

The set of $\{I, X, Y, Z, S, H, \text{CNOT}\}$ forms the second Clifford hierarchy, \mathcal{C}_2 and the Clifford group. We will explain why these hierarchies are important in the next section. Let us consider a single qubit. If we only use the single qubit gates above, the states that I can simulate are going to be on the x , y , and z axis of the Bloch sphere, with nothing

in between them. The states that are in superposition are going to be in equal superposition and we can not get any intermediate angles. We can expand this gate set to also access more intricate superpositions.

T-gate. T-gate is a single-qubit gate, denoted by T , and it gives the qubit a $\pi/4$ phase. Its matrix form and its action on the basis $|0\rangle$ and $|1\rangle$ defined as,

$$T = \begin{pmatrix} 1 & 0 \\ 0 & e^{i\frac{\pi}{4}} \end{pmatrix}, \quad T|0\rangle = |0\rangle, \quad T|1\rangle = e^{i\frac{\pi}{4}}|1\rangle \quad (1.11)$$

Rotations. The rotation gates are single-qubit gates, denoted by $\{R_x(\theta), R_y(\theta), R_z(\theta)\}$, and they rotate the qubit along the given axis and give angle. Their matrix form and action on the basis $|0\rangle$ and $|1\rangle$ defined as,

$$R_x(\theta) = \begin{pmatrix} \cos\frac{\theta}{2} & -i\sin\frac{\theta}{2} \\ -i\sin\frac{\theta}{2} & \cos\frac{\theta}{2} \end{pmatrix}, \quad R_x(\theta)|0\rangle = \cos\frac{\theta}{2}|0\rangle - i\sin\frac{\theta}{2}|1\rangle \quad (1.12)$$

$$R_x(\theta)|1\rangle = -i\sin\frac{\theta}{2}|0\rangle + \cos\frac{\theta}{2}|1\rangle$$

$$R_y(\theta) = \begin{pmatrix} \cos\frac{\theta}{2} & -\sin\frac{\theta}{2} \\ \sin\frac{\theta}{2} & \cos\frac{\theta}{2} \end{pmatrix}, \quad R_y(\theta)|0\rangle = \cos\frac{\theta}{2}|0\rangle + \sin\frac{\theta}{2}|1\rangle \quad (1.13)$$

$$R_y(\theta)|1\rangle = -\sin\frac{\theta}{2}|0\rangle + \cos\frac{\theta}{2}|1\rangle$$

$$R_z(\theta) = \begin{pmatrix} e^{-i\frac{\theta}{2}} & 0 \\ 0 & e^{i\frac{\theta}{2}} \end{pmatrix}, \quad R_z(\theta)|0\rangle = e^{-i\frac{\theta}{2}}|0\rangle \quad (1.14)$$

$$R_z(\theta)|1\rangle = e^{i\frac{\theta}{2}}|1\rangle$$

It is useful to mention that rotation gates for some specific rotation angles can reduce to some of the gates in the second Clifford Hierarchy.

The set of gates described in this section is universal, i.e. one can reach *any* point in the Hilbert space with these gates.

The true potential of quantum computers was unleashed by the introduction of a few algorithms¹ for quantum computers that could, in principle, surpass the classical ones. Some notable algorithms include the Deutsch-Josza algorithm [5], Shor's algorithm [6] and Grover's algorithm [7]. Since then there has been a great effort worldwide to realize quantum computers in practice. The current stage of quantum computing is known as the Noisy Intermediate-Scale Quantum (NISQ) era, where quantum processors contain up to 1000 qubits and are not yet advanced enough for fault-tolerance. However, they are useful to study, for example, many-body quantum systems, that would be challenging for classical computers [8].

¹The word algorithm is the Latinization of the name of the Persian scientist and polymath Al-Khwarizmi's name for the honour of his works on Algebra and Arithmetic

Aside from the algorithms that exist nowadays in the quantum computing community, there is a great effort to show that the existing quantum computers are performing tasks that are infeasible for classical computers. These studies are focused on simulating random quantum circuits on a scale that is impossible for any classical computer [9–11].

A particularly useful concept for exploring the physics of quantum computers was that of a random quantum system or random quantum circuit. Since the quantum system reaches a steady state rapidly in the framework of random circuits, it allows us to study some universal features of quantum physics more easily. Examples of such universal features are entanglement, mutual information, and non-linear correlation functions of reduced density matrix [12]. We will return to this concept in the following sections.

1.3. NON-STABILIZERNESS OR MAGIC

Since the introduction of quantum mechanics, there have been many non-trivial effects (some of them are mentioned above). However, entanglement was at the heart of quantum mechanics from early on [13]. Traditionally, detecting entanglement in an experimental set-up is a criterion for us to consider that system a quantum system. However, for quantum computational purposes, there is an added complexity to the story.

As mentioned in the previous section, the second Clifford hierarchy, \mathcal{C}_2 , has an important place in quantum computation. It forms a group called Clifford group, such that

$$C = \{U \in \mathcal{C}_2 | UPU^\dagger = e^{i\phi} P'\}, \quad (1.15)$$

where $P, P' \in \mathcal{P}_N$ and \mathcal{P}_N is the set of all Pauli strings for N -qubits. Pauli strings defined as, $\mathcal{P}_N = \{\sigma_1 \otimes \sigma_2 \otimes \dots \otimes \sigma_N \mid \sigma_i \in \{I, X, Y, Z\}\}$. The Clifford group can produce arbitrarily high entangled states since CNOT and Hadamard are in the Clifford group. However, the states resulting from the Clifford gates do not offer any quantum advantage in computation!

The Gottesman-Knill theorem [14] guarantees that any circuit consisting solely of Clifford gates can be simulated efficiently in a polynomial time on a classical computer. Additionally, the Clifford circuits are not *universal*. We can see that every N -qubit superposition resulting from this set of gates is always an *equal* superposition, up to a sign or phase. The states that one can simulate via Clifford circuits are called **Stabilizer States**, where they are only a subset of the whole Hilbert space.

From the perspective of classical simulatability, we need to define new criteria for having a quantum advantage in computation *and* have universal unitary circuits. This criteria is known as **Magic** or **Non-stabilizer** [15]. In order to inject magic into the state, we need to have gates outside of Clifford group in the circuit. Examples of such gates are T-gates and rotation gates, which were introduced in the previous section.

Non-stabilizer or magic plays a crucial role in fault-tolerant regimes of quantum computation. A big class of error correction code, stabilizer codes, are designed such that they inherently support a subset of quantum operations, particularly Clifford operations, in a fault-tolerant manner, often implemented transversely [16, 17]. We call them "cheap" gates. Since we need non-Clifford gates as well and they are non-transversal, we call them the "expensive" gates. With all this knowledge about Clifford and non-Clifford gates, it is safe to say that non-stabilizer or magic can be considered a resource for

quantum computation [15].

Recently, there has been a great effort to quantify non-stabilizerness. Similarly to how entanglement can be quantified by defining a distance from a product state, we can quantify non-stabilizerness as the distance from the stabilizer group. Notable measures for non-stabilizerness are Magical Cross-Entropy, Mana [15], Robustness of Magic [18, 19] and Stabilizer Entropies (SE) [20]. There has been other measures introduced recently [21–24]. In this thesis, I mainly focus on the Stabilizer Entropies because of their favourable scaling in comparison to other quantifiers.

The class of Stabilizer Entropies is diverse, but a key quantity for this thesis is stabilizer Renyi- n entropy for N qubit pure-state that is defined as,

$$M_n(|\Psi_N\rangle) = (1-n)^{-1} \log_2 \sum_{P \in \mathcal{P}_N} \frac{\langle \Psi_N | P | \Psi_N \rangle^{2n}}{2^N}, \quad (1.16)$$

where \mathcal{P}_N is the set of all Pauli strings as defined before. It has been shown that $n \geq 2$ is a magic monotone and can be extended to the mixed-states as well [25, 26]. Although I stated that Stabilizer Entropies are scaling favourably, it does not mean that they are easy to calculate for a given state. The summation in Eq. 1.16 is over all possible Pauli strings, where the number of Pauli strings scales as 4^N for N qubits. The state itself also scales as 2^N so we are still suffering from the exponential scaling here.

One powerful method to scale up the Stabilizer Entropies comes with the help of Tensor Network models [27]. So far the main focus of the Tensor Network community in the the Stabilizer Entropies has been on Matrix Product States (MPS) representation [28–31].

Non-stabilizerness also has close relationships to other physical properties of the system. Obviously, one of the most important physical properties, whose relationship to non-stabilizerness is very interesting, is entanglement. For example, a direct connection between non-stabilizerness and entanglement spectrum flatness has been observed [32]. Another systematic study on the role of magic in entanglement was conducted, and the entanglement dominant and magic dominant phases were separated. It is shown that in the entanglement dominant phase, sample efficient and time efficient algorithms for entanglement tasks are not computationally intractable in the magic dominant phase [33].

Another direction for studying the non-stabilizerness is in the context of quantum many-body systems. The non-stabilizerness has been studied in the generalized Rokhsar-Kivelson wavefunctions [29], in the critical regime of spin chains [34, 35], in frustrated and unfrustrated regimes of many-body systems [36].

1.4. INFORMATION SCRAMBLING

Another important concept relevant to the investigation of quantum systems is that of information scrambling. A generic isolated quantum state, $\rho = |\psi\rangle\langle\psi|$, typically will reach the thermal equilibrium after some unitary time evolution. For example in case we are interested in the subsystem A of the state with the compliment \bar{A} ,

$$\rho_A = \text{tr}_{\bar{A}} \rho, \quad (1.17)$$

where local measurements on A allow us to extract all necessary information about this subsystem. However, after the thermalization, only macroscopic information of A can be extracted and the microscopic information of the initial state is apparently lost and inaccessible via local measurements [37]. In case our initial state is a product state, after thermalization, ρ_A will become a maximally mixed state.

Let us consider this concept in the example of entanglement entropy, which is defined as

$$S(\rho_A) = -\text{tr} \rho_A \log_2 \rho_A. \quad (1.18)$$

We can see that entanglement is zero at the beginning of a quantum process for a product state as an initial state. The entanglement grows with the thermalization. This effect is independent of the initial state, where we can choose two orthogonal product states and see the entanglement growth in a similar way. There are some exceptions to this logic like Anderson localization in the presence of disorder [38], but they are not central to this thesis.

In order to quantify the thermalization, entropy-based methods were proposed [39, 40]. Like the previous case, we begin by dividing the system into subsystems, A , and its complement \bar{A} . If we consider another subsystem, B , and its complement \bar{B} , we can define thermalization or scrambling quantifier, called mutual information, as

$$I(A : B) = S(\rho_A) + S(\rho_B) - S(\rho_{AB}), \quad (1.19)$$

The mutual information quantifies the dependencies or correlations between the two subsystems A and B .

We can also define other entropy-based quantifiers of information scrambling like tripartite information [41].

There is a very different way to look at information scrambling. Specifically, we can assess it through the lens of correlation functions. Considering a local operator, W , we can write its time evolution in the Heisenberg picture as

$$W(t) = U^\dagger(t) W U(t), \quad (1.20)$$

for a generic unitary $U(t)$. We can see that the local operator W will become non-local as we go forward in time. By considering another local operator, V , we can quantify the thermalization or information scrambling resulting from unitary $U(t)$, by considering the overlap of these two operators $W(t)$ and V . This overlap can be defined as the squared commutator [37],

$$C \equiv \langle [W(t), V]^\dagger [W(t), V] \rangle. \quad (1.21)$$

Alternatively, we can write

$$\langle [W(t), V]^\dagger [W(t), V] \rangle = 2(1 - \text{Re} \langle W^\dagger(t) V^\dagger W(t) V \rangle), \quad (1.22)$$

The decay of the $\text{Re} \langle W^\dagger(t) V^\dagger W(t) V \rangle$ has been used as a reliable quantifier of information scrambling. This term is known as Out-of-Time Ordered Correlator (OTOC) and it is defined as

$$\text{OTOC} = \text{Re}\langle W^\dagger(t) V^\dagger W(t) V \rangle. \quad (1.23)$$

OTOCs have been extensively studied in the context of black hole physics [42], many-body localization in condensed matter physics [43] and operator spreading in quantum circuits [44].

Later we will see how information scrambling is related to non-stabilizerness, both with correlators and entropic-based quantifiers. I covered them in chapters 2 and 3.

1.5. VARIATIONAL QUANTUM STATES

Aside from the fundamental properties of the quantum world, described in the previous sections, there is a practical problem to study these systems. Due to the exponential scaling of the Hilbert space, known as the exponential scaling, we can not study them on large scales. The approximate methods have been proposed to tackle this problem. The variational quantum states are an example of such approximation [45–47].

The majority of the literature on the variational quantum states is developed to simulate the quantum systems on classical computers. An important class of examples of the variational states are known as the Variational Monte Carlo (VMC) states. The VMC states are a class of probabilistic frameworks used to study the different features of a quantum system. For example, finding the ground state energy of a k -local many-body Hamiltonian is a problem that can be approximated via VMC methods.

The modern applications of VMC come with training the neural networks for studying quantum systems. The Neural Network Quantum States (NQS) has been introduced recently [48] and shown to be a powerful and Hamiltonian agnostic ansatz. One important model of classical neural networks is known as the Restricted Boltzmann Machine (RBM) [48].

The structure of the neural network for RBM is just a simple one hidden layer fully connected neural network with restrictions on having only intra-layer connections. The schematic structure of RBM is shown in Fig. 1.1 and the ansatz for the probability amplitude is given as

$$\psi_{\theta}(\mathbf{s}) = \sum_{\mathbf{h}} e^{\sum_j a_j \sigma_j + \sum_i b_i h_i + \sum_{ij} W_{ij} h_i \sigma_j}, \quad (1.24)$$

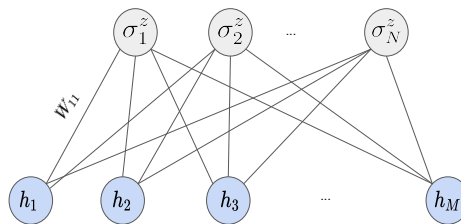


Figure 1.1: The neural network diagram for Restricted Boltzmann Machine (RBM) with N visible units and M hidden units connecting via W_{ij} weights.

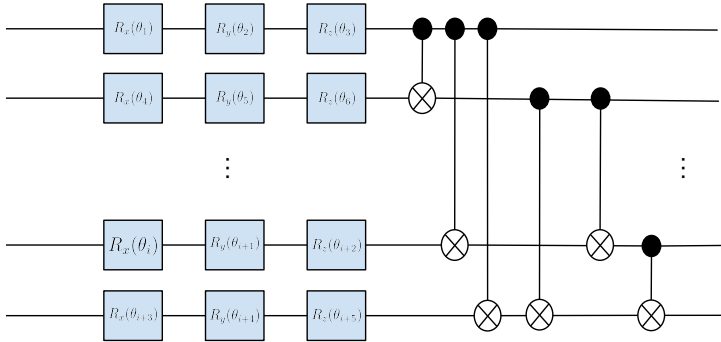


Figure 1.2: One layer of VQE ansatz consists of rotation gates and an entangling gate, CNOT, on every two pairs of qubits.

where $\theta = \{\mathbf{a}, \mathbf{b}, \mathbf{W}\}$. We refer to \mathbf{W} as weights, \mathbf{b} hidden biases and \mathbf{a} visible biases. These are the trainable parameters of the neural networks, and $\mathbf{s} = (\sigma_1, \sigma_2, \dots, \sigma_N)$ is the sample of the configuration of the states such that $\sigma_i = \pm 1$. For the ground state search problem, we need to find the optimal values for θ such that for a given Hamiltonian, H ,

$$E_{gs} \approx \frac{\langle \psi_{\theta} | H | \psi_{\theta} \rangle}{|\psi_{\theta}|^2}. \quad (1.25)$$

However for RBM as we can see from Eq. 1.24, we need to sample the required configurations \mathbf{s} . The sampling process relies on the probability $P(\mathbf{s})$,

$$P(\mathbf{s}) = \frac{|\psi_{\theta}(\mathbf{s})|^2}{\sum_{\mathbf{s}'} |\psi_{\theta}(\mathbf{s}')|^2} \quad (1.26)$$

To briefly explain the simplified sampling process, by proposing a new configuration each time step, e.g. from $\mathbf{s} \rightarrow \mathbf{s}'$, the acceptance probability of the new configuration is

$$A(\mathbf{s} \rightarrow \mathbf{s}') = \min \left(1, \frac{P(\mathbf{s}')}{P(\mathbf{s})} \right), \quad (1.27)$$

and by repeating this process we can have the desired number of samples to train our neural networks. This was a primary example of VMC processes, in general, we can use more complex and case-specific ways of sampling methods depending on the problem we wish to solve. The last step to find our desired ground state is to find the optimal values for θ that minimises the right-hand side of Eq. 1.25. There is a big class of optimizers that can achieve this goal, notable examples are stochastic gradient descent or Adam.

So far I have only described the classical variational quantum states where every part of the calculation is meant to be performed on a classical computer. However, a class of variational states has recently been proposed to tackle the same problems, e.g., ground state search, in hybrid quantum-classical manner. A flagship example of such an algorithm is known as Variational Quantum Eigensolver (VQE) [49].

Similar to the classical variational quantum states, in VQE we also have an ansatz that comes with a parameterized quantum circuit. In digital quantum computation, we have

discrete gate sets, one way that we can have continuous parameters is to use the rotation gates and vary the angle of rotations. By placing rotation gates with rotation parameters θ , and CNOTs on every pair of neighbouring qubits, we can have a general parameterized circuit. In Fig. 1.2 we can see one layer of such a parameterized circuit. Similar to RBM, where we can increase the number of hidden units, here we can increase the depth of the circuit and increase the number of trainable parameters (rotational angles).

Analogously to the classical variational algorithms, we aim to find the optimal values for θ such that minimises $\langle \psi_\theta | H | \psi_\theta \rangle$. The optimisation part is the duty of classical computers in this hybrid architecture and is performed by classical optimizers analogously to classical variational methods.

1.6. OUTLINE OF THE CHAPTERS OF THIS THESIS

In Chapter 2 of this thesis, we will explore the relationship between Out-of-Time Ordered Correlators (OTOCs) and non-stabilizerness. We show a relationship between fluctuations of OTOCs in random t-doped circuits and various measures of non-stabilizerness. We explore this relationship both analytically and numerically. Specifically, we show that very few OTOCs are needed to approximate mana (for qutrits) and Stabilizer 2-Renyi entropy for qubits.

In Chapter 3 of this thesis, we generalize the mutual dependence of non-stabilizerness and fluctuations to another class of information scrambling quantifiers: the entropic-based measures. We observe that the fluctuations of the mutual information also show the same behaviour as OTOC in random t-doped circuits. To connect these observations to entanglement, we also explore the effect of non-stabilizerness in entanglement phase transition in measurement induced.

In Chapter 4 of this thesis, we analyse the non-stabilizerness of the approximated quantum states via variational methods with the ultimate goal of establishing a common framework for classical and quantum notions of exact and approximate simulatability. We analyze the trade-off between the ground state energy accuracy and non-stabilizerness of the same state, for both classical and quantum variational states. We observe better accuracy in the ground state energy is necessary but not a sufficient condition for good non-stabilizerness accuracy. This result suggests that only optimizing a state based on one parameter, here ground state energy, does not necessarily yield better accuracy on other types of parameters, like non-stabilizerness.

In Chapter 5, we provide an overview of and a broader perspective on our results. We discuss how this thesis fits into the field of resource theory of quantum computation and variational methods.

1.7. AUTHOR'S CONTRIBUTIONS

In this section, I will clarify my contributions to the chapters of this thesis.

In Chapter 2, the idea of using fluctuations of OTOC for quantifying non-stabilizerness emerged from my discussion with my supervisor Eliska Greplova. Through her valuable supervision, I could do all the necessary simulations that yielded the results presented here. Later, we received valuable insights from anonymous reviewers of our first submission. Finally, the paper was enriched with the analytical relation for the fluctuations of

OTOC and stabilizer 2-Renyi entropy, provided by Lorenzo Leone, one of the reviewers of the manuscripts in SciPost Physics journal. I am grateful for this productive peer-review experience.

In Chapter 3, with the help of my supervisor Eliska Greplova, I conceived the project and wrote the code for mutual information simulation and data analysis. Jonas Helsen derived the analytical relation for mutual information fluctuations and non-stabilizerness in t -doped random circuits. As a part of the master's thesis, Cagan Karaca simulated the measurement-induced circuits and analysed the phase transition point with insights from Eliska Greplova and me, he found the relationship between fluctuations of mutual information and non-stabilizerness in measurement-induced circuits and produced the figures for that section. The project was supervised by Eliska Greplova and the manuscript was written by Jonas Helsen, Eliska Greplova and me.

In Chapter 4, myself, Eliska Greplova, and Tom Spriggs, designed the project. Myself and Tom Spriggs wrote the code for the neural network and the exact diagonalization simulation. I performed the non-stabilizerness calculations. Bokai Chen performed the VQE simulation as a part of his master's thesis, and later his results were enhanced and expanded on by Tom Spriggs. A similar simulation was done for the Fermi-Hubbard model by Yitao Sun during his internship at QMAI group. While those results are not included in this thesis, I learned a lot and benefited from this collaboration. Tom Spriggs performed the MPS simulations and plotted the paper figures. The manuscript was written by Eliska Greplova, Tom Spriggs, and me.

BIBLIOGRAPHY

1. Feynman, R. P. Simulating physics with computers. *International Journal of Theoretical Physics* **21**, 467–488 (June 1982).
2. Schrödinger, E. An Undulatory Theory of the Mechanics of Atoms and Molecules. *Physical Review* **28**, 1049–1070 (Dec. 1926).
3. Sakurai, J. J. *Modern Quantum Mechanics (Revised Edition)* ISBN: 0-201-53929-2. <http://www.scribd.com/doc/3035203/J-J-Sakurai-Modern-Quantum-Mechanics> (1994).
4. Gottesman, D. & Chuang, I. L. Demonstrating the viability of universal quantum computation using teleportation and single-qubit operations. *Nature* **402**, 390–393 (1999).
5. Deutsch, D. & Jozsa, R. Rapid solution of problems by quantum computation. *Proceedings of the Royal Society of London. Series A: Mathematical and Physical Sciences* **439**, 553–558 (1992).
6. Shor, P. *Algorithms for quantum computation: discrete logarithms and factoring in Proceedings 35th Annual Symposium on Foundations of Computer Science* (1994), 124–134.
7. Grover, L. K. *A fast quantum mechanical algorithm for database search in Proceedings of the Twenty-Eighth Annual ACM Symposium on Theory of Computing* (Association for Computing Machinery, Philadelphia, Pennsylvania, USA, 1996), 212–219. ISBN: 0897917855. <https://doi.org/10.1145/237814.237866>.
8. Preskill, J. Quantum Computing in the NISQ era and beyond. *Quantum* **2**, 79. ISSN: 2521-327X. <https://doi.org/10.22331/q-2018-08-06-79> (Aug. 2018).
9. Arute, F. *et al.* Quantum supremacy using a programmable superconducting processor. *Nature* **574**, 505–510 (2019).
10. Bouland, A., Fefferman, B., Nirkhe, C. & Vazirani, U. On the complexity and verification of quantum random circuit sampling. *Nature Physics* **15**, 159–163 (2019).
11. Movassagh, R. The hardness of random quantum circuits. *Nature Physics* **19**, 1719–1724 (2023).
12. Fisher, M. P., Khemani, V., Nahum, A. & Vijay, S. Random Quantum Circuits. *Annual Review of Condensed Matter Physics* **14**, 335–379. ISSN: 1947-5462. <http://dx.doi.org/10.1146/annurev-conmatphys-031720-030658> (Mar. 2023).
13. Einstein, A., Podolsky, B. & Rosen, N. Can Quantum-Mechanical Description of Physical Reality Be Considered Complete? *Phys. Rev.* **47**, 777–780. <https://link.aps.org/doi/10.1103/PhysRev.47.777> (10 May 1935).

14. Gottesman, D. The Heisenberg Representation of Quantum Computers. *arXiv:quant-ph/9807006*. <https://arxiv.org/abs/quant-ph/9807006> (1998).
15. Veitch, V., Hamed Mousavian, S. A., Gottesman, D. & Emerson, J. The resource theory of stabilizer quantum computation. *New Journal of Physics* **16**, 013009. ISSN: 1367-2630. <http://dx.doi.org/10.1088/1367-2630/16/1/013009> (Jan. 2014).
16. Gottesman, D. Stabilizer Codes and Quantum Error Correction. *arXiv:quant-ph/9705052*. <https://arxiv.org/abs/quant-ph/9705052> (1997).
17. Gottesman, D. Theory of fault-tolerant quantum computation. *Physical Review A* **57**, 127–137. ISSN: 1094-1622. <http://dx.doi.org/10.1103/PhysRevA.57.127> (Jan. 1998).
18. Howard, M. & Campbell, E. Application of a Resource Theory for Magic States to Fault-Tolerant Quantum Computing. *Phys. Rev. Lett.* **118**, 090501. <https://link.aps.org/doi/10.1103/PhysRevLett.118.090501> (9 Mar. 2017).
19. Hamaguchi, H., Hamada, K. & Yoshioka, N. Handbook for Efficiently Quantifying Robustness of Magic. *arXiv:2311.01362*. <https://arxiv.org/abs/2311.01362> (2024).
20. Leone, L., Oliviero, S. F. E. & Hamma, A. Stabilizer Rényi Entropy. *Physical Review Letters* **128**. ISSN: 1079-7114. <http://dx.doi.org/10.1103/PhysRevLett.128.050402> (Feb. 2022).
21. Haug, T. & Kim, M. Scalable Measures of Magic Resource for Quantum Computers. *PRX Quantum* **4**. ISSN: 2691-3399. <http://dx.doi.org/10.1103/PRXQuantum.4.010301> (Jan. 2023).
22. Liu, Z.-W. & Winter, A. Many-Body Quantum Magic. *PRX Quantum* **3**. ISSN: 2691-3399. <http://dx.doi.org/10.1103/PRXQuantum.3.020333> (May 2022).
23. Garcia, R. J., Bu, K. & Jaffe, A. Resource theory of quantum scrambling. *Proceedings of the National Academy of Sciences* **120**. ISSN: 1091-6490. <http://dx.doi.org/10.1073/pnas.2217031120> (Apr. 2023).
24. Garcia, R. J. *et al.* *On the Hardness of Measuring Magic* 2024. <https://arxiv.org/abs/2408.01663>.
25. Leone, L. & Bittel, L. *Stabilizer entropies are monotones for magic-state resource theory* 2024. arXiv: 2404.11652 [quant-ph]. <https://arxiv.org/abs/2404.11652>.
26. Haug, T. & Piroli, L. Stabilizer entropies and nonstabilizerness monotones. *Quantum* **7**, 1092. ISSN: 2521-327X. <http://dx.doi.org/10.22331/q-2023-08-28-1092> (Aug. 2023).
27. Orús, R. A practical introduction to tensor networks: Matrix product states and projected entangled pair states. *Annals of Physics* **349**, 117–158. ISSN: 0003-4916. <https://www.sciencedirect.com/science/article/pii/S0003491614001596> (2014).

28. Haug, T. & Piroli, L. Quantifying nonstabilizerness of matrix product states. *Physical Review B* **107**. ISSN: 2469-9969. <http://dx.doi.org/10.1103/PhysRevB.107.035148> (Jan. 2023).
29. Tarabunga, P. S., Tirrito, E., Bañuls, M. C. & Dalmonte, M. Nonstabilizerness via Matrix Product States in the Pauli Basis. *Physical Review Letters* **133**. ISSN: 1079-7114. <http://dx.doi.org/10.1103/PhysRevLett.133.010601> (July 2024).
30. Lami, G. & Collura, M. Nonstabilizerness via Perfect Pauli Sampling of Matrix Product States. *Phys. Rev. Lett.* **131**, 180401. <https://link.aps.org/doi/10.1103/PhysRevLett.131.180401> (18 Oct. 2023).
31. Lami, G. & Collura, M. Unveiling the Stabilizer Group of a Matrix Product State. *Phys. Rev. Lett.* **133**, 010602. <https://link.aps.org/doi/10.1103/PhysRevLett.133.010602> (1 July 2024).
32. Tirrito, E. *et al.* Quantifying nonstabilizerness through entanglement spectrum flatness. *Phys. Rev. A* **109**, L040401. <https://link.aps.org/doi/10.1103/PhysRevA.109.L040401> (4 Apr. 2024).
33. Gu, A., Oliviero, S. F. E. & Leone, L. Magic-induced computational separation in entanglement theory. *arXiv:2403.19610*. <https://arxiv.org/abs/2403.19610> (2024).
34. Tarabunga, P. S. Critical behaviors of non-stabilizerness in quantum spin chains. *Quantum* **8**, 1413. ISSN: 2521-327X. <http://dx.doi.org/10.22331/q-2024-07-17-1413> (July 2024).
35. White, C. D., Cao, C. & Swingle, B. Conformal field theories are magical. *Physical Review B* **103**. ISSN: 2469-9969. <http://dx.doi.org/10.1103/PhysRevB.103.075145> (Feb. 2021).
36. Odavić, J. *et al.* Complexity of frustration: A new source of non-local non-stabilizerness. *SciPost Phys.* **15**, 131. <https://scipost.org/10.21468/SciPostPhys.15.4.131> (2023).
37. Xu, S. & Swingle, B. Scrambling Dynamics and Out-of-Time-Ordered Correlators in Quantum Many-Body Systems. *PRX Quantum* **5**, 010201. <https://link.aps.org/doi/10.1103/PRXQuantum.5.010201> (1 Jan. 2024).
38. Anderson, P. W. Absence of Diffusion in Certain Random Lattices. *Phys. Rev.* **109**, 1492–1505. <https://link.aps.org/doi/10.1103/PhysRev.109.1492> (5 Mar. 1958).
39. Touil, A. & Deffner, S. Information scrambling —A quantum thermodynamic perspective. *Europhysics Letters* **146**, 48001. ISSN: 1286-4854. <http://dx.doi.org/10.1209/0295-5075/ad4413> (May 2024).
40. Alba, V. & Calabrese, P. Quantum information scrambling after a quantum quench. *Phys. Rev. B* **100**, 115150. <https://link.aps.org/doi/10.1103/PhysRevB.100.115150> (11 Sept. 2019).
41. Monaco, G. L. *et al.* An operational definition of quantum information scrambling. *arXiv:2312.11619*. <https://arxiv.org/abs/2312.11619> (2023).

42. Hayden, P. & Preskill, J. Black holes as mirrors: quantum information in random subsystems. *Journal of High Energy Physics* **2007**, 120. <https://dx.doi.org/10.1088/1126-6708/2007/09/120> (Sept. 2007).
43. Basko, D., Aleiner, I. & Altshuler, B. Metal–insulator transition in a weakly interacting many-electron system with localized single-particle states. *Annals of Physics* **321**, 1126–1205. ISSN: 0003-4916. <https://www.sciencedirect.com/science/article/pii/S0003491605002630> (2006).
44. Mi, X. *et al.* Information scrambling in quantum circuits. *Science* **374**, 1479–1483. eprint: <https://www.science.org/doi/pdf/10.1126/science.abg5029>. <https://www.science.org/doi/abs/10.1126/science.abg5029> (2021).
45. Jastrow, R. Many-Body Problem with Strong Forces. *Phys. Rev.* **98**, 1479–1484. <https://link.aps.org/doi/10.1103/PhysRev.98.1479> (5 June 1955).
46. Gutzwiller, M. C. Effect of Correlation on the Ferromagnetism of Transition Metals. *Phys. Rev. Lett.* **10**, 159–162. <https://link.aps.org/doi/10.1103/PhysRevLett.10.159> (5 Mar. 1963).
47. Gutzwiller, M. C. Effect of Correlation on the Ferromagnetism of Transition Metals. *Phys. Rev.* **134**, A923–A941. <https://link.aps.org/doi/10.1103/PhysRev.134.A923> (4A May 1964).
48. Carleo, G. & Troyer, M. Solving the quantum many-body problem with artificial neural networks. *Science* **355**, 602–606. eprint: <https://www.science.org/doi/pdf/10.1126/science.aag2302>. <https://www.science.org/doi/abs/10.1126/science.aag2302> (2017).
49. Schuld, M. & Petruccione, F. *Machine Learning with Quantum Computers* 2nd. ISBN: 978-3-030-83097-3 (Springer, 2021).

2

QUANTIFYING NON-STABILIZERNESS VIA INFORMATION SCRAMBLING

The advent of quantum technologies brought forward much attention to the theoretical characterization of the computational resources they provide. A method to quantify quantum resources is to use a class of functions called magic monotones and stabilizer entropies, which are, however, notoriously hard and impractical to evaluate for large system sizes. In recent studies, a fundamental connection between information scrambling, the magic monotone mana and 2-Renyi stabilizer entropy was established. This connection simplified magic monotone calculation, but this class of methods still suffers from exponential scaling with respect to the number of qubits. In this work, we establish a way to sample an out-of-time-order correlator that approximates magic monotones and 2-Renyi stabilizer entropy. We numerically show the relation of these sampled correlators to different non-stabilizer measures for both qubit and qutrit systems and provide an analytical relation to 2-Renyi stabilizer entropy. Furthermore, we put forward and simulate a protocol to measure the monotonic behaviour of magic for the time evolution of local Hamiltonians.

⁰The work in this chapter has been published as: **A. Ahmadi**, E. Greplova, Quantifying non-stabilizer via information scrambling, *SciPost Physics* 16 (2), 043 (2024)

2.1. INTRODUCTION

The field of quantum computing introduced the concept that quantum systems can deliver a significant computational speed-up in a variety of settings [1–6]. Yet, although increasingly large quantum processors are available, the question remains of how to rigorously quantify the computational resources of a quantum computer. One successful approach towards determining quantum resources of a quantum state is to calculate how “far away” the state is from being possible to simulate efficiently with a classical computer [7].

A specific example of quantum states that are tractable to represent and simulate on a classical computer are the so-called stabilizer states [8]. These states result from quantum circuits produced by Clifford gates which are elements of the Clifford group generated by the Hadamard gate, the phase gate and the entangling control-NOT gate [9]. In order to get any quantum advantage over classical computers, we need to add additional gates outside of the Clifford group. By injecting more non-Clifford gates into a quantum circuit, we obtain a quantum state with further distance from a stabilizer state. This distance is in literature referred to as magic or non-stabilizeress[10]. The states that are not stabilizer states are called *magic states*. Interestingly, the Clifford operations could be easier both at the experimental level and for quantum error correction [11–13], while universal gate-sets are achieved by the distillation of a large number of noisy magic states into a less-noisy magic state which subsequently provides the computational resources for the fault-tolerant quantum computation [7, 14–17]

Examples of magic monotones include magical cross-entropy, mana [10], and robustness of magic [15]. These measures are, however, computationally expensive to evaluate and their calculation requires exact knowledge of the wave-function combined with complex optimization [10], which excludes the study of large quantum circuits. More recently introduced magic monotones such as the Gottesman-Kitaev-Preskill magic measure and the stabilizer Renyi entropy, [18, 19], offer simplified scaling which enables exact calculation of magic for a few qubits using conventional computers.

Different approaches to describe how far a quantum state is from the stabilizer states, can also be related to the amount of quantum correlations in the system. The out-of-time ordered correlators (OTOCs) quantify quantum information scrambling [20–25]. Quantum information scrambling describes the spread of the local information in a quantum system [24]. Through the time evolution of a closed quantum system, the in-

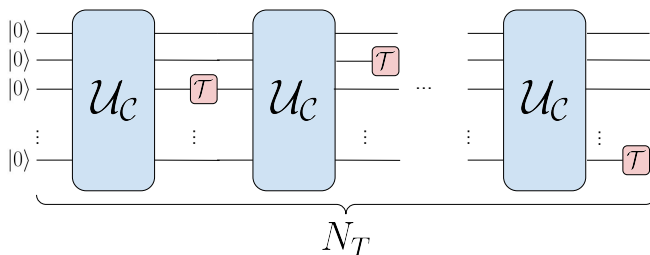


Figure 2.1: The schematic structure of a t-doped quantum circuit. We are using a block of the random Clifford gates, \mathcal{U}_C followed by a T-gate on a random qudit. We repeat this process N_T times.

formation about initial state of the system can become very hard to access due to quantum correlations in the system [26]. Even though the information is still encoded in the system it is not directly accessible without measuring all its degrees of freedom. Information scrambling has recently attracted an increasing amount of attention due to the relation with the anti-de Sitter/conformal field theory (AdS/CFT) correspondence [27]. The AdS/CFT correspondence draws a duality that relates the noise in quantum error correction codes to information scrambling in black holes [20, 22, 23]. Another application of this concept emerged in condensed matter physics such as many-body localization [28] and non-Fermi liquid behaviours [29].

Moreover, it was recently experimentally demonstrated that OTOCs can be used as an indicator of the degree of non-stabilizerness of scrambled quantum circuits [30]. In parallel, recent work has shown an analytical relation between the non-stabilizerness and OTOC [19, 31].

In this work, we show the relation between a randomised sampling of OTOC fluctuations and mana for qutrit systems and stabilizer Renyi entropy for qubit systems. We show numerical evidence that this method requires dramatically lesser number of OTOC measurements in comparison to the exact methods of calculating magic monotones. Capitalizing on this relation, we put forward an experimentally feasible way to approximate magic using the evaluation of OTOCs. Our work might lay the foundation to approximate magic in a scalable way in larger systems, as our protocol is designed to be adaptable for both numerical techniques such as tensor networks [32] and neural networks [33] as well as experimental measurements [30].

2.2. METHODS

2.2.1. MAGIC

The concept of magic in quantum information science arises from the field of resource theory [34]. The Gottesman-Knill theorem [8] guarantees that the subset of the physical states known as *stabilizer* states are efficiently simulatable on a classical computer. More precisely, the stabilizer states are the second level of the Clifford hierarchy [9].

Since the first level (the Pauli gates) and the second level, (the Clifford gates) of the Clifford hierarchy are insufficient for universal quantum computing, we need to use the third-level gates. This level of Clifford's hierarchy includes, for example, a T-gate. Another set of important non-Clifford gates are the rotation gates $\{R_x(\theta), R_y(\theta), R_z(\theta)\}$, where θ is the angle of rotation. These gates are particularly important in problems that require a continuous set of parameters to tune, i.e. quantum machine learning algorithms [5, 6].

The amount of non-stabilizerness, or magic, of any state is measured using *magic monotones*. Magic monotones such as the robustness of magic [10] are based on an optimization over all stabilizer states, which make them practically hard to compute. However, one example of a magic monotone that does not require any optimization is known as mana, \mathcal{M} [10]. This magic monotone has another limitation, namely that it is only definable for odd-prime dimensional Hilbert spaces. Additionally, mana is practically very hard to calculate since it is based on calculating discrete Wigner functions which in practice limits current calculations to at most 6 qudits. More details regarding

the definition and evaluation of mana are available in Appendix 2.6.

Another method introduced to measure magic for qubits is the Stabilizer Renyi Entropy [19]. For a system of N qubits, the Stabilizer Renyi Entropy of order n is defined as

$$M_n(|\Psi_N\rangle) = (1-n)^{-1} \log \sum_{P \in \mathcal{P}_N} \frac{\langle \Psi_N | P | \Psi_N \rangle^{2n}}{2^N}, \quad (2.1)$$

where \mathcal{P}_N is the set of all N -qubit Pauli strings and the number of the Pauli strings in \mathcal{P}_N we are summing over scales as 4^N .

2.2.2. INFORMATION SCRAMBLING

A well-known measure of information scrambling is the out-of-time-order correlators (OTOCs) which are commonly used in high-energy physics and condensed matter physics [20–25, 28, 29]. OTOC is evaluated for any two operators A and B , where $[A, B] = 0$, as

$$\text{OTOC}(t) = \text{Re}(\langle A^\dagger(t) B^\dagger A(t) B \rangle), \quad (2.2)$$

where

$$A(t) = U^\dagger(t) A(0) U(t), \quad (2.3)$$

or equivalently

$$\text{OTOC}(U) = \frac{1}{d} \text{tr}(U^\dagger(t) A^\dagger(0) U(t) B^\dagger U^\dagger(t) A(0) U(t) B) \quad (2.4)$$

and $U(t)$ is the time evolution operator, which could either result from the time evolution of a Hamiltonian or from a quantum circuit. Here we will consider a N qudit system, $A(0) = X_{N-1}$ and $B = Z_1$ where X_i and Z_i are the conventional Pauli operators and the subscript indicates the i -th qudit. As long as the commutation relation above holds, these Pauli operators can be placed on arbitrary qubit pairs. In this case, $A(0)$ plays the role of the butterfly operator related to chaotic quantum systems. The reason for using the butterfly operator is that by including a small perturbation (in this case a bit flip) we are disturbing the reversibility of the system, which is a signature of chaos [35]. The information scrambling measured through OTOC describes how information spreads in the system and becomes inaccessible in later times [20–25]. Information scrambling also describes how local Heisenberg operators grow in time [30, 36, 37]. A way to assess how the OTOC value fluctuates over a set of random circuits is the OTOC fluctuation, δ_{OTOC} , defined as the standard deviation of OTOC over all measured instances of OTOC. Let $U = C_1 V C_2$, where V is a generic unitary operator. Defining the average over C_1, C_2 as

$$\mathbb{E}_C \text{OTOC}(V) := \int dC_1 dC_2 \text{OTOC}(V) \quad (2.5)$$

and define the fluctuations around the average

$$\delta_{\text{OTOC}}(V) := \mathbb{E}_C \text{OTOC}^2(V) - [\mathbb{E}_C \text{OTOC}(V)]^2. \quad (2.6)$$

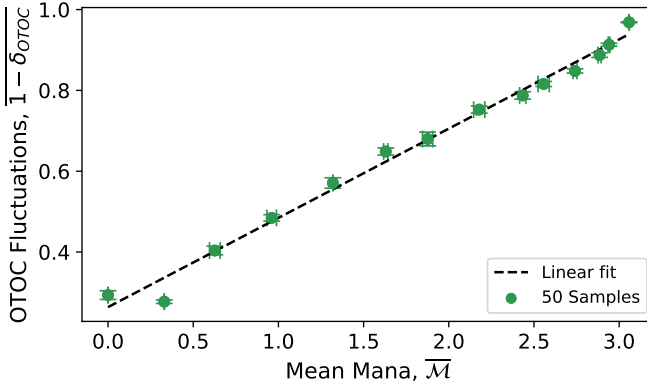


Figure 2.2: The fluctuation of OTOC, $\overline{1 - \delta_{OTOC}}$ as a function of the mean value of mana, $\overline{\mathcal{M}}$. We see a linear behaviour between these two magic monotones for 6 qutrit t-doped circuits. Here we show results for 50 (green dots) random samples of OTOC on the y-axis. On the x-axis, we calculated mana for 10 of the samples and we fit a linear dependence (dashed line). The vertical error bar is the statistical error calculated by repeating the process above 10 more times to get the error by the standard deviation of the sampled δ_{OTOC} instances and the horizontal error bar corresponds to the standard deviation of mana.

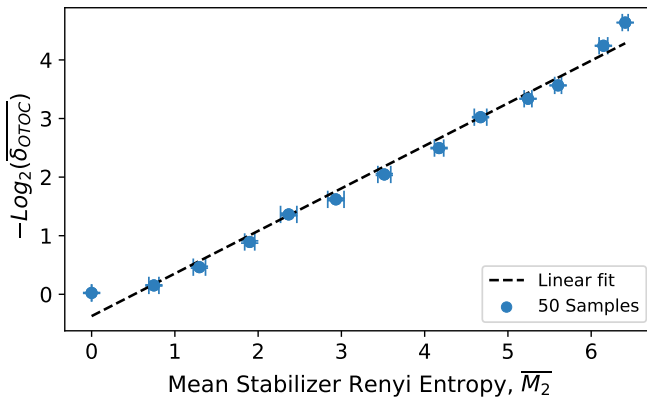


Figure 2.3: The log of fluctuation of OTOC, $-\text{Log}_2(\overline{\delta_{OTOC}})$ over 50 (blue dots) samples as a function of the mean value of stabilizer Renyi entropy (dashed line), $\overline{M_2}$ over 10 samples. The vertical error bar is the statistical error calculated by repeating the process above 10 more times to get the error by the standard deviation of the sampled δ_{OTOC} instances, and the horizontal error bar corresponds to the standard deviation of the stabilizer Renyi entropy M_2 .

2.3. RESULTS

We will now numerically investigate the relation between the fluctuations of OTOC, which was experimentally observed in Ref. [30] to decrease with the growing non-stabilizerness of the quantum circuit, and the measure for magic, mana, \mathcal{M} for $q = 3$ and the stabilizer Renyi entropy, M_2 for $q = 2$ where q is the dimension of the local Hilbert space. To this end, we design random quantum circuits with Clifford and non-Clifford gates, known as t-doped quantum circuits.

2.3.1. MANA AND OTOC

First, we consider N qudits in q -dimensional Hilbert space where $q = 3$. The circuits consist of M cycles of Clifford gates. In each cycle, we first apply one single Clifford gate, randomly chosen from the set $\mathcal{S} = \{H, S, X, Y, Z, I\}$ on each qudit. Then we add two CSUM gates on two randomly chosen qudits, where the CSUM gate is the counterpart of CNOT in Hilbert spaces with $q > 2$. Here we have a fixed number of $M = 10$ random cycles for each block of random Cliffords. Finally, we add a single non-Clifford gate, T , on a randomly chosen qudit. We increase the magic in the circuit by increasing the number of layers of the random Cliffords followed by a T-gate.

We begin by analyzing the relationship of mana and OTOC in the Hilbert space of dimension $q = 3$ for circuits containing four qudits such that mana is well-defined and computationally tractable. We use the qudit Clifford gates introduced in [38]. We provide detailed definitions of all gates in Appendix 2.7.

We observe an increasing monotonous relation between the mean value of mana, $\overline{\mathcal{M}}$ and the OTOC fluctuations, $1 - \delta_{\text{OTOC}}$, see Fig. 2.2. In Fig. 2.2, we observe a linear dependence between $1 - \delta_{\text{OTOC}}$ and $\overline{\mathcal{M}}$. This relationship corresponds to the linear fit $1 - \delta_{\text{OTOC}} \approx 0.22\overline{\mathcal{M}} + 0.26$. We simulated the OTOC instances of 50 circuit runs and the number of T-gates in the circuit is $N_T \in [0, 20]$. For the simulation of the quantum circuits, we have used the Cirq package [39].

2.3.2. THE STABILIZER RENEYI ENTROPY AND OTOC

Mana, discussed in the previous section, is not only challenging from the scaling point of view but also only defined for odd-dimensional local Hilbert space; because it is related to the negativity of discrete Wigner functions, and thus not possible to evaluate for qubits [40, 41]. In this section, we investigate the relation of 4-OTOC fluctuations, δ_{OTOC} , with the stabilizer Renyi entropy, M_2 , which is well-defined for even-dimensional Hilbert spaces. To evaluate the stabilizer Renyi entropy we use Eq. (4.8) for $q = 2$ and $n = 2$. The authors of Ref. [19] have shown the relation of the stabilizer Renyi entropy with 8-OTOC. The main difference between our approach with the existing analytical formula in Ref. [19] is the random sampling of a constant number of OTOCs as opposed to the exponential scaling of the number of 8-OTOC terms in the Renyi entropy formula [19].

We use the same random circuits as described in the previous subsection (see Fig. 2.1), this time for qubits. This way we obtain a comparison between δ_{OTOC} and the exact stabilizer Renyi entropy. In Fig. 2.3, we show OTOC fluctuations as a function of mean Renyi entropy, $\overline{M_2}$ and find a dependence corresponding to the fit $\overline{M_2} \approx -1.38 \log_2 \overline{\delta_{\text{OTOC}}} + 0.51$. We repeat the process 10 times to average over different δ_{OTOC} to obtain statistical error bars. The circuit used for Fig. 2.3 is a 12 qubit t-doped Clifford and we calculate $\overline{M_2}$ from

10 random instances. Each point in Fig. 2.3 belongs to a certain number of T-gates in the circuit, $N_T \in [0, 26]$. We note that the range of N_T was motivated by the fact that it has been shown that we need more than or equal to $2N$ T-gates to saturate the magic [42]. We see that regardless of the number of T-gates (and hence the amount of magic in the circuit), our ability to approximate the stabilizer Renyi entropy using OTOC fluctuations remains similar.

For the explanation of the relation observed in Fig. 2.3, we formulate the following lemma:

Lemma 1. Let $M_2(|V\rangle)$ be the stabilizer entropy of the Choi state [43] $|V\rangle$ associated to the unitary V and $d = 2^N$, then

$$\mathbb{E}_C \delta_{\text{OTOC}}(V) = \left(\frac{d^2}{d^2 - 1} \right)^2 2^{-M_2(|V\rangle)} - \frac{2d^2}{(d^2 - 1)^2}. \quad (2.7)$$

Proof. See Appendix 2.8.

From the Lemma 1 and the numerical results in Fig 3, we can conclude that sampling OTOC fluctuations could lead to more efficiency in measuring $M_2(|V\rangle)$.

For the case of random t-doped Clifford circuits, it generally holds that

$$\mathbb{E}_{C_t} 2^{-M_2(|C_t\rangle)} = \mathbb{E}_{C_t} 2^{-M_2(C_t|0\rangle)} + O(d^{-1}). \quad (2.8)$$

Therefore, in the case of a t-doped Clifford circuit, there is no distinction between the stabilizer entropy of $V|0\rangle$ and $|V\rangle$ for sufficiently large d .

It is worth noting that the relation of 4-OTOC fluctuations with the averaged 8-OTOC has been studied in Ref. [44]. In contrast, here we describe the relationship to 2-Renyi entropy.

2.3.3. THE MAGIC GENERATED BY TIME EVOLUTION OF A HAMILTONIAN

In this section, we propose a protocol to measure the magic generated by time evolution under the general Hamiltonian. The time evolution unitary operator of a general time-independent Hamiltonian is a fixed operator. Since, in our method, scrambling is an essential feature, in order to have such a low number of samples we need to create diversity in measured instances of OTOC by introducing additional randomisation in the circuit. We achieve this goal by including two extra blocks of random Clifford circuits, one before the time evolution and one after, see Fig. 2.4a. Since Clifford gates do not produce any magic by definition, we do not lose any generality for the circuit's magic calculation, but importantly we enhance the scrambling. It is important to keep in mind that the depth of the random Clifford circuit needs to be sufficient to fully scramble the state.

Here, as an example, we consider the Hamiltonian of the transverse-field Ising Hamiltonian,

$$H = -J \sum_i Z_i Z_{i+1} - h \sum_i X_i. \quad (2.9)$$

The system is in the open boundary condition and Z_i and X_i are the Pauli matrices on the i -th qubit. For this simulation, we fix $J = 1$ and $h = 0.5$. The schematic structure of the circuit we consider for its time evolution is shown in Fig. 2.4(a).

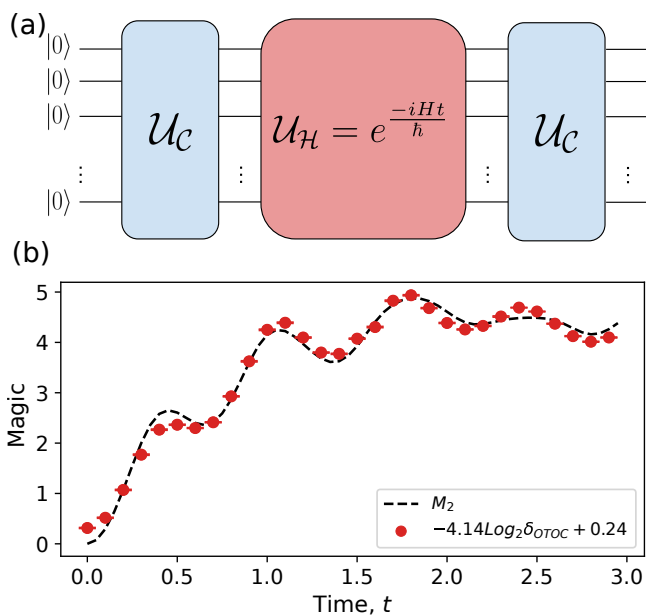


Figure 2.4: (a) The schematic structure of measuring magic of a time evolution of the Hamiltonian, \mathcal{U}_H . The protocol consists of two random Clifford blocks, before and after the desired time evolution block. (b) The comparison of OTOC fluctuations (blue dots) with the exact stabilizer Renyi entropy density (dashed line). The simulation is done for 10 qubits for the Choi state of a chain of length 5.

We are considering a chain of $N = 5$ for the Hamiltonian of Eq.2.9 and the Choi isomorphism, $|V\rangle \equiv \mathbb{1} \otimes V |I\rangle$ where $V = \mathcal{U}_\epsilon \mathcal{U}_\mathcal{H} \mathcal{U}_\epsilon$ and $|I\rangle \equiv 2^{-N/2} \sum_{i=1}^{2^N} |i\rangle \otimes |i\rangle$. From Fig.2.4(b) we can see that M_2 for the local Hamiltonian of the Eq.2.9 and OTOC fluctuations show similar behaviour, although the prediction accuracy is lower than for the random t-doped circuits. In this simulation, we used 5 qubits with 50 instances of sampled OTOCs. The time evolves for a total time of $3/J$. We see the same trend of increase in magic in the early time and oscillatory behaviour and stabilization in both stabilizer Renyi entropy and approximated OTOC fluctuations. We used the Qiskit package [45] for this simulation.

2.4. CONCLUSION AND DISCUSSION

We have shown aspects of the relation between mana and random sampling of OTOC fluctuations for t-doped circuits which were previously unexplored. In addition to that, we provided numerical evidence that OTOC fluctuation sampling in the scrambled circuits is useful for measuring magic. We were able to mirror behavior for stabilizer Renyi entropy and for mana with significantly lower number measurements. Since the structure of the random circuits is challenging to scale for N qubits, the scalability of this method remains inconclusive, but for up-to 12 qubits we obtained remarkably precise magic estimate with constant number of samples. We also observed that the relation of δ_{OTOC} and magic is not universal, it showed \log_2 behaviour for 2-Renyi entropy and linear behaviour for mana.

Ref. [31] puts forward a statement that the fluctuations of OTOC are always smaller or equal to a specific type of magic monotone. In this work, we complement this statement by numerically showing the relation of OTOC fluctuations to the stabilizer Renyi entropy. We analyzed the accuracy of stabilizer Renyi entropy approximation as a function of the number of samples drawn from scrambled random circuits. While the majority of our simulated data points fulfil the inequality derived in Ref. [31], it is not always the case. This observation is an interesting starting point for further investigation. Also, the analytical relations here could be the starting point for the investigation of the relation between the stabilizer Renyi entropy and the introduced magic measure in Ref. [31].

Additionally, we also extended the method of sampling scrambling random circuits to approximate magic to Hamiltonian evolution and numerically calculated magic for the time evolution governed by an Ising Hamiltonian in a transverse field with very good results in comparison with stabilizer Renyi entropy of the Choi state of the time evolved state of the Hamiltonian. Interestingly the reached agreement is lesser than that of t-doped circuits, but our method still captures general trends of magic behavior during Hamiltonian evolution.

Interesting research direction going forward is to combine our sampling approach with experiment [30] or approximate numerical methods such as tensor networks [32, 46] and neural networks [33]. Our method can be used alongside or as a complement to other existing approximation methods [47–52]. Specifically, the algorithm introduced in [48] is an efficient method for measuring Tsallis stabilizer entropy which has a direct relation to stabilizer Renyi entropy. In Ref. [53] lower number of samples comes with

doubling the dimension of the Hilbert space. The fact the analytical relationship in Eq. (2.7) between δ_{OTOC} and Stabilizer Renyi entropy involves Choi state of a unitary operator might hint at a possible link between these approaches.

All code required to reproduce results presented in this manuscript is available at [54].

2

2.5. ACKNOWLEDGMENTS

We thank Lorenzo Leone for extremely productive peer review process, insightful discussions and the proof of Lemma 1.

2.6. APPENDIX-1: MANA

One of the magic monotones is known as *mana*. The restriction of mana is that it is only well-defined for odd prime-dimensional Hilbert spaces. Here, we introduce it for q -dim Hilbert spaces [10] with q an odd prime number. To show how to calculate mana, we first need to define the clock and shift operators corresponding to the q -dimensional Pauli Z gate and Pauli X gate [38],

$$Z = \sum_{n=0}^{q-1} \omega^n |n\rangle \langle n|, \quad X = \sum_{n=0}^{q-1} |n+1 \bmod q\rangle \langle n|, \quad (2.10)$$

with $\omega = e^{2\pi i/q}$. The other necessary definition is the Heisenberg-Weyl operators in prime dimensions,

$$T_{aa'} = \omega^{-2^{-1}aa'} Z^a X^{a'}, \quad (2.11)$$

where $2^{-1} = \frac{q+1}{2}$ (the multiplicative inverse of 2 mod q) and $(a, a') \in \mathbb{Z}_q \times \mathbb{Z}_q$. By following this definition, we can define Pauli strings as

$$T_{\mathbf{a}} = T_{a_1 a'_1} \otimes T_{a_2 a'_2} \cdots \otimes T_{a_N a'_N}. \quad (2.12)$$

Now, we can define a new basis set for the Hilbert space, known as phase space point operators,

$$A_{\mathbf{b}} = q^{-N} T_{\mathbf{b}} \left(\sum_{\mathbf{a}} T_{\mathbf{a}} \right) T_{\mathbf{b}}^\dagger, \quad (2.13)$$

and these phase space point operators form a complete basis set for $\mathbb{C}^{q^N \otimes q^N}$. Thus, we can expand any density matrix ρ in this basis,

$$\rho = \sum_{\mathbf{u}} W_\rho(\mathbf{u}) A_{\mathbf{u}}, \quad (2.14)$$

The coefficients $W_\rho(\mathbf{u})$ are called discrete Wigner functions and we can define mana as

$$\mathcal{M}(\rho) = \log \sum_{\mathbf{u}} |W_\rho(\mathbf{u})|. \quad (2.15)$$

As we already stated in the main text, we are dealing with Clifford and non-Clifford operations. The Clifford gates map Pauli strings to other Pauli strings, up to an arbitrary phase [55],

$$C = \{U : UT_{\mathbf{a}}U^\dagger = e^{i\phi} T_{\mathbf{b}}\}, \quad (2.16)$$

Since the Clifford gates map each of these Pauli strings to each other, each Clifford unitaries also map the computational basis to one of the eigenstates of Pauli strings. These eigenstates are called stabilizer states. Since stabilizer states are prepared with only Clifford gates, their mana is *zero*.

2.7. APPENDIX-2: CLIFFORD AND NON-CLIFFORD GATES DEFINITIONS

In this appendix, we are introducing the gates that we have used in this study. We introduce both 2-dimensional Hilbert spaces and higher-dimensional Hilbert spaces.

2.7.1. CLIFFORD GATES

The set of Clifford gates is the second level of Clifford hierarchy [9] that are the following gates in 2-dimensional Hilbert spaces,

$$H_2 = \frac{1}{\sqrt{2}} \begin{bmatrix} 1 & 1 \\ 1 & -1 \end{bmatrix}, \quad P_2 = \begin{bmatrix} 1 & 0 \\ 0 & i \end{bmatrix}, \quad (2.17)$$

$$\text{CNOT} = |0\rangle\langle 0| \otimes I + |1\rangle\langle 1| \otimes X.$$

The generalization of these gates is straightforward [56]. The d -dimensional Hadamard gate, H_d , is

$$H_d |j\rangle = \frac{1}{\sqrt{d}} \sum_{i=0}^{d-1} \omega^{ij} |i\rangle \quad j \in \{0, 1, 2, \dots, d-1\}, \quad (2.18)$$

where $\omega := e^{2\pi i/d}$. The next gate is the d -dimensional Phase gate, P_d ,

$$P_d |j\rangle = \omega^{j(j-1)/2} |j\rangle, \quad (2.19)$$

and, finally, the generalized CNOT gate that is known as $CSUM_d$ gate and defined as

$$CSUM_d |i, j\rangle = |i, i + j \pmod{d}\rangle \quad i, j \in \{0, 1, 2, \dots, d-1\}, \quad (2.20)$$

2.7.2. NON-CLIFFORD GATES

Clifford gates are not sufficient for universal quantum computation and we at least need one non-Clifford gate to have this universality [57, 58]. One of these gates is the T-gate that emerges from the third level Clifford hierarchy. The definition of T-gate for 2-dimensional Hilbert space is

$$T_2 = \begin{bmatrix} 1 & 0 \\ 0 & e^{i\pi/4} \end{bmatrix}. \quad (2.21)$$

The generalization of T-gate to higher dimensional Hilbert spaces is not so straightforward [38]. Here, we only write down the matrices of the T-gate for 3-dimensional Hilbert spaces which are useful for us. The 3-dimensional Hilbert space T-gate is

$$T_3 = \begin{bmatrix} 1 & 0 & 0 \\ 0 & e^{2\pi i/9} & 0 \\ 0 & 0 & e^{-2\pi i/9} \end{bmatrix}. \quad (2.22)$$

2.8. APPENDIX-3: PROOF OF LEMMA 1

In order to show lemma 1, we need to have a close look at the first term in δ_{OTOC} ,

$$\mathbb{E}_C \text{OTOC}^2(V) = \int dC_1 dC_2 \frac{1}{d^2} \text{tr} \left(T_{(12)(34)} V^{\dagger \otimes 4} C_1^{\dagger \otimes 4} A^{\otimes 4} C_1^{\otimes 4} V^{\otimes 4} C_2^{\otimes 4} B^{\otimes 4} C_2^{\dagger \otimes 4} \right) \quad (2.23)$$

By averaging over C_1 we will have [42, 59]

$$\int dC_1 C_1^{\dagger \otimes 4} A^{\otimes 4} C_1^{\otimes 4} = \frac{1}{d^2 - 1} \sum_{P \in \mathbb{P}_n \setminus \{\mathbb{I}\}} P^{\otimes 4}, \quad (2.24)$$

By averaging over Clifford circuits we will get a flat distribution over the Pauli group \mathbb{P}_n but the identity. By defining $Q := d^{-2} \sum_{P \in \mathbb{P}_n} P^{\otimes 4}$, the Eq. 2.24 becomes

$$\int dC_1 C_1^{\dagger \otimes 4} A^{\otimes 4} C_1^{\otimes 4} = \frac{d^2}{d^2 - 1} Q - \frac{1}{d^2 - 1} \mathbb{I}^{\otimes 4}, \quad (2.25)$$

we get similar results for averaging over C_2 on the non-identity Pauli operator B . So Eq. 2.23 would become

$$\mathbb{E}_C \text{OTOC}^2(V) = \frac{1}{d^2} \left(\frac{d^2}{d^2 - 1} \right)^2 \text{tr}(QV^{\otimes 4} QV^{\dagger \otimes 4}) - \frac{2d^2 - 1}{(d^2 - 1)^2}, \quad (2.26)$$

where we used the fact that $\text{tr}(\mathcal{O}QT_{(12)(34)}) = \text{tr}(\mathcal{O}Q)$ for every \mathcal{O} [42]. From Ref. [25] we know that the average $\mathbb{E}_C \text{OTOC}(U) = -(d^2 - 1)^{-1}$. So the final equation would be

$$\mathbb{E}_C \delta_{\text{OTOC}}(V) = \left(\frac{d^2}{d^2 - 1} \right)^2 2^{-M_2(|V\rangle)} - \frac{2d^2}{(d^2 - 1)^2}, \quad (2.27)$$

we know that from Ref. [59] the second stabilizer Renyi entropy of the Choi state of the unitary V is

$$M_2(|V\rangle) = -\log \frac{1}{d^2} \text{tr}(QV^{\otimes 4} QV^{\dagger \otimes 4}), \quad (2.28)$$

We see that from Eq. 2.7 the second stabilizer Renyi entropy is related to the Choi state $|V\rangle$ associated with the unitary V and not the second stabilizer Renyi entropy of the state $V|0\rangle$. Fortunately, in the case of V being a random t-doped circuit, C_t , from Ref. [59] we have

$$\begin{aligned} \mathbb{E}_{C_t} \delta_{\text{OTOC}}(C_t) &= \frac{d^4}{(d^2 - 1)^2} \left[\frac{4(6 - 9d^2 + d^4)}{d^4(d^2 - 9)} + \frac{d^2 - 1}{d^2} \left(\frac{(d+2)(d+4)f_+^t}{6d(d+3)} \right. \right. \\ &\quad \left. \left. + \frac{(d-2)(d-4)f_-^t}{6d(d-3)} + 2 \frac{(d^2 - 4)(\frac{f_+ + f_-}{2})^t}{3d^2} \right) \right] - 2 \frac{d^2}{(d^2 - 1)^2}, \end{aligned} \quad (2.29)$$

where

$$f_{\pm} = \frac{3d^2 \mp 3d - 4}{5(d^2 - 1)}, \quad (2.30)$$

for d being large we have

$$\mathbb{E}_{C_t} \delta_{\text{OTOC}}(C_t) = \left(\frac{3}{4} \right)^t + O(d^{-2}). \quad (2.31)$$

In Ref. [19], the average value of 2-stabilizer entropy over a t-doped Clifford circuit is given as

$$-\log \left(\frac{4 + (d-1)f_+^t}{3+d} \right) \leq \mathbb{E}_{C_t} M_2(C_t | 0\rangle) \leq \begin{cases} t, & t < N-1 \\ N-1, & t \geq N-1 \end{cases}. \quad (2.32)$$

From Eq. 2.29 and Eq. 2.32, it is straightforward to show that for a random t -doped Clifford circuit,

$$\mathbb{E}_{C_t} 2^{-M_2(C_t)} = \mathbb{E}_{C_t} 2^{-M_2(C_t|0)} + O(d^{-1}). \quad (2.33)$$

2

2.9. APPENDIX-4: PROPAGATION OF ERROR

Let us analyze how errors propagate in Eq.2.7. We can write the error in M_2 in terms of δ_{OTOC} as

$$\Delta M_2 = \frac{\partial M_2}{\partial \delta_{OTOC}} \Delta(\delta_{OTOC}). \quad (2.34)$$

At the same time, we can rewrite Eq.2.7 as

$$M_2 = -\log_2 \frac{\mathbb{E} \delta_{OTOC} + \beta}{\alpha}. \quad (2.35)$$

This formula allows us to evaluate the derivative on the right-hand side of (2.34) as

$$\frac{\partial M_2}{\partial \delta_{OTOC}} = -\frac{1}{(\mathbb{E} \delta_{OTOC} + \beta) \ln 2}. \quad (2.36)$$

Combining (2.34) and (2.36) we obtain

$$\Delta M_2 = -\frac{1}{(\mathbb{E} \delta_{OTOC} + \beta) \ln 2} \Delta(\delta_{OTOC}). \quad (2.37)$$

Error in M_2 is thus proportional to the error in δ_{OTOC} with an inverse factor of the expectation value of δ_{OTOC} .

BIBLIOGRAPHY

1. Shor, P. W. Polynomial-Time Algorithms for Prime Factorization and Discrete Logarithms on a Quantum Computer. *SIAM Review* **41**, 303–332. <https://doi.org/10.1137/S0036144598347011> (1999).
2. Grover, L. K. *A Fast Quantum Mechanical Algorithm for Database Search* in *Proceedings of the Twenty-Eighth Annual ACM Symposium on Theory of Computing* (Association for Computing Machinery, Philadelphia, Pennsylvania, USA, 1996), 212–219. ISBN: 0897917855. <https://doi-org.tudelft.idm.oclc.org/10.1145/237814.237866>.
3. Aaronson, S. & Arkhipov, A. The Computational Complexity of Linear Optics. *Theory of Computing* **9**, 143–252. <http://www.theoryofcomputing.org/articles/v009a004> (2013).
4. Cao, Y. *et al.* Quantum Chemistry in the Age of Quantum Computing. *Chemical Reviews* **119**. PMID: 31469277, 10856–10915. eprint: <https://doi.org/10.1021/acs.chemrev.8b00803>. <https://doi.org/10.1021/acs.chemrev.8b00803> (2019).
5. Kandala, A. *et al.* Hardware-efficient variational quantum eigensolver for small molecules and quantum magnets. *Nature* **549**, 242–246. ISSN: 1476-4687. <http://dx.doi.org/10.1038/nature23879> (Sept. 2017).
6. Farhi, E., Goldstone, J. & Gutmann, S. A Quantum Approximate Optimization Algorithm. arXiv: [1411.4028 \[quant-ph\]](https://arxiv.org/abs/1411.4028). <https://doi.org/10.48550/arXiv.1411.4028> (2014).
7. Bravyi, S. & Kitaev, A. Universal quantum computation with ideal Clifford gates and noisy ancillas. *Phys. Rev. A* **71**, 022316. <https://link.aps.org/doi/10.1103/PhysRevA.71.022316> (2 Feb. 2005).
8. Gottesman, D. The Heisenberg representation of quantum computers. *arXiv preprint quant-ph/9807006*. <https://www.osti.gov/biblio/319738> (June 1998).
9. Gottesman, D. & Chuang, I. L. Demonstrating the viability of universal quantum computation using teleportation and single-qubit operations. *Nature* **402**, 390–393 (1999).
10. Veitch, V., Mousavian, S. A. H., Gottesman, D. & Emerson, J. The resource theory of stabilizer quantum computation. *New Journal of Physics* **16**, 013009 (2014).
11. Gottesman, D. Theory of fault-tolerant quantum computation. *Physical Review A* **57**, 127–137. <https://doi.org/10.1103/PhysRevA.57.127> (Jan. 1998).
12. Shor, P. W. Fault-tolerant quantum computation. *arXiv:quant-ph/9605011*. <https://doi.org/10.48550/arXiv.quant-ph/9605011> (1997).

13. Gottesman, D. Stabilizer Codes and Quantum Error Correction. *arXiv:quant-ph/9705052*. <https://doi.org/10.48550/arXiv.quant-ph/9705052> (1997).
14. Beverland, M., Campbell, E., Howard, M. & Kliuchnikov, V. Lower bounds on the non-Clifford resources for quantum computations. *Quantum Science and Technology* **5**, 035009. <https://dx.doi.org/10.1088/2058-9565/ab8963> (May 2020).
15. Howard, M. & Campbell, E. Application of a Resource Theory for Magic States to Fault-Tolerant Quantum Computing. *Physical Review Letters* **118**. <https://doi.org/10.1103/PhysRevLett.118.090501> (Mar. 2017).
16. Campbell, E. T. & O’Gorman, J. An efficient magic state approach to small angle rotations. *Quantum Science and Technology* **1**, 015007 (Dec. 2016).
17. Campbell, E. T. Catalysis and activation of magic states in fault-tolerant architectures. *Physical Review A* **83** (Mar. 2011).
18. Hahn, O., Ferraro, A., Hultquist, L., Ferrini, G. & Garca-lvarez, L. Quantifying Qubit Magic Resource with Gottesman-Kitaev-Preskill Encoding. *Physical Review Letters* **128** (May 2022).
19. Leone, L., Oliviero, S. F. & Hama, A. Stabilizer Renyi Entropy. *Physical Review Letters* **128**. <https://doi.org/10.1103/PhysRevLett.128.050402> (Feb. 2022).
20. Hayden, P. & Preskill, J. Black holes as mirrors: quantum information in random subsystems. *Journal of High Energy Physics* **2007**, 120–120. ISSN: 1029-8479. <http://dx.doi.org/10.1088/1126-6708/2007/09/120> (Sept. 2007).
21. Sekino, Y. & Susskind, L. Fast scramblers. *Journal of High Energy Physics* **2008**, 065–065. <https://doi.org/10.1088/1126-6708/2008/10/065> (Oct. 2008).
22. Shenker, S. H. & Stanford, D. Black holes and the butterfly effect. en. *Journal of High Energy Physics* **2014**, 67. ISSN: 1029-8479. (2021) (Mar. 2014).
23. Maldacena, J., Shenker, S. H. & Stanford, D. A bound on chaos. *Journal of High Energy Physics* **2016**. ISSN: 1029-8479. [http://dx.doi.org/10.1007/JHEP08\(2016\)106](http://dx.doi.org/10.1007/JHEP08(2016)106) (Aug. 2016).
24. Hosur, P., Qi, X.-L., Roberts, D. A. & Yoshida, B. Chaos in quantum channels. *Journal of High Energy Physics* **2016**. ISSN: 1029-8479. [http://dx.doi.org/10.1007/JHEP02\(2016\)004](http://dx.doi.org/10.1007/JHEP02(2016)004) (Feb. 2016).
25. Roberts, D. A. & Yoshida, B. Chaos and complexity by design. *Journal of High Energy Physics* **2017**. [https://doi.org/10.1007/JHEP04\(2017\)29121](https://doi.org/10.1007/JHEP04(2017)29121) (Apr. 2017).
26. Zhang, Y. Information Scrambling in Quantum Many-Body Systems. *Dissertation (Ph.D.)* <https://resolver.caltech.edu/CaltechTHESIS:02262020-182938837> (Feb. 2020).
27. Almheiri, A., Dong, X. & Harlow, D. Bulk locality and quantum error correction in AdS/CFT. *Journal of High Energy Physics* **2015** (2015).

28. Basko, D., Aleiner, I. & Altshuler, B. Metal–insulator transition in a weakly interacting many-electron system with localized single-particle states. *Annals of Physics* **321**, 1126–1205. ISSN: 0003-4916. <http://dx.doi.org/10.1016/j.aop.2005.11.014> (May 2006).
29. Ben-Zion, D. & McGreevy, J. Strange metal from local quantum chaos. *Physical Review B* **97**. ISSN: 2469-9969. <http://dx.doi.org/10.1103/PhysRevB.97.155117> (Apr. 2018).
30. Mi, X. *et al.* Information scrambling in quantum circuits. *Science* **374**, 1479–1483. ISSN: 1095-9203. <http://dx.doi.org/10.1126/science.abg5029> (Dec. 2021).
31. Garcia, R. J., Bu, K. & Jaffe, A. Resource theory of quantum scrambling. *Proceedings of the National Academy of Sciences* **120**, e2217031120. eprint: <https://www.pnas.org/doi/pdf/10.1073/pnas.2217031120>. <https://www.pnas.org/doi/abs/10.1073/pnas.2217031120> (2023).
32. Xu, S. & Swingle, B. Scrambling Dynamics and Out-of-Time Ordered Correlators in Quantum Many-Body Systems: a Tutorial. *arXiv:2202.07060*. <https://arxiv.org/abs/2202.07060> (2022).
33. Wu, Y., Duan, L.-M. & Deng, D.-L. Artificial neural network based computation for out-of-time-ordered correlators. *Physical Review B* **101** (June 2020).
34. Chitambar, E. & Gour, G. Quantum resource theories. *Reviews of Modern Physics* **91**. ISSN: 1539-0756. <http://dx.doi.org/10.1103/RevModPhys.91.025001> (Apr. 2019).
35. Chen, X., Nandkishore, R. M. & Lucas, A. Quantum butterfly effect in polarized Floquet systems. *Physical Review B* **101**. <https://doi.org/10.1103/PhysRevB.101.064307> (Feb. 2020).
36. Qi, X.-L. & Streicher, A. Quantum epidemiology: operator growth, thermal effects, and SYK. *Journal of High Energy Physics* **2019**. [https://doi.org/10.1007/JHEP08\(2019\)29012](https://doi.org/10.1007/JHEP08(2019)29012) (Aug. 2019).
37. Parker, D. E., Cao, X., Avdoshkin, A., Scaffidi, T. & Altman, E. A Universal Operator Growth Hypothesis. *Physical Review X* **9**. <https://doi.org/10.1103/PhysRevX.9.041017> (Oct. 2019).
38. Wang, Y., Hu, Z., Sanders, B. C. & Kais, S. Qudits and High-Dimensional Quantum Computing. *Frontiers in Physics* **8** (2020).
39. Developers, C. *Cirq* version v0.12.0. See full list of authors on Github: <https://github.com/quantumlib/Cirq/graphs/contributors>. Aug. 2021. <https://doi.org/10.5281/zenodo.5182845>.
40. Mari, A. & Eisert, J. Positive Wigner Functions Render Classical Simulation of Quantum Computation Efficient. *Phys. Rev. Lett.* **109**, 230503. <https://link.aps.org/doi/10.1103/PhysRevLett.109.230503> (23 Dec. 2012).
41. Schmid, D., Du, H., Selby, J. H. & Pusey, M. F. Uniqueness of Noncontextual Models for Stabilizer Subtheories. *Physical Review Letters* **129**. <https://doi.org/10.1103/PhysRevLett.129.120403> (Sept. 2022).

42. Leone, L., Oliviero, S. F. E., Zhou, Y. & Hamma, A. Quantum Chaos is Quantum. *Quantum* **5**, 453. ISSN: 2521-327X. <https://doi.org/10.22331/q-2021-05-04-453> (May 2021).
43. Choi, M.-D. Completely positive linear maps on complex matrices. *Linear Algebra and its Applications* **10**, 285–290. ISSN: 0024-3795. <https://www.sciencedirect.com/science/article/pii/0024379575900750> (1975).
44. Leone, L., Oliviero, S. F. E., Piemontese, S., True, S. & Hamma, A. Retrieving information from a black hole using quantum machine learning. *Physical Review A* **106**. <https://doi.org/10.1103/PhysRevA.106.062434> (Dec. 2022).
45. ANIS, M. S. *et al.* *Qiskit: An Open-source Framework for Quantum Computing* 2021.
46. Haug, T. & Piroli, L. Quantifying nonstabilizerness of matrix product states. *Physical Review B* **107** (Jan. 2023).
47. Haug, T. & Kim, M. Scalable Measures of Magic Resource for Quantum Computers. *PRX Quantum* **4**. <https://doi.org/10.1103/PRXQuantum.4.010301> (Jan. 2023).
48. Haug, T., Lee, S. & Kim, M. S. Efficient stabilizer entropies for quantum computers. *arXiv:2305.19152*. <https://doi.org/10.48550/arXiv.2305.19152> (2023).
49. Tarabunga, P. S., Tirrito, E., Chanda, T. & Dalmonte, M. Many-Body Magic Via Pauli-Markov Chains—From Criticality to Gauge Theories. *PRX Quantum* **4**, 040317. <https://link.aps.org/doi/10.1103/PRXQuantum.4.040317> (4 Oct. 2023).
50. Tirrito, E. *et al.* *Quantifying non-stabilizerness through entanglement spectrum flatness* 2023. <https://doi.org/10.48550/arXiv.2304.01175>.
51. Turkeshi, X., Schirò, M. & Sierant, P. Measuring nonstabilizerness via multifractal flatness. *Physical Review A* **108**. ISSN: 2469-9934. <http://dx.doi.org/10.1103/PhysRevA.108.042408> (Oct. 2023).
52. Lami, G. & Collura, M. Nonstabilizerness via Perfect Pauli Sampling of Matrix Product States. *Phys. Rev. Lett.* **131**, 180401. <https://link.aps.org/doi/10.1103/PhysRevLett.131.180401> (18 Oct. 2023).
53. Odavić, J. *et al.* Complexity of frustration: A new source of non-local non-stabilizerness. *SciPost Phys.* **15**, 131. <https://scipost.org/10.21468/SciPostPhys.15.4.131> (2023).
54. Ahmadi, A. & Greplova, E. *Magic Info Scrambling* <https://gitlab.com/QMAI/papers/magicinfoscrambling>.
55. White, C. D., Cao, C. & Swingle, B. Conformal field theories are magical. *Physical Review B* **103** (2021).
56. Gottesman, D. Fault-Tolerant Quantum Computation with Higher-Dimensional Systems. *Chaos, Solitons & Fractals* **10**, 1749–1758. ISSN: 0960-0779. [http://dx.doi.org/10.1016/S0960-0779\(98\)00218-5](http://dx.doi.org/10.1016/S0960-0779(98)00218-5) (Sept. 1999).
57. Barenco, A. *et al.* Elementary gates for quantum computation. *Physical Review A* **52**, 3457–3467. <https://doi.org/10.1103/PhysRevA.52.3457> (Nov. 1995).

58. Boykin, P, Mor, T., Pulver, M., Roychowdhury, V. & Vatan, F A new universal and fault-tolerant quantum basis. *Information Processing Letters* **75**, 101–107. ISSN: 0020-0190. <https://www.sciencedirect.com/science/article/pii/S0020019000000843> (2000).
59. Leone, L., Oliviero, S. F. E. & Hamma, A. Nonstabilizerness determining the hardness of direct fidelity estimation. *Phys. Rev. A* **107**, 022429. <https://link.aps.org/doi/10.1103/PhysRevA.107.022429> (2 Feb. 2023).

3

MUTUAL INFORMATION FLUCTUATIONS AND NON-STABILIZERNESS IN RANDOM CIRCUITS

The emergence of quantum technologies has brought much attention to the characterization of quantum resources as well as the classical simulatability of quantum processes. Quantum resources, as quantified by non-stabilizeress, have in one theoretical approach been linked to a family of entropic, monotonic functions. In this work, we demonstrate both analytically and numerically a simple relationship between non-stabilizeress and information scrambling using the fluctuations of an entropy-based quantifier. Specifically, we find that the non-stabilizeress generated by a random quantum circuit is proportional to fluctuations of mutual information. Furthermore, we explore the role of non-stabilizeress in measurement-induced entanglement phase transitions. We find that the fluctuations of mutual information decrease with increasing non-stabilizeress yielding potentially easier identification of the transition point. Our work establishes a key connection between quantum resource theory, information scrambling and measurement-induced entanglement phase transitions.

⁰The work in this chapter is currently under peer review and is available at: **A. Ahmadi**, J. Helsen, C. Karaca, E. Greplova, Mutual information fluctuations and non-stabilizeress in random circuits, *arXiv:2408.03831*

3.1. INTRODUCTION

Since the formulation of quantum theory, entanglement has been known to be one of the unique signatures of quantum theory [1]. While entanglement is one of the key features of distinguishing the quantum world from the classical, it is known that entanglement alone is insufficient for having an advantage from the *computational* point of view. In particular, the stabilizer states are a set of states that can be highly entangled and at the same time can be simulated efficiently on classical computers [2–7].

The missing feature for quantum computation to have an advantage over classical computation is a concept known as non-stabilizerlessness or *magic* [8]. In quantum circuit language, in the fault-tolerant regime, the gates that are known to be "cheap" gates [8] are Clifford gates, and magic is injected into the state by adding non-Clifford gates to the circuit. It is also known that the Clifford operations could have easier implementation both at the experimental level and for quantum error correction [2, 4, 9, 10]. This feature makes magic the resource for quantum computation.

Various measures for non-stabilizerlessness, or magic, have been proposed. Some of the notable ones are magical cross-entropy, mana [8], robustness of magic [11, 12], stabilizer entropies (SE) [13] and others [14–18]. Due to the favourable scaling of the stabilizer entropies these measures received much attention from the community to study the properties of non-stabilizerlessness of quantum systems [19–25]. Additionally, there has been a significant effort to scale up the computability of stabilizer entropies [26–30].

Diverse studies confirmed there exists a relationship between non-stabilizerlessness and information scrambling [13, 16, 31]. Information scrambling describes the spread of local information in a generic quantum system [32]. Information scrambling has been shown to be one of the most powerful measures for various quantum properties of quantum systems, from black holes [33–36] to many-body quantum systems [37] to quantum circuits [31, 38]. There are a number of known methods for measuring information scrambling. One of the well-known approaches is based on the measurement of correlator functions, namely Out-of-Time Ordered Correlators (OTOCs) [33, 36, 38–41]. Another approach for studying information scrambling are entropy-based measures [32, 42–48].

In this paper, we describe numerically and analytically a general relationship between non-stabilizerlessness and *fluctuations* of entropy-based measures of information scrambling. A specific instance of this relation has been observed earlier by connecting fluctuations of OTOCs to non-stabilizerlessness [13, 31]. In the present work, we generalize this behaviour to fluctuations of generic mutual information measures of disjoint regions of the quantum circuit on t-doped circuits. The observed link between non-stabilizerlessness and mutual information creates a bridge to the theory of phase transitions in measurement-induced random quantum circuits, where mutual information plays a crucial role [49–81]. Here we show that non-stabilizerlessness is an ingredient in reducing the spread of entanglement phase transition in random quantum circuits and also reduces the fluctuations of the measured mutual information.

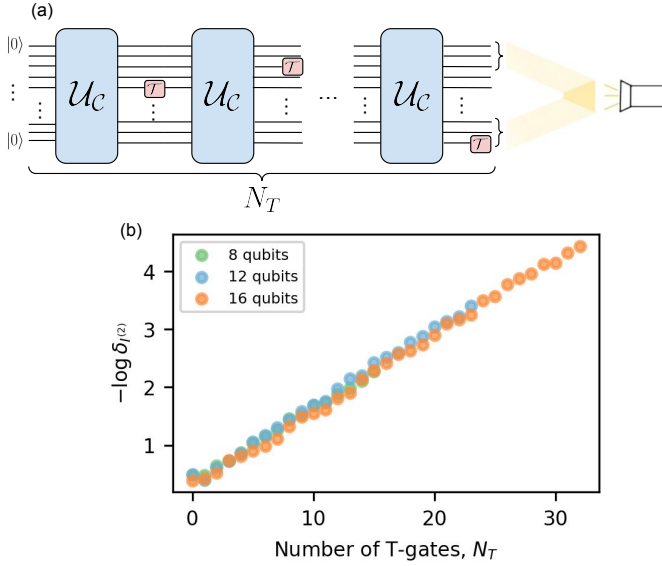


Figure 3.1: (a) The schematic structure of the t-doped Clifford circuits and the disjoint area of measuring scrambling. (b) The log of fluctuations of the mutual information, $-\ln \delta_{I^{(2)}}$ as a function of the number of T-gates, N_T , on the circuit for the number of qubits, $N = 8, 12, 16$ and the number of samples is 500.

3.2. RANDOM CIRCUITS AND MUTUAL INFORMATION

3.2.1. DEFINITIONS AND NOTATION

The structure of the T-doped circuits that we use in this study consists of blocks of random Clifford operations followed by single T-gates on random qubits in the circuit. The blocks of random Clifford consist of single Clifford gates drawn randomly from the set $\{I, X, Y, Z, H, S\}$ followed by three CNOT gates on two random qubits. We apply both single and double Clifford gates until the state gets fully scrambled (in our case after $2N$ operations, where N is the number of qubits in the system). Each Clifford block (of depth $2N$) is followed by a T-gate performed on a randomly selected qubit. This Clifford block plus T-gate sequence is then repeated N_T times. The structure of the circuit is shown in Fig. 3.1 (a).

A popular entropy-based measure for quantifying scrambling is mutual information [42] of disjoint areas A and B which is defined as

$$I^{(2)} := S_A^{(2)} + S_B^{(2)} - S_{AB}^{(2)}, \quad (3.1)$$

where $S_X^{(2)}$ is the Renyi-2 entropy defined as $S_X^{(2)} \equiv -\log_2 \text{Tr} \rho_X^2$ for the subsystem X and ρ_X is the reduced density matrix of subsystem X . We chose the subsystems A and B such that they have $N_A = N_B = N/4$ of the first and last qubits as shown in Fig. 3.1 (a).

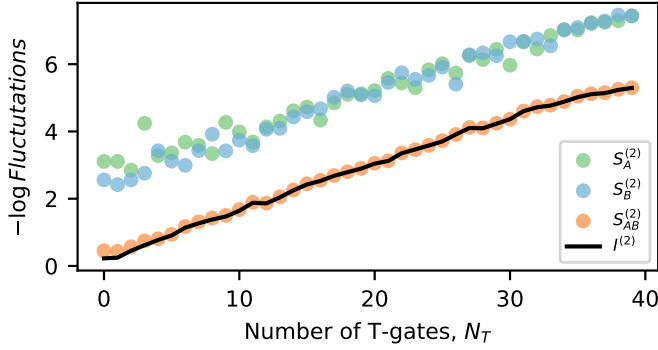


Figure 3.2: The comparison of the $-\ln \text{fluctuations}$ of all terms in the mutual information definition, $S_A^{(2)}$, $S_B^{(2)}$, $S_{AB}^{(2)}$, and the mutual information as a function of the number of T-gates, N_T for a 16-qubit system.

3.2.2. RELATION OF MUTUAL INFORMATION FLUCTUATIONS AND MAGIC

By measuring a sample of different instances of $I^{(2)}$ for a fixed number of T-gates, we observed a trend in the fluctuations, i.e. the standard deviation, of these instances

$$\delta_{I^{(2)}} = (\mathbb{E}[(I^{(2)})^2] - \mathbb{E}[I^{(2)}]^2)^{1/2},$$

as a function of the number of T-gates, N_T , in the random circuit. We observe a linear relationship between the number of T-gates in the circuit and $-\ln \delta_{I^{(2)}}$ as shown in Fig. 3.1 (b). We have a circuit of $N = 8, 12, 16$ qubits and the number of T-gates in each circuit is $N_T \in \{0, \dots, 2N\}$ which is where magic increases linearly with the number of qubits [31, 82]. We fit this linear behavior and obtain $-\ln \delta_{I^{(2)}} \approx 0.13N_T + 0.32$ dependency. Interestingly, this behaviour is similar to that previously observed for the fluctuations of out-of-time-order correlations [31].

In order to interpret the results in Fig. 3.1 (b), we analyze Eq. 3.1 term by term and assess the contribution of these terms to the observed fluctuation behaviour. Eq. 3.1 have three terms of entanglement Renyi-2 entropy, where subsystems A and B have the size of $N/4$ and subsystem AB has the size of $N/2$. By evaluating the fluctuations of $S_A^{(2)}$, $S_B^{(2)}$ and $S_{AB}^{(2)}$ alongside the total fluctuations of the mutual information, we find that the fluctuations of $S_{AB}^{(2)}$ are the leading term in behaviour of fluctuations of mutual information, $\delta_{I^{(2)}}$. This result is shown in Fig. 3.2.

Specifically, in Fig. 3.2, we show all contributions to the fluctuations of the mutual information for a 16-qubit system and observe the fluctuation of the mutual information overlaps with the fluctuations of the entanglement Renyi-2 entropy of the subsystem AB .

We also explored the effect of measuring the total spin of the subsystems A and B and their statistical relation to non-stabilizeress in Appendix 3.8.

3.2.3. ANALYTICAL RELATION OF N_T AND $\ln(\delta_{I^{(2)}})$

Due to the non-linear nature of the entropy, it is difficult to analytically recover the behaviour seen in Fig. 3.1. However if one instead averages *inside* the logarithm exact calculation becomes tractable (this can be thought of as the first step towards a replica-trick

calculation, which we will not attempt here) and we can explain the key features of the relation between magic and entropic fluctuations. Accordingly, we define the quantities

$$\begin{aligned}\tilde{S}_{AB}^{(2)} &:= -\log_2(\mathbb{E}[\text{Tr}(\rho_{AB}^2)]), \\ \tilde{\delta} &:= (-\log_2(\mathbb{E}[\text{Tr}(\rho_{AB}^2)]^2) - (\tilde{S}_{AB}^{(2)})^2),\end{aligned}$$

where the average is taken over the circuit set described in Fig. 3.1. A simple calculation shows that $\tilde{S}_{AB}^{(2)}$ is independent of N_T . On the other hand $\tilde{\delta}$ shows a clear linear dependence. Suppressing various subleading contributions, we can prove the following relation:

$$-\ln(\tilde{\delta}) \approx N_T \ln(1/\lambda) \quad (3.2)$$

for $\lambda = 3/4$ and thus $\ln(1/\lambda) \approx 0.28$. This captures the linear behaviour seen in Fig. 3.1 but does not give the correct rate. We expect that the correct rate can only be obtained through a full replica calculation, similar to the behaviour of the velocity of entanglement observed in [83]. The proof of Eq. (3.2) requires calculating the fourth moments of the Clifford group and is rather involved. We defer it to Appendix 3.9. It must be noted that although establishing this result requires calculating a fourth moment of the Clifford group, it does not hold for any quartic invariant of the Clifford group. In Appendix 3.9, both analytics and numerics of quartic and octic invariants support our statement.

3.3. EFFECT OF MAGIC ON MEASUREMENT-INDUCED PHASE TRANSITION

In recent years, there have been diverse and rich studies on the entanglement phase transition in random quantum circuits [49–81]. Interestingly, the detection of these phase transitions typically relies on the study of the behaviour of the mutual information in the random quantum circuit [81, 84]. These studies mainly focused on two types of circuits. One type is the Clifford circuits, because of their scalability which is guaranteed by Gottesman-Knill theorem [5, 7] so they are widely used to study the phase transition more accurately [49, 50, 54, 65, 68, 70, 71, 74]. The second case is the Haar random circuits that are being used because of their universality in randomness. The possible drawback of using the Haar structures is that they are difficult to scale up and usually have been studied for small-scale systems of qubits [51, 52, 66, 67, 84]. In this section, we study specifically the effect of magic in entanglement phase transition. Specifically, the two research directions mentioned above either avoid non-stabilizer resources altogether or use Haar randomness. Here, we analyze magic injected into the entanglement phase transition circuits in a controlled way and study its effect through the lens of fluctuations analysis developed in Sec. 3.2.2.

It is important to mention that, in parallel, there are ongoing studies in phase transitions in magic as well [85–90]. However the purpose of this section is to show the effect of magic solely on the entanglement phase transition identified by the mutual information.

The circuit structure for measurement-induced phase transition we use here inspired by Ref. [49, 50, 54, 65, 68, 70, 74] consists of two-qubit blocks of random Clifford gates on the neighbouring qubits. The block of random Clifford gates is generated using the canonical form for uniformly randomly distributed 2-Clifford gate described in [91]. Here,

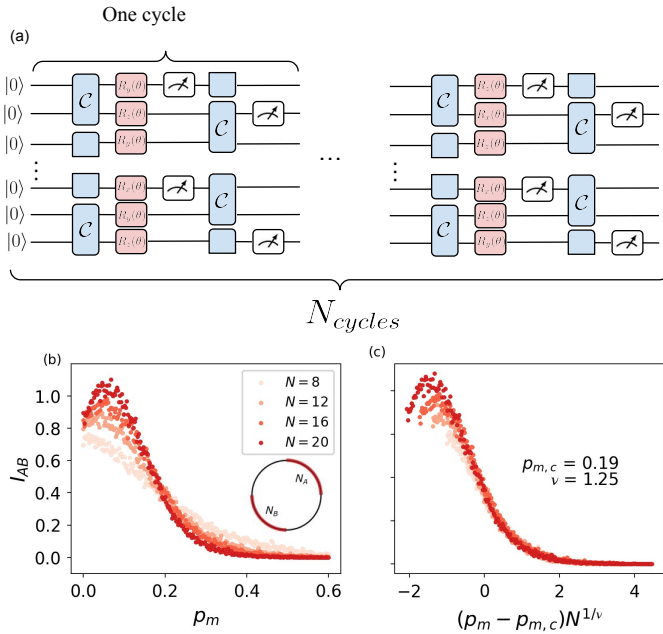


Figure 3.3: (a) The schematic structure of measurement-induced phase transition. The blue block shows the random two-qubit Clifford gate and the red single-qubit gates are random rotation gates followed by a projective measurement with probability p_m . The whole circuit consists of repeating each cycle N_{cycle} times. (b) The mutual information of two disjoint partitions of the system, namely the first and third quarters ($N_B = N_B = N/4$), averaged over 800 instances and $N_{cycle} = 125$ for different system sizes and the rotation angle, $\theta = 0$. (c) The finite size scaling of the mutual information for the critical parameters $p_{m,c} = 0.19$ and $\nu = 1.25$.

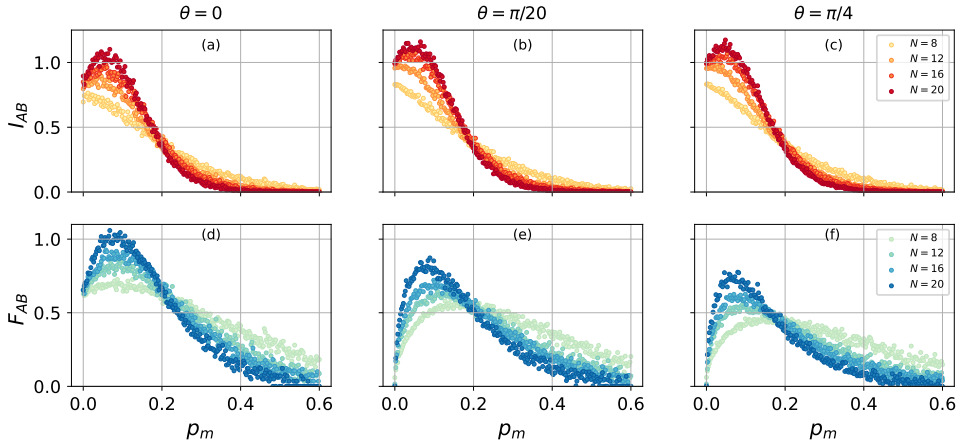


Figure 3.4: The upper panels correspond to averaged mutual information for different numbers of qubits as a function of measurement rate, p_m for different levels of non-stabilizerness in the circuit, and the lower panels correspond to the fluctuations of the mutual information for the same system. The number of instances for averaging and fluctuations is 800 shots. (a) The mutual information of measurement-induced circuit where the angle of rotation, θ , in the rotation gates, is zero and the circuit is Clifford as a function of measurement rate, p_m . (b) The mutual information of the measurement-induced circuit where the angle of rotation, θ , is $\pi/20$ and magic is at an intermediate level, as a function of measurement rate, p_m . (c) The mutual information of the measurement-induced circuit where the angle of rotation, θ , is $\pi/4$ and magic is maximum per rotation gate, as a function of measurement rate, p_m . (d) The fluctuations of the mutual information for Clifford gates, as a function of measurement rate, p_m . (e) The fluctuations of mutual information where the angle of rotation, θ is $\pi/20$ as a function of measurement rate, p_m . (f) The fluctuations of mutual information where the angle of rotation, θ is $\pi/4$ as a function of measurement rate, p_m .

in order to inject magic in a controlled way, we follow the two-qubit random Clifford gates by a randomly chosen rotation gate from the set of $\{R_x(\theta), R_y(\theta), R_z(\theta)\}$. Afterwards, we induce the projective measurement on each qubit with probability p_m in the z-basis. This process is followed by another set of random Cliffords this time on the odd pairs of qubits. Here, we introduce a periodic boundary condition by connecting the first and the last qubit. After performing Cliffords on odd pairs of qubit, we again follow by projective measurement (again with probability p_m). This process forms one cycle of the circuit, as the schematic structure of the circuit is shown in Fig. 3.3 (a) and is repeated N_{cycles} times.

In this random circuit set-up, we know that in the absence of measurements, $p_m = 0$, the entanglement obeys volume-law scaling $S^{(2)} \propto N_s$, and persists up to a critical measurement rate $p_{m,c}$. It is known that above the criticality measurement rate, the entanglement entropy follows a scaling known as area law scaling $S^{(2)} \propto \ln \xi$, where $\xi \sim |p_m - p_{m,c}|^{-\nu}$ shows a divergence in the correlation length at criticality [50]. As illustrated in previous studies, the entanglement data for different system sizes collapse on a single curve with the scaling form of $|S^{(2)}(p_m) - S^{(2)}(p_{m,c})| = F_S[(p_m - p_{m,c})N^{1/\nu}]$ [50]. It is also shown that for the same critical measurement rate, $p_{m,c}$ and critical exponent ν , similar finite-size scaling relation can be seen from mutual information $I_{AB} = F_I[(p_m - p_{m,c})N^{1/\nu}]$ near criticality [84]. Assuming the collapse of mutual information data for different system sizes on a single curve with the standard scaling form $I_{AB} = F_I[(p_m - p_{m,c})N^{1/\nu}]$ for granted, allows us to extract the critical measurement, $p_{m,c}$, rate and critical exponent, ν .

We use the mutual information as defined in Eq. 3.1 to identify the entanglement phase transition from area law entanglement to volume law entanglement [84]. The partitions that we consider for mutual information are the first and third quarters of the whole system. First, we confirm that there is an entanglement phase transition present at all by checking the Clifford case with zero injected magic, i.e. $\theta = 0$, for system sizes $N = \{8, 12, 16, 20\}$. We average the measured mutual information over 800 instances and use the circuit depth of $N_{cycles} = 125$. Due to the small system size, we need to employ finite-size scaling to estimate the critical exponent, ν , and the critical measurement rate, $p_{m,c}$. For this range of system sizes after finite-size scaling, we find that the critical measurement rate, $p_{m,c} = 0.19$ and the critical exponent, $\nu = 1.25$ (see also Fig. 3.3 (b) and (c)). For extracting these values, we expanded the function $F_I(p_m, N) \approx ax^2 + bx + c$ where $x = (p_m - p_{m,c})N^{1/\nu}$. We can extract $p_{m,c}$ and ν using the least-square optimization method on the data of the mutual information. In other words $p_{m,c}, \nu = \text{argmin}(a, b, c) \sum_{I_{AB}} (ax^2 + bx + c - I_{AB})^2$.

The next step is to inject magic into the system. By increasing the rotation angle to $\theta = \pi/4$, we inject magic into the system. We set the number of cycles and non-Clifford gates to $N_{cycle} = 125$ to ensure we gradually saturate the non-stabilizerlessness in the random circuit. Given the number of effective T-gates in the circuit, namely $125 * N$, we expect that this random structure shows similar behaviour to the Haar random circuit. In order to study non-stabilizerlessness behaviour of an intermediate case, where magic is non-zero but also not maximal, we repeat the same numerical experiment, but with rotation angle $\theta = \pi/20$.

We show the result of these simulations in the upper panels of Fig. 3.4, where we plot mutual information, I_{AB} , as a function of measurement probability. p_m for rota-

tion angles $\theta \in \{0, \pi/20, \pi/4\}$. First, we notice that there is no difference in the critical measurement rate, $p_{m,c}$ nor in the critical exponent, ν . However, when we analyze fluctuations of I_{AB} , $F_{AB} = (\mathbb{E}[(I^{(2)})^2] - \mathbb{E}[I^{(2)}]^2)^{1/2}$, we immediately observe a reduction in fluctuations with increasing non-stabilizerness as we expect from the previous section on t-doped circuits. The consequence of this fluctuation reduction is better separation of data from different system sizes, which in turn allows for the phase transition point to be more easily identified from mutual information data from the statistical point of view. However, we need to point out the fact that it is obvious that by increasing the non-stabilizerness, simulating large circuits becomes harder, and also, implementation of such circuits could become harder on a fault-tolerant quantum computer.

3.4. DISCUSSION AND CONCLUSIONS

We have shown, both analytically and numerically, that for t-doped Clifford circuits, the fluctuations of the mutual information are proportional to the non-stabilizerness of the system. This observation creates a direct relation between fluctuations of entropic quantity and magic. In Appendix 3.9 we show that this behaviour is fundamentally different than that of Renyi-4 entropy (meaning that our observations are not merely a consequence of the fluctuation being a “fourth-moment quantity”). The relation of magic to the fluctuation of quantum information quantity (OTOC) was previously observed in [31], which is also related to quantum information scrambling. Additionally, similar fluctuations behaviour has already been observed for entanglement entropy [92–94], which could be related to a special case of mutual information. Specifically, when we have a pure state and the bi-partition spans the whole system, mutual information reduces to a scaled entanglement entropy.

We also observed that the injection of magic into the measurement-induced phase transition in random circuits decreases the fluctuations of mutual information around the entanglement phase transition, potentially simplifying the identification of this transition from data. It then of course depends on the experimental platform, whether additional rotation gates are feasible to implement. Since we observed that adding *any* amount of magic is beneficial, presumably the phase of these gates would not need to be implemented with high precision, as long as the gate is outside of the Clifford group.

The main open question going forward is that of large-scale simulation of the random circuits with injection of the entanglement. These types of circuits present a particular challenge for approximate methods: they require relatively long time evolution as well as rapid entanglement growth. One candidate that could possibly go beyond these limitations is the Neural Network Quantum States (NQS) [95, 96] which could be an interesting future research direction.

3.5. AUTHOR CONTRIBUTIONS

AA conceived the project with input from EG. AA wrote the code for mutual information fluctuation analysis, analyzed the data and created the figures. CK wrote the code and created figures for the entanglement phase transition analysis with the help of AA and EG. JH derived the analytical proof of the information fluctuation theorem. AA, JH, and EG wrote the manuscript. EG supervised the project.

3.6. DATA AVAILABILITY

A GitLab repository containing this project is available at [97]. All the data and code to analyze them is available at [98]. For the simulations of this paper, we used Qiskit and Cirq [99, 100] simulators.

3.7. ACKNOWLEDGEMENTS

We acknowledge useful discussions with Thomas E. Spriggs, Mohammed Boky, Ana Silva and Ali G. Moghaddam. This work is part of the project Engineered Topological Quantum Networks (Project No.VI.Veni.212.278) of the research program NWO Talent Programme Veni Science domain 2021 which is financed by the Dutch Research Council (NWO). JH acknowledges funding from the Dutch Research Council (NWO) through Veni No.VI.Veni.222.331 and the Quantum Software Consortium (NWO Zwaartekracht Grant No.024.003.037).

3.8. APPENDIX-1:FOURTH MOMENT OF SPIN MEASUREMENTS

Inspired by the relation between measuring spin fluctuations of a subsystem and entanglement entropy [101] and mutual information [84, 102], we observed that the fourth moment (Kurtosis) of spin measurement of the subsystem also relates to non-stabilizerness on t-doped circuits.

We considered the circuit of the same structure as in Fig. 3.1. Instead of measuring entanglement entropy, $S^{(2)}$, of subsystems A and B , we measured the total spin of those subsystems, $S_z = \sum_{n \in N_l} s_{n,z}$ where $l \in \{A, B\}$. We define $Kurt(S_z)_{A,B}$ as

$$Kurt(S_z)_{A,B} := Kurt(\langle S_z \rangle_A) + Kurt(\langle S_z \rangle_B) - Kurt(\langle S_z \rangle_{AB}). \quad (3.3)$$

The Kurtosis of a random variable X is the standardized fourth moment, defined as, $\frac{\mathbb{E}[(X-\mu)^4]}{\sigma^4}$ where μ is the mean and σ is the standard deviation.

The results of the simulation in Fig. 3.5 show that there is a linear trend in $-\ln Kurt(S_z)_{A,B}$ as a function of the number of T-gates in the circuit. In this case, the number of T gates, N_T , and the number of samples are both 500. This linear trend depending on the number of qubits, can be observed for an effective number of T-gates. As it is shown in Fig. 3.5, for an 8 qubit circuit, this effect can be observed from $N_T = 0$ while for a 12 qubit circuit, the effective number of T-gates is $N_T = 5$ and for 16 qubit circuit, it is $N_T = 12$.

One possible explanation for the behaviour of small N_T in Fig. 3.5 for not following the linear trend, could be that for measuring spins in each subsystem for Clifford circuits, we have

$$\langle S_{z,j} \rangle = \text{Tr}(\sigma_{z,j} \rho) = \sum_i c_i \text{Tr}(\sigma_{z,j} P_i), \quad (3.4)$$

given the fact that $\text{Tr}(P_i P_j) = \delta_{ij}$ [103], so that we obtain

$$\langle S_{z,j} \rangle = c_j. \quad (3.5)$$

Suppose the Clifford circuit is in the scrambling regime $c_j \approx O(4^{-N})$ for $N \gg 1$, $c_j \ll 1$. Given all instances of spin measurements being a small value, their kurtosis also becomes small and $-\ln Kurt(S_z) > 1$. So we expect the linear behaviour of $-\ln Kurt(S_z)_{A,B}$ as a function of N_T to fail for the small N_T with respect to the system size.

3.9. APPENDIX-2:ANALYTICAL TREATMENT OF ENTROPY FLUCTUATIONS

In this Supplementary we state a refined version of Eq. (2) in the main text, and prove it. We will make use of the "super-ket" notation: denoting density matrices ρ as $|\rho\rangle\rangle$ and observables E as $\langle\langle E|$, with the trace inner product $\langle\langle E|\rho\rangle\rangle = \text{Tr}(E^\dagger \rho)$. Quantum channels Λ act linearly: $\Lambda|\rho\rangle\rangle = |\Lambda(\rho)\rangle\rangle$. For unitary channels we emphasise the difference between channel and unitary with calligraphic letters, i.e. $|\mathcal{U}\rho\mathcal{U}^\dagger\rangle\rangle = \mathcal{U}|\rho\rangle\rangle$. Before we move on to the proof we briefly review relevant representation theory for the unitary and Clifford groups.

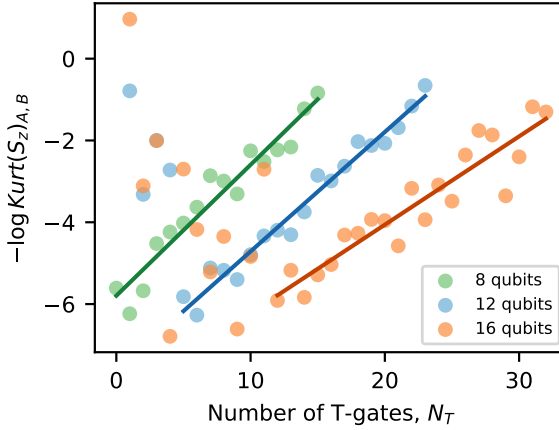


Figure 3.5: The log of kurtosis of the spin measurements, $-\ln \text{Kurt}(S_z)_{A,B}$ as a function of the number of T-gates, N_T , on the circuit for the number of qubits, $N = 8, 12, 16$ and the number of samples is 500.

3.9.1. MOMENTS OF THE UNITARY AND CLIFFORD GROUPS

We review the theory of polynomial invariants of the unitary group and the Clifford group. We will focus on quoting results required for the proof. For more detailed explanations see [104](unitary group) and [105–108](Clifford group). We begin by discussing the unitary group, and then make adaptations where needed for the Clifford group (focusing in particular on the case of quartic polynomials). The polynomial invariants of degree t of the unitary group are captured collectively by the t -th moment (super)operator, which is defined by

$$\mathcal{M}^{U(2^N), (t)} = \int_{U(2^n)} dU \mathcal{U}^{\otimes t}. \tag{3.6}$$

This operator (via Schur-Weyl duality) can be expressed in terms of permutation operators: for $\pi \in S_t$ we define

$$R_\pi = r_\pi^{\otimes N} \quad \text{where} \quad r_\pi = \sum_{x \in \{0,1\}^t} |x_{\pi(1)}, \dots, x_{\pi(t)}\rangle \langle x_1, \dots, x_t|.$$

The moment operator is a projector onto the space spanned by these permutation operators, and we can write

$$\mathcal{M}_t = \sum_{\pi', \pi \in S_t} W_{\pi', \pi}^{U(2^N), (t)} |R_{\pi'}\rangle \langle R_\pi|, \tag{3.7}$$

where $W_{\pi', \pi}^{U(2^N), (t)}$ is the so-called Weingarten matrix, the (pseudo) inverse of the Gram matrix $G_{\pi, \pi'}^{U(2^N), (t)} := \langle \langle R_\pi | R_{\pi'} \rangle \rangle$ of the permutation operators. A key fact about the Weingarten matrix is that it is diagonally dominant for fixed t and large n , we have:

$$W^{U(2^N), (t)} = 2^{-tN} (I + 2^{-N} F), \tag{3.8}$$

where F is a matrix with bounded (as a function of n) entries. In particular for $t = 4$ we have $\|F\| \leq 16$.

Next we consider the Clifford group. The moment operator has an analogous but more complicated expression, which we will only discuss in detail for $t = 4$. We have:

$$\mathcal{M}^{\mathbb{C}_N,(4)} = \frac{1}{|\mathbb{C}_N|} \sum_{C \in \mathbb{C}_N} \mathcal{C}^{\otimes 4}. \quad (3.9)$$

This operator differs from that of the Haar measure, as the Clifford group is *not* a 4-design. For $n \geq 3$, the dimension of its image is 30, and a basis is given by the 24 permutation operators R_π , parameterized by $\pi \in S_4$, and six more operators R_T . The latter can be written in the form $R_{\hat{\pi}}\Pi_4$, where $\hat{\pi}$ ranges over the subgroup $S_3 \subseteq S_4$ of permutations acting on the final three subsystems. and

$$\Pi_4 := 2^{-n} (I^{\otimes 4} + X^{\otimes 4} + Y^{\otimes 4} + Z^{\otimes 4})^{\otimes n} =: \pi_4^{\otimes n}. \quad (3.10)$$

We will denote this set of six operators as $\hat{S}_3 = \{\pi_4, \pi_4 \cdot (23), \pi_4 \cdot (34), \pi_4 \cdot (24), \pi_4 \cdot (234), \pi_4 \cdot (324)\}$ where we use the dot to emphasise multiplication. Following convention we will denote the total set of 30 operators as $\Sigma_{4,4} = S_4 \cup \hat{S}_3$. In terms of these operators the moment operator (3.9) is given by

$$\mathcal{M}^{\mathbb{C}_N,(4)} = \sum_{T', T \in \Sigma_{4,4}} W_{T', T}^{\mathbb{C}_N,(4)} |R_{T'}\rangle\rangle \langle\langle R_T|. \quad (3.11)$$

where $W^{\mathbb{C}_N,(4)}$ is the *Clifford-Weingarten matrix*. We note that $W^{\mathbb{C}_N,(4)}$ is also diagonally dominant for large N . In particular for $t = 4$ we have

$$W^{\mathbb{C}_N,(4)} = 2^{-4N} (I + 2^{-N} F), \quad (3.12)$$

where $\|F\| \leq 16$.

Finally we will need a lemma from [109] that characterises the action of the T -gate on the commutant of the Clifford group:

Lemma 1. *Let \mathcal{T} denote the quantum channel acting by the T -gate $T = \begin{pmatrix} 1 & 0 \\ 0 & e^{i\pi/4} \end{pmatrix}$ on the first qubit of an N -qubit state. Then we have, for every $\pi, \pi' \in \hat{S}_3$, that*

$$\langle\langle R_\pi \Pi_4 | \mathcal{T}^{\otimes 4} | R_{\pi'} \Pi_4 \rangle\rangle \begin{cases} = (2^4 - 4)2^{4(N-1)} = \frac{3}{4}2^{4N} & \text{if } \pi = \pi', \\ \leq (2^3 - 4)2^{3(N-1)} = \frac{1}{2}2^{3N} & \text{if } \pi \neq \pi'. \end{cases}$$

3.9.2. MAIN THEOREM

With the necessary representation theory reviewed we can prove the relation in Eq. 2 in the main text. For precision's sake we restate the result as a theorem.

Theorem 2. *Let ψ_{N_T} be the N -qubit state generated by the application of N_T T gates (on a fixed qubit) interspersed with random N -qubit Clifford gates, and let ρ_{AB} be its reduced state on $N/2$ qubits. Averaged over the random Clifford gates we have*

$$\tilde{S}_{AB}^{(2)} := -\log(\mathbb{E} \text{Tr}(\rho_{AB}^2)) = 1 + N/2 + O(2^{-N}) \quad (3.13)$$

$$\tilde{\delta} := (-\log(\mathbb{E} \text{Tr}(\rho_{AB}^2)^2) - (\tilde{S}_{AB}^{(2)})^2) = \left(\frac{3}{4}\right)^{N_T} + O(2^{-N}). \quad (3.14)$$

Proof. We begin by calculating $\tilde{S}_{AB}^{(2)}$. We have

$$\mathbb{E} \text{Tr}(\rho_{AB}^2) = \frac{1}{|\mathbb{C}_N|} \sum_{C_0, \dots, C_{N_T}} \langle \langle \mathbb{F}_{AB} \otimes \mathbb{1}_{AB} | \mathcal{C}_{N_T}^{\otimes 2} \mathcal{T}^{\otimes 2} \dots \mathcal{T}^{\otimes 2} \mathcal{C}_0^{\otimes 2} | 0^{\otimes 2} \rangle \rangle, \quad (3.15)$$

where \mathbb{F} is the permutation operator exchanging two copies of the AB subsystem. Here we used the trace identities $\text{tr}(A)^2 = \text{tr}(A^{\otimes 2})$ and $\text{tr}(A^2) = \text{tr}(\mathbb{F}A^{\otimes 2})$. We can simplify this equation by noting that the Clifford group is a 2 design, and hence

$$\frac{1}{|\mathbb{C}_N|} \sum_{C \in \mathbb{C}_N} \mathcal{C}^{\otimes 2} = \mathcal{M}^{U(2^N), (2)}, \quad (3.16)$$

where $\mathcal{M}^{U(2^N), (2)}$ is the quadratic moment operator of the *unitary group*. By Haar invariance, the action of $\mathcal{T}^{\otimes 2}$ is easily seen to be absorbed, and since $\mathcal{M}^{U(2^N), (2)}$ is a projector, we have

$$\mathbb{E} \text{Tr}(\rho_{AB}^2) = \langle \langle \mathbb{F}_{AB} | \mathcal{M}^{U(2^N), (2)} | 0^{\otimes 2} \rangle \rangle. \quad (3.17)$$

This already shows that $\tilde{S}_{AB}^{(2)}$ is independent of N_T . We can calculate the associated value exactly by using the well known formula (see e.g. [107])

$$\mathcal{M}^{U(2^N), (2)} | 0^{\otimes 2} \rangle \rangle = \frac{1}{2^N(2^N + 1)} \sum_{\pi \in S_2} |R_\pi\rangle\rangle. \quad (3.18)$$

Using the fact that $\mathbb{F}_{AB} = r_{(12)}^{\otimes N_{AB}}$ and $R_\pi = r_\pi^{\otimes N}$ separate across qubits we can now calculate

$$\mathbb{E} \text{Tr}(\rho_{AB}^2) = \frac{1}{2^N(2^N + 1)} \sum_{\pi \in S_2} \text{tr}(\mathbb{F}r_\pi)^{N_{AB}} \text{tr}(r_\pi)^{N - N_{AB}}. \quad (3.19)$$

By direct calculation we have $\text{tr}(r_{(12)}) = 2$ and $\text{tr}(r_e) = 4$. With a little calculus we thus get

$$\mathbb{E} \text{Tr}(\rho_{AB}^2) = \frac{2^{N_{AB}} 4^{N - N_{AB}} + 2^{N - N_{AB}} 4^{N_{AB}}}{2^N(2^N + 1)}. \quad (3.20)$$

Using $N_{AB} = N/2$ we can see that

$$\mathbb{E} \text{Tr}(\rho_{AB}^2) = 22^{-N/2} + O(2^{-N}). \quad (3.21)$$

Calculating the variance term $\mathbb{E} \text{Tr}(\rho_{AB}^2)^2$ is similar but messier. Again through trace identities we obtain

$$\mathbb{E} \text{Tr}(\rho_{AB}^2)^2 = \frac{1}{|\mathbb{C}_N|^{N_T+1}} \sum_{C_0, \dots, C_{N_T}} \langle \langle (\mathbb{F}_{AB} \otimes \mathbb{1}_{AB})^{\otimes 2} | \mathcal{C}_{N_T}^{\otimes 4} \mathcal{T}^{\otimes 4} \dots \mathcal{T}^{\otimes 4} \mathcal{C}_0^{\otimes 4} | 0^{\otimes 4} \rangle \rangle. \quad (3.22)$$

Since the Clifford group is not a 4-design we can no longer simplify this expression. Instead we directly insert

$$\frac{1}{|\mathbb{C}_N|} \sum_{C \in \mathbb{C}_N} \mathcal{C}^{\otimes 4} = \mathcal{M}^{\mathbb{C}_N, (4)} = \sum_{T', T \in \Sigma_{4,4}} W_{T', T}^{\mathbb{C}_N, (4)} |R_{T'}\rangle\rangle \langle\langle R_T|. \quad (3.23)$$

Defining the matrix

$$Q_{T,T'} = \langle\langle R_T | \mathcal{T} | R_{T'} \rangle\rangle, \quad (3.24)$$

and the vectors

$$v_T = \langle\langle (\mathbb{F}_{AB} \otimes \mathbb{1}_{AB})^{\otimes 2} | R_T \rangle\rangle \quad (3.25)$$

$$u_T = \langle\langle R_T | 0^{\otimes 4} \rangle\rangle, \quad (3.26)$$

we can write the above expression as a matrix vector inner product

$$\mathbb{E} \text{Tr}(\rho_{AB}^2)^2 = v^\dagger W Q W \dots Q W u = v^\dagger (W Q)^{N_T} W u. \quad (3.27)$$

At this point it is worth noting that u is the all ones vector, and that the vector v has the property

$$v_T \begin{cases} = 2^{3N} & \text{if } T \in \{e, (12)(34), (12), (34), \pi_4 \cdot (34)\}, \\ \leq 2^{5N/2} & \text{otherwise,} \end{cases} \quad (3.28)$$

where we used explicitly that $N_{AB} = N/2$ and that $\mathbb{F}_{AB}^{\otimes 2} = r_{(12)(34)}^{\otimes N_{AB}}$. Next we make some approximations valid in the large N regime. We will use big O notation to suppress constants that can in principle be calculated. We have that

$$W = 2^{-4n} I + O(2^{-5N}) \quad (3.29)$$

and (via lemma 1) that

$$Q = 2^{4N} \begin{pmatrix} I_{24} & 0 \\ 0 & \frac{3}{4} I_6 \end{pmatrix} + O(2^{3N}). \quad (3.30)$$

Consequently we have

$$v^\dagger (W Q)^{N_T} W u = 2^{-4N} v^\dagger \begin{pmatrix} I_{24} & 0 \\ 0 & \frac{3}{4} I_6 \end{pmatrix} u + O(2^{-2N}) \quad (3.31)$$

$$= 2^{-4N} \left(4 \cdot 2^{3N} + \left(\frac{3}{4}\right)^{N_T} 2^{3N} \right) + O(2^{-2N}) \quad (3.32)$$

$$= \left(4 + \left(\frac{3}{4}\right)^{N_T} \right) 2^{-N} + O(2^{-2N}), \quad (3.33)$$

which finishes this part of the calculation. With this in hand we can compute $\tilde{\delta}$:

$$\tilde{\delta} = (-\log(\mathbb{E} \text{Tr}(\rho_A^2)^2) - (\tilde{S}_A^{(2)})^2) \approx \log\left(1 + \left(\frac{3}{4}\right)^{N_T} O(2^{-N})\right) \approx \left(\frac{3}{4}\right)^{N_T} + O(2^{-N}), \quad (3.34)$$

where the last approximation is the first order of the Taylor expansion of $\log(1+x)$. \square

The key detail of this calculation is the extra term appearing at order 2^{3N} in the expression of the vector v . This term is due to the generator $\pi_4 \cdot (34)$ which is present in the commutant of the Clifford group and not that of the unitary group. We also see that due to lemma 1 it vanishes quickly with increasing N_T , as we also observe numerically. It is important to note that this is not merely a consequence of the fluctuation of the Renyi-2 entropy being a quartic invariant. In other quartic invariants such as the Renyi-4 entropy,

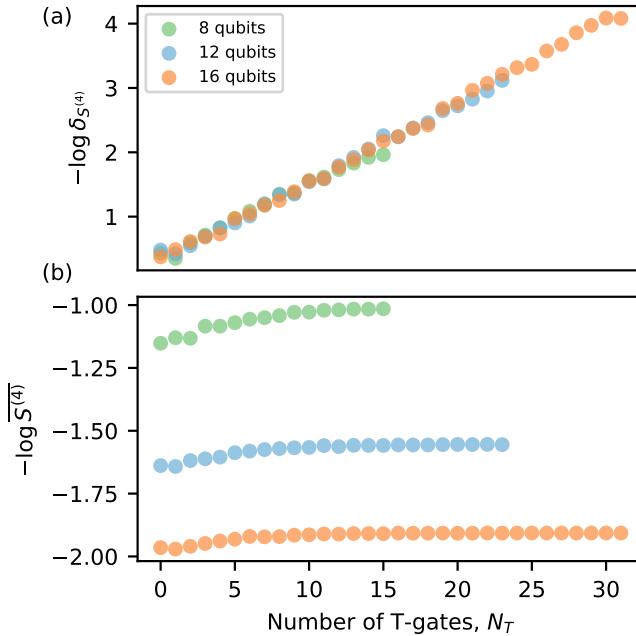


Figure 3.6: (a) The log of fluctuations of Renyi-4 entropy, $-\ln \delta_{S^{(4)}}$ as a function of the number of T-gates, N_T , on the circuit. (b) The log of the average of Renyi-4 entropy, $-\log \overline{S^{(4)}}$ as a function of the number of T-gates, N_T on the circuit. The number of qubits, $N = 8, 12, 16$ and the number of samples is 500.

a similar calculation can be made but there the contributions from the non-permutation generators are all suppressed by a factor of 2^{-N} making them invisible even at moderate qubit numbers. We confirm this observation numerically and show the results in Fig. 3.6 (b): The averaged instances of Renyi-4 entropy do not show the linear behaviour, however, the fluctuations of Renyi-4 entropy do in Fig. 3.6 (a) showing the behavior is encoded in the fluctuations, not in the order of Renyi entropy. Similarly, it is vital that $|AB| = N/2$. If $|AB|$ is substantially smaller or larger than this (e.g. $|AB| = N/8$), then the contribution of the generator $\pi_4 \cdot (34)$ becomes subleading even in the fluctuation of the Renyi-2 entropy. A numerical illustration of how different subsystem sizes influence the result is shown in Fig. 3.7 for the subsystem size of $|AB| = N/4$, where we see that a gap opened for 8-qubit and 16-qubit system sizes, thus making the proportionality between mutual information fluctuations and the number of T-gates system size dependent.

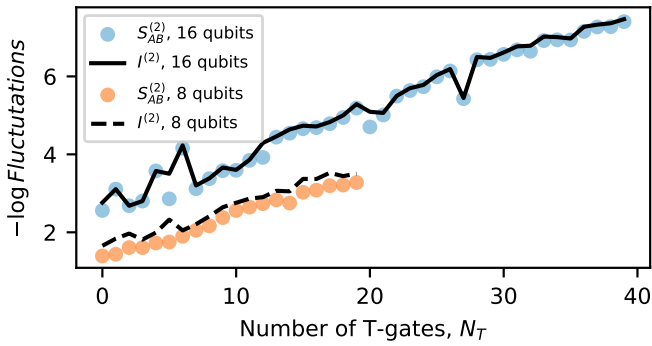


Figure 3.7: The log of fluctuations of mutual information $-\ln \delta_{I^{(2)}}$ and Renyi-4 entropy, $-\ln \delta_{S^{(2)}}$ as a function of the number of T-gates, N_T , on the circuit for the subsystem size $N_A = N_B = N/8$. The number of qubits, $N = 8, 16$ and the number of samples is 500.

BIBLIOGRAPHY

1. Einstein, A., Podolsky, B. & Rosen, N. Can Quantum-Mechanical Description of Physical Reality Be Considered Complete? *Phys. Rev.* **47**, 777–780. <https://link.aps.org/doi/10.1103/PhysRev.47.777> (10 May 1935).
2. Gottesman, D. Stabilizer Codes and Quantum Error Correction. *arXiv:quant-ph/9705052v1*. eprint: [quant-ph/9705052](https://doi.org/10.48550/arXiv.quant-ph/9705052) (quant-ph). <https://doi.org/10.48550/arXiv.quant-ph/9705052> (1997).
3. Nielsen, M. A. & Chuang, I. L. *Quantum Computation and Quantum Information: 10th Anniversary Edition* <https://doi.org/10.1017/CB09780511976667> (Cambridge University Press, 2010).
4. Gottesman, D. Theory of fault-tolerant quantum computation. *Phys. Rev. A* **57**, 127–137. <https://link.aps.org/doi/10.1103/PhysRevA.57.127> (1 Jan. 1998).
5. Aaronson, S. & Gottesman, D. Improved simulation of stabilizer circuits. *Phys. Rev. A* **70**, 052328. <https://link.aps.org/doi/10.1103/PhysRevA.70.052328> (5 Nov. 2004).
6. Gottesman, D. Class of quantum error-correcting codes saturating the quantum Hamming bound. *Phys. Rev. A* **54**, 1862–1868. <https://link.aps.org/doi/10.1103/PhysRevA.54.1862> (3 Sept. 1996).
7. Gottesman, D. The Heisenberg Representation of Quantum Computers. *arXiv:quant-ph/9807006*. <https://doi.org/10.48550/arXiv.quant-ph/9807006> (1998).
8. Veitch, V., Mousavian, S. A. H., Gottesman, D. & Emerson, J. The resource theory of stabilizer quantum computation. *New Journal of Physics* **16**, 013009. <https://dx.doi.org/10.1088/1367-2630/16/1/013009> (Jan. 2014).
9. Shor, P. W. Fault-tolerant quantum computation. *arXiv:quant-ph/9605011*. <https://doi.org/10.48550/arXiv.quant-ph/9605011> (1997).
10. Beverland, M., Campbell, E., Howard, M. & Kliuchnikov, V. Lower bounds on the non-Clifford resources for quantum computations. *Quantum Science and Technology* **5**, 035009. <https://dx.doi.org/10.1088/2058-9565/ab8963> (May 2020).
11. Howard, M. & Campbell, E. Application of a Resource Theory for Magic States to Fault-Tolerant Quantum Computing. *Physical Review Letters* **118**. ISSN: 1079-7114. <http://dx.doi.org/10.1103/PhysRevLett.118.090501> (Mar. 2017).
12. Hamaguchi, H., Hamada, K. & Yoshioka, N. Handbook for Efficiently Quantifying Robustness of Magic. *arXiv:2311.01362*. <https://doi.org/10.48550/arXiv.2311.01362> (2023).

13. Leone, L., Oliviero, S. F. E. & Hamma, A. Stabilizer Rényi Entropy. *Phys. Rev. Lett.* **128**, 050402. <https://link.aps.org/doi/10.1103/PhysRevLett.128.050402> (5 Feb. 2022).
14. Haug, T. & Kim, M. Scalable Measures of Magic Resource for Quantum Computers. *PRX Quantum* **4**, 010301. <https://link.aps.org/doi/10.1103/PRXQuantum.4.010301> (1 Jan. 2023).
15. Liu, Z.-W. & Winter, A. Many-Body Quantum Magic. *PRX Quantum* **3**, 020333. <https://link.aps.org/doi/10.1103/PRXQuantum.3.020333> (2 May 2022).
16. Garcia, R. J., Bu, K. & Jaffe, A. Resource theory of quantum scrambling. *Proceedings of the National Academy of Sciences* **120**, e2217031120. eprint: <https://www.pnas.org/doi/pdf/10.1073/pnas.2217031120>. <https://www.pnas.org/doi/abs/10.1073/pnas.2217031120> (2023).
17. Turkeshi, X., Tirrito, E. & Sierant, P. Magic spreading in random quantum circuits. *arXiv:2407.03929*. <https://arxiv.org/abs/2407.03929> (2024).
18. Garcia, R. J. *et al.* On the Hardness of Measuring Magic. *arXiv:2408.01663*. <https://arxiv.org/abs/2408.01663> (2024).
19. Leone, L., Oliviero, S. F. E., Esposito, G. & Hamma, A. Phase transition in stabilizer entropy and efficient purity estimation. *Physical Review A* **109**. ISSN: 2469-9934. <http://dx.doi.org/10.1103/PhysRevA.109.032403> (Mar. 2024).
20. Rattacaso, D., Leone, L., Oliviero, S. F. E. & Hamma, A. Stabilizer entropy dynamics after a quantum quench. *Physical Review A* **108**. ISSN: 2469-9934. <http://dx.doi.org/10.1103/PhysRevA.108.042407> (Oct. 2023).
21. Oliviero, S. F. E., Leone, L., Zhou, Y. & Hamma, A. Stability of topological purity under random local unitaries. *SciPost Phys.* **12**, 096. <https://scipost.org/10.21468/SciPostPhys.12.3.096> (2022).
22. Leone, L., Oliviero, S. F. E. & Hamma, A. Learning t-doped stabilizer states. *Quantum* **8**, 1361. ISSN: 2521-327X. <http://dx.doi.org/10.22331/q-2024-05-27-1361> (May 2024).
23. Leone, L., Oliviero, S. F. E. & Hamma, A. Nonstabilizerness determining the hardness of direct fidelity estimation. *Phys. Rev. A* **107**, 022429. <https://link.aps.org/doi/10.1103/PhysRevA.107.022429> (2 Feb. 2023).
24. Oliviero, S. F. E., Leone, L. & Hamma, A. Magic-state resource theory for the ground state of the transverse-field Ising model. *Phys. Rev. A* **106**, 042426. <https://link.aps.org/doi/10.1103/PhysRevA.106.042426> (4 Oct. 2022).
25. Odavić, J. *et al.* Complexity of frustration: A new source of non-local non-stabilizerness. *SciPost Phys.* **15**, 131. <https://scipost.org/10.21468/SciPostPhys.15.4.131> (2023).
26. Haug, T., Lee, S. & Kim, M. S. Efficient stabilizer entropies for quantum computers. *arXiv:2305.19152*. <https://doi.org/10.48550/arXiv.2305.19152> (2023).
27. Haug, T. & Piroli, L. Quantifying nonstabilizerness of matrix product states. *Phys. Rev. B* **107**, 035148. <https://link.aps.org/doi/10.1103/PhysRevB.107.035148> (3 Jan. 2023).

28. Tarabunga, P. S., Tirrito, E., Banuls, M. C. & Dalmonte, M. Nonstabilizerness via matrix product states in the Pauli basis. *arXiv:2401.16498*. <https://doi.org/10.48550/arXiv.2401.16498> (2024).
29. Lami, G. & Collura, M. Nonstabilizerness via Perfect Pauli Sampling of Matrix Product States. *Phys. Rev. Lett.* **131**, 180401. <https://link.aps.org/doi/10.1103/PhysRevLett.131.180401> (18 Oct. 2023).
30. Lami, G. & Collura, M. Unveiling the Stabilizer Group of a Matrix Product State. *Phys. Rev. Lett.* **133**, 010602. <https://link.aps.org/doi/10.1103/PhysRevLett.133.010602> (1 July 2024).
31. Ahmadi, A. & Greplova, E. Quantifying non-stabilizerness via information scrambling. *SciPost Phys.* **16**, 043. <https://scipost.org/10.21468/SciPostPhys.16.2.043> (2024).
32. Hosur, P., Qi, X.-L., Roberts, D. A. & Yoshida, B. Chaos in quantum channels. *Journal of High Energy Physics* **2016**. ISSN: 1029-8479. [http://dx.doi.org/10.1007/JHEP02\(2016\)004](http://dx.doi.org/10.1007/JHEP02(2016)004) (Feb. 2016).
33. Hayden, P. & Preskill, J. Black holes as mirrors: quantum information in random subsystems. *Journal of High Energy Physics* **2007**, 120–120. ISSN: 1029-8479. <http://dx.doi.org/10.1088/1126-6708/2007/09/120> (Sept. 2007).
34. Sekino, Y. & Susskind, L. Fast scramblers. *Journal of High Energy Physics* **2008**, 065–065. ISSN: 1029-8479. <http://dx.doi.org/10.1088/1126-6708/2008/10/065> (Oct. 2008).
35. Shenker, S. H. & Stanford, D. Black holes and the butterfly effect. *Journal of High Energy Physics* **2014**. ISSN: 1029-8479. [http://dx.doi.org/10.1007/JHEP03\(2014\)067](http://dx.doi.org/10.1007/JHEP03(2014)067) (Mar. 2014).
36. Swingle, B. Unscrambling the physics of out-of-time-order correlators. *Nature Physics* **14**, 988–990. <https://doi.org/10.1038/s41567-018-0295-5> (Oct. 2018).
37. Basko, D., Aleiner, I. & Altshuler, B. Metal–insulator transition in a weakly interacting many-electron system with localized single-particle states. *Annals of Physics* **321**, 1126–1205. ISSN: 0003-4916. <https://www.sciencedirect.com/science/article/pii/S0003491605002630> (2006).
38. Mi, X. *et al.* Information scrambling in quantum circuits. *Science* **374**, 1479–1483. eprint: <https://www.science.org/doi/pdf/10.1126/science.abg5029>. <https://www.science.org/doi/abs/10.1126/science.abg5029> (2021).
39. Khemani, V., Vishwanath, A. & Huse, D. A. Operator Spreading and the Emergence of Dissipative Hydrodynamics under Unitary Evolution with Conservation Laws. *Phys. Rev. X* **8**, 031057. <https://link.aps.org/doi/10.1103/PhysRevX.8.031057> (3 Sept. 2018).
40. Aleiner, I. L., Faoro, L. & Ioffe, L. B. Microscopic model of quantum butterfly effect: Out-of-time-order correlators and traveling combustion waves. *Annals of Physics* **375**, 378–406. ISSN: 0003-4916. <https://www.sciencedirect.com/science/article/pii/S0003491616301919> (2016).

41. Roberts, D. A. & Stanford, D. Diagnosing Chaos Using Four-Point Functions in Two-Dimensional Conformal Field Theory. *Phys. Rev. Lett.* **115**, 131603. <https://link.aps.org/doi/10.1103/PhysRevLett.115.131603> (13 Sept. 2015).
42. Alba, V. & Calabrese, P. Quantum information scrambling after a quantum quench. *Phys. Rev. B* **100**, 115150. <https://link.aps.org/doi/10.1103/PhysRevB.100.115150> (11 Sept. 2019).
43. Touil, A. & Deffner, S. Information scrambling—A quantum thermodynamic perspective. *Europhysics Letters* **146**, 48001. ISSN: 1286-4854. <http://dx.doi.org/10.1209/0295-5075/ad4413> (May 2024).
44. Monaco, G. L. *et al.* An operational definition of quantum information scrambling. *arXiv:2312.11619*. eprint: [2312.11619](https://doi.org/10.48550/arXiv.2312.11619) (quant-ph). <https://doi.org/10.48550/arXiv.2312.11619> (2023).
45. Nahum, A., Ruhman, J., Vijay, S. & Haah, J. Quantum Entanglement Growth under Random Unitary Dynamics. *Phys. Rev. X* **7**, 031016. <https://link.aps.org/doi/10.1103/PhysRevX.7.031016> (3 July 2017).
46. Hama, A., Giampaolo, S. M. & Illuminati, F. Mutual information and spontaneous symmetry breaking. *Phys. Rev. A* **93**, 012303. <https://link.aps.org/doi/10.1103/PhysRevA.93.012303> (1 Jan. 2016).
47. Schnaack, O. *et al.* Tripartite information, scrambling, and the role of Hilbert space partitioning in quantum lattice models. *Physical Review B* **100**. ISSN: 2469-9969. <http://dx.doi.org/10.1103/PhysRevB.100.224302> (Dec. 2019).
48. Pappalardi, S. *et al.* Scrambling and entanglement spreading in long-range spin chains. *Phys. Rev. B* **98**, 134303. <https://link.aps.org/doi/10.1103/PhysRevB.98.134303> (13 Oct. 2018).
49. Li, Y., Chen, X. & Fisher, M. P. A. Quantum Zeno effect and the many-body entanglement transition. *Phys. Rev. B* **98**, 205136. <https://link.aps.org/doi/10.1103/PhysRevB.98.205136> (20 Nov. 2018).
50. Li, Y., Chen, X. & Fisher, M. P. A. Measurement-driven entanglement transition in hybrid quantum circuits. *Phys. Rev. B* **100**, 134306. <https://link.aps.org/doi/10.1103/PhysRevB.100.134306> (13 Oct. 2019).
51. Skinner, B., Ruhman, J. & Nahum, A. Measurement-Induced Phase Transitions in the Dynamics of Entanglement. *Phys. Rev. X* **9**, 031009. <https://link.aps.org/doi/10.1103/PhysRevX.9.031009> (3 July 2019).
52. Chan, A., Nandkishore, R. M., Pretko, M. & Smith, G. Unitary-projective entanglement dynamics. *Phys. Rev. B* **99**, 224307. <https://link.aps.org/doi/10.1103/PhysRevB.99.224307> (22 June 2019).
53. Jian, C.-M., You, Y.-Z., Vasseur, R. & Ludwig, A. W. W. Measurement-induced criticality in random quantum circuits. *Phys. Rev. B* **101**, 104302. <https://link.aps.org/doi/10.1103/PhysRevB.101.104302> (10 Mar. 2020).
54. Gullans, M. J. & Huse, D. A. Dynamical Purification Phase Transition Induced by Quantum Measurements. *Phys. Rev. X* **10**, 041020. <https://link.aps.org/doi/10.1103/PhysRevX.10.041020> (4 Oct. 2020).

55. Fisher, M. P., Khemani, V., Nahum, A. & Vijay, S. Random Quantum Circuits. *Annual Review of Condensed Matter Physics* **14**, 335–379. eprint: <https://doi.org/10.1146/annurev-conmatphys-031720-030658>. <https://doi.org/10.1146/annurev-conmatphys-031720-030658> (2023).
56. Cao, X., Tilloy, A. & Luca, A. D. Entanglement in a fermion chain under continuous monitoring. *SciPost Phys.* **7**, 024. <https://scipost.org/10.21468/SciPostPhys.7.2.024> (2019).
57. Bao, Y., Choi, S. & Altman, E. Theory of the phase transition in random unitary circuits with measurements. *Phys. Rev. B* **101**, 104301. <https://link.aps.org/doi/10.1103/PhysRevB.101.104301> (10 Mar. 2020).
58. Zabalo, A. *et al.* Critical properties of the measurement-induced transition in random quantum circuits. *Phys. Rev. B* **101**, 060301. <https://link.aps.org/doi/10.1103/PhysRevB.101.060301> (6 Feb. 2020).
59. Tang, Q. & Zhu, W. Measurement-induced phase transition: A case study in the nonintegrable model by density-matrix renormalization group calculations. *Phys. Rev. Res.* **2**, 013022. <https://link.aps.org/doi/10.1103/PhysRevResearch.2.013022> (1 Jan. 2020).
60. Fuji, Y. & Ashida, Y. Measurement-induced quantum criticality under continuous monitoring. *Phys. Rev. B* **102**, 054302. <https://link.aps.org/doi/10.1103/PhysRevB.102.054302> (5 Aug. 2020).
61. Iaconis, J., Lucas, A. & Chen, X. Measurement-induced phase transitions in quantum automaton circuits. *Phys. Rev. B* **102**, 224311. <https://link.aps.org/doi/10.1103/PhysRevB.102.224311> (22 Dec. 2020).
62. Lang, N. & Büchler, H. P. Entanglement transition in the projective transverse field Ising model. *Phys. Rev. B* **102**, 094204. <https://link.aps.org/doi/10.1103/PhysRevB.102.094204> (9 Sept. 2020).
63. Nahum, A., Roy, S., Skinner, B. & Ruhman, J. Measurement and Entanglement Phase Transitions in All-To-All Quantum Circuits, on Quantum Trees, and in Landau-Ginsburg Theory. *PRX Quantum* **2**, 010352. <https://link.aps.org/doi/10.1103/PRXQuantum.2.010352> (1 Mar. 2021).
64. Lavasani, A., Alavirad, Y. & Barkeshli, M. Measurement-induced topological entanglement transitions in symmetric random quantum circuits. *Nature Physics* **17**, 342–347. <https://doi.org/10.1038/s41567-020-01112-z> (Jan. 2021).
65. Sang, S. & Hsieh, T. H. Measurement-protected quantum phases. *Phys. Rev. Res.* **3**, 023200. <https://link.aps.org/doi/10.1103/PhysRevResearch.3.023200> (2 June 2021).
66. Lunt, O. & Pal, A. Measurement-induced entanglement transitions in many-body localized systems. *Phys. Rev. Res.* **2**, 043072. <https://link.aps.org/doi/10.1103/PhysRevResearch.2.043072> (4 Oct. 2020).

67. Szyniszewski, M., Romito, A. & Schomerus, H. Universality of Entanglement Transitions from Stroboscopic to Continuous Measurements. *Phys. Rev. Lett.* **125**, 210602. <https://link.aps.org/doi/10.1103/PhysRevLett.125.210602> (21 Nov. 2020).
68. Gullans, M. J., Krastanov, S., Huse, D. A., Jiang, L. & Flammia, S. T. Quantum Coding with Low-Depth Random Circuits. *Phys. Rev. X* **11**, 031066. <https://link.aps.org/doi/10.1103/PhysRevX.11.031066> (3 Sept. 2021).
69. Alberton, O., Buchhold, M. & Diehl, S. Entanglement Transition in a Monitored Free-Fermion Chain: From Extended Criticality to Area Law. *Phys. Rev. Lett.* **126**, 170602. <https://link.aps.org/doi/10.1103/PhysRevLett.126.170602> (17 Apr. 2021).
70. Turkeshi, X., Fazio, R. & Dalmonte, M. Measurement-induced criticality in $(2 + 1)$ -dimensional hybrid quantum circuits. *Phys. Rev. B* **102**, 014315. <https://link.aps.org/doi/10.1103/PhysRevB.102.014315> (1 July 2020).
71. Ippoliti, M., Gullans, M. J., Gopalakrishnan, S., Huse, D. A. & Khemani, V. Entanglement Phase Transitions in Measurement-Only Dynamics. *Phys. Rev. X* **11**, 011030. <https://link.aps.org/doi/10.1103/PhysRevX.11.011030> (1 Feb. 2021).
72. Li, Y. & Fisher, M. P. A. Statistical mechanics of quantum error correcting codes. *Phys. Rev. B* **103**, 104306. <https://link.aps.org/doi/10.1103/PhysRevB.103.104306> (10 Mar. 2021).
73. Fan, R., Vijay, S., Vishwanath, A. & You, Y.-Z. Self-organized error correction in random unitary circuits with measurement. *Phys. Rev. B* **103**, 174309. <https://link.aps.org/doi/10.1103/PhysRevB.103.174309> (17 May 2021).
74. Lavasani, A., Alavirad, Y. & Barkeshli, M. Topological Order and Criticality in $(2 + 1)$ D Monitored Random Quantum Circuits. *Phys. Rev. Lett.* **127**, 235701. <https://link.aps.org/doi/10.1103/PhysRevLett.127.235701> (23 Dec. 2021).
75. Van Regemortel, M., Cian, Z.-P., Seif, A., Dehghani, H. & Hafezi, M. Entanglement Entropy Scaling Transition under Competing Monitoring Protocols. *Phys. Rev. Lett.* **126**, 123604. <https://link.aps.org/doi/10.1103/PhysRevLett.126.123604> (12 Mar. 2021).
76. Claeys, P. W., Henry, M., Vicary, J. & Lamacraft, A. Exact dynamics in dual-unitary quantum circuits with projective measurements. *Phys. Rev. Res.* **4**, 043212. <https://link.aps.org/doi/10.1103/PhysRevResearch.4.043212> (4 Dec. 2022).
77. Agrawal, U. *et al.* Entanglement and Charge-Sharpener Transitions in $U(1)$ Symmetric Monitored Quantum Circuits. *Phys. Rev. X* **12**, 041002. <https://link.aps.org/doi/10.1103/PhysRevX.12.041002> (4 Oct. 2022).
78. Block, M., Bao, Y., Choi, S., Altman, E. & Yao, N. Y. Measurement-Induced Transition in Long-Range Interacting Quantum Circuits. *Phys. Rev. Lett.* **128**, 010604. <https://link.aps.org/doi/10.1103/PhysRevLett.128.010604> (1 Jan. 2022).

79. Noel, C. *et al.* Measurement-induced quantum phases realized in a trapped-ion quantum computer. *Nature Physics* **18**, 760–764. <https://doi.org/10.1038/s41567-022-01619-7> (June 2022).
80. Koh, J. M., Sun, S.-N., Motta, M. & Minnich, A. J. Measurement-induced entanglement phase transition on a superconducting quantum processor with mid-circuit readout. *Nature Physics* **19**, 1314–1319. <https://doi.org/10.1038/s41567-023-02076-6> (June 2023).
81. Oshima, H. & Fuji, Y. Charge fluctuation and charge-resolved entanglement in a monitored quantum circuit with $U(1)$ symmetry. *Phys. Rev. B* **107**, 014308. <https://link.aps.org/doi/10.1103/PhysRevB.107.014308> (1 Jan. 2023).
82. Leone, L., Oliviero, S. F. E., Zhou, Y. & Hamma, A. Quantum Chaos is Quantum. *Quantum* **5**, 453. ISSN: 2521-327X. <http://dx.doi.org/10.22331/q-2021-05-04-453> (May 2021).
83. Zhou, T. & Nahum, A. Emergent statistical mechanics of entanglement in random unitary circuits. *Physical Review B* **99**, 174205. <https://link.aps.org/doi/10.1103/PhysRevB.99.174205> (2019).
84. Moghaddam, A. G., Pöyhönen, K. & Ojanen, T. Exponential Shortcut to Measurement-Induced Entanglement Phase Transitions. *Physical Review Letters* **131**. ISSN: 1079-7114. <http://dx.doi.org/10.1103/PhysRevLett.131.020401> (July 2023).
85. Bejan, M., McLauchlan, C. & Béri, B. Dynamical Magic Transitions in Monitored Clifford+T Circuits. *arXiv:2312.00132*. <https://doi.org/10.48550/arXiv.2312.00132> (2023).
86. Niroula, P. *et al.* Phase transition in magic with random quantum circuits. *arXiv:2304.10481*. <https://doi.org/10.48550/arXiv.2304.10481> (2024).
87. Fux, G. E., Tirrito, E., Dalmonte, M. & Fazio, R. Entanglement-magic separation in hybrid quantum circuits. *arXiv:2312.02039*. <https://doi.org/10.48550/arXiv.2312.02039> (2023).
88. Gu, A., Oliviero, S. F. E. & Leone, L. Magic-induced computational separation in entanglement theory. *arXiv:2403.19610*. <https://doi.org/10.48550/arXiv.2403.19610> (2024).
89. Leone, L., Oliviero, S. F. E., Esposito, G. & Hamma, A. Phase transition in stabilizer entropy and efficient purity estimation. *Phys. Rev. A* **109**, 032403. <https://link.aps.org/doi/10.1103/PhysRevA.109.032403> (3 Mar. 2024).
90. Tarabunga, P. S. & Tirrito, E. Magic transition in measurement-only circuits. *arXiv:2407.15939*. <https://arxiv.org/abs/2407.15939> (2024).
91. Bravyi, S. & Maslov, D. Hadamard-Free Circuits Expose the Structure of the Clifford Group. *IEEE Transactions on Information Theory* **67**, 4546–4563. ISSN: 1557-9654. <http://dx.doi.org/10.1109/TIT.2021.3081415> (July 2021).
92. True, S. & Hamma, A. Transitions in Entanglement Complexity in Random Circuits. *Quantum* **6**, 818. ISSN: 2521-327X. <http://dx.doi.org/10.22331/q-2022-09-22-818> (Sept. 2022).

93. Piemontese, S., Roscilde, T. & Hama, A. Entanglement complexity of the Rokhsar-Kivelson-sign wavefunctions. *Phys. Rev. B* **107**, 134202. <https://link.aps.org/doi/10.1103/PhysRevB.107.134202> (13 Apr. 2023).
94. Oliviero, S. F., Leone, L. & Hama, A. Transitions in entanglement complexity in random quantum circuits by measurements. *Physics Letters A* **418**, 127721. ISSN: 0375-9601. <https://www.sciencedirect.com/science/article/pii/S0375960121005855> (2021).
95. Wu, Y., Duan, L.-M. & Deng, D.-L. Artificial neural network based computation for out-of-time-ordered correlators. *Phys. Rev. B* **101**, 214308. <https://link.aps.org/doi/10.1103/PhysRevB.101.214308> (21 June 2020).
96. Wang, Z. & Davis, E. J. Calculating Rényi entropies with neural autoregressive quantum states. *Physical Review A* **102**. ISSN: 2469-9934. <http://dx.doi.org/10.1103/PhysRevA.102.062413> (Dec. 2020).
97. Ahmadi, A., Helsen, J., Karaca, C. & Greplova, E. Mutual info fluctuations. <https://gitlab.com/QMAI/papers/mutualfluctuations> (2024).
98. Ahmadi, A., Helsen, J., Karaca, C. & Greplova, E. Mutual info fluctuations. <https://zenodo.org/records/13151079> (2024).
99. Aleksandrowicz, G. *et al.* *Qiskit: An Open-source Framework for Quantum Computing* version 0.7.2. Feb. 2019. <https://doi.org/10.5281/zenodo.2562111>.
100. Developers, C. *Cirq* version v0.12.0. Aug. 2021. <https://doi.org/10.5281/zenodo.5182845>.
101. Pöyhönen, K., Moghaddam, A. G. & Ojanen, T. Many-body entanglement and topology from uncertainties and measurement-induced modes. *Phys. Rev. Res.* **4**, 023200. <https://link.aps.org/doi/10.1103/PhysRevResearch.4.023200> (2 June 2022).
102. Pöyhönen, K., Moghaddam, A. G., Ivaki, M. N. & Ojanen, T. Scalable approach to monitored quantum dynamics and entanglement phase transitions. *arXiv:2406.19052*. <https://arxiv.org/abs/2406.19052> (2024).
103. Gambetta, J. M. *et al.* Characterization of Addressability by Simultaneous Randomized Benchmarking. *Physical Review Letters* **109**. ISSN: 1079-7114. <http://dx.doi.org/10.1103/PhysRevLett.109.240504> (Dec. 2012).
104. Collins, B., Matsumoto, S. & Novak, J. The Weingarten calculus. *Notices of the AMS* **69**, 734–745. <http://dx.doi.org/10.1090/noti2474> (2022).
105. Zhu, H., Kueng, R., Grassl, M. & Gross, D. The Clifford group fails gracefully to be a unitary 4-design. *arXiv preprint arXiv:1609.08172*. eprint: 1609.08172. <https://doi.org/10.48550/arXiv.1609.08172> (2016).
106. Helsen, J., Wallman, J. J. & Wehner, S. Representations of the multi-qubit Clifford group. *Journal of Mathematical Physics* **59**, 072201. <http://dx.doi.org/10.1063/1.4997688> (2018).

107. Gross, D., Nezami, S. & Walter, M. Schur-Weyl Duality for the Clifford Group with applications: Property Testing, a Robust Hudson Theorem, and de Finetti Representations. *Communications in Mathematical Physics*, 1–69. <https://doi.org/10.1007/s00220-021-04118-7> (2021).
108. Montealegre-Mora, F. & Gross, D. Rank-deficient representations in the theta correspondence over finite fields arise from quantum codes. *Representation Theory* **25**, 193–223. <https://doi.org/10.1090/ert/563> (2021).
109. Helsen, J. & Walter, M. Thrifty shadow estimation: Reusing quantum circuits and bounding tails. *Physical Review Letters* **131**, 240602. <https://link.aps.org/doi/10.1103/PhysRevLett.131.240602> (2023).

4

QUANTUM RESOURCES OF QUANTUM AND CLASSICAL VARIATIONAL METHODS

Variational techniques have long been at the heart of atomic, solid-state, and many-body physics. They have recently extended to quantum and classical machine learning, providing a basis for representing quantum states via neural networks. These methods generally aim to minimize the energy of a given ansatz, though open questions remain about the expressivity of quantum and classical variational ansätze. The connection between variational techniques and quantum computing, through variational quantum algorithms, offers opportunities to explore the quantum complexity of classical methods. We demonstrate how the concept of non-stabilizerness, or magic, can create a bridge between quantum information and variational techniques and we show that energy accuracy is a necessary but not always sufficient condition for accuracy in non-stabilizerness. Through systematic benchmarking of neural network quantum states, matrix product states, and variational quantum methods, we show that while classical techniques are more accurate in non-stabilizerness, not accounting for the symmetries of the system can have a severe impact on this accuracy. Our findings form a basis for a universal expressivity characterization of both quantum and classical variational methods.

⁰The work in this chapter has been published as: T. Spriggs* **A. Ahmadi***, B. Chen and E. Greplova, Quantum resources of quantum and classical variational methods, *Accepted at Machine Learning: Science and Technology*, (2025) DOI: [10.1088/2632-2153/adaca2](https://doi.org/10.1088/2632-2153/adaca2)

*indicates equal contribution

4.1. INTRODUCTION

Due to the prohibitive scaling of large scale quantum wavefunctions, approximate methods are typically employed to numerically find ground states and time evolve quantum systems. Classical variational methods have rich track record and span physics intuition driven parametrization of the trial wavefunction [1–5], ansätze capturing specific entanglement properties [6, 7], and, more recently, physics-agnostic wavefunctions based on neural networks [8–13].

In parallel to this progress, quantum variational methods were formulated with the same goal: to capture potentially complicated wavefunctions using a small number of degrees of freedom [14–17]. In this instance, the variational ansatz is formulated as a quantum circuit. Quantum operations in such circuits are then parametrized and the parameters of the quantum gates are updated, using classical optimization techniques, until the energy of the output of the circuit well approximates the energy of the sought-after quantum state.

In search for ground states of specific Hamiltonians, both classical and quantum variational techniques rely on the energy variational principle: the expectation value of the Hamiltonian is evaluated with respect to the trial state and then minimized. The lowest achievable value is then considered a good approximation for the true ground state energy of the system.

Once we optimize the energy of our ansatz, the question arises regarding how well is the quantum state itself represented by our approximate representation. While variational minimization brings the system to the point in Hilbert space with the required energy, it is far from certain that the optimized state will structurally reflect the global properties of the system. In particular, especially long range correlations are known to pose a challenge.

In this work, we assess the expressivity of both quantum and classical variational methods from a quantum computational complexity point of view: we analyze the amount of quantum resources that the variational ansatz expresses when optimized in accordance with the classical energy variational principle.

In quantum computing, one way of assessing quantum resources is to measure how far a given state is from being efficiently and exactly simulated on a classical computer [18]. The quantum operations that allow for efficient, exact classical simulation are elements of the Clifford group. All the other operations are referred to as non-Clifford. To quantify how ‘far’ a given operation is from the Clifford group, a measure called magic, or non-stabilizerness, was introduced [19].

Non-stabilizerness has recently been at the forefront of quantum information literature as more scalable techniques have emerged to quantitatively evaluate it [20–24]. This progress allowed for the first exploration of non-stabilizerness evaluation for tensor networks [22, 25, 26].

At first sight, the notions of non-stabilizerness and classical variational principle are unrelated. One is designed to determine areas of potential quantum-computational advantage, the other to assess performance of classical, few-parameter ansätze. However, a key property we want from a variational ansatz is to faithfully approximate the sought-after state, beyond just its energy. An interesting interplay with quantum information arises: classical variational ansätze are unrestricted by, for example, the Gottesmann-

Knill theorem [18], and are allowed to converge to any point in the Hilbert space that minimize the energy regardless of where the exact solution lies with respect to the Clifford group.

In this work, we perform a systematic benchmark for non-stabilizerness expressivity of classical and quantum variational ansätze using the transverse-field Ising model (TFIM), a common testbed model for variational methods. Specifically, we compare non-stabilizerness expressivity of neural quantum states, matrix product states, and a variational quantum eigensolver. We find that high energy precision is a necessary, but not always sufficient, condition for the few-parameter variational ansätze to express the non-stabilizerness of the model correctly. We observe that quantum variational methods generally show worse performance compared to the state-of-the-art classical methods. In the context of this work it means that even though the ansatz itself is quantum, it is worse at predicting the energy and non-stabilizerness of the exact wavefunction. Moreover, the variations in energy and non-stabilizerness accuracy across multiple repeats are generally much larger for the quantum variational method compared to the results from neural quantum states.

The outline of this paper is as follows. Section 4.2 provides an overview of methods and techniques used in this work: Section 4.2.1 briefly elucidates the specific Hamiltonian with which this work explores, Section 4.2.2 details the three algorithms used for finding the ground state of the given Hamiltonian, and Section 4.2.3 presents the measure of quantum resources that we use to assess the non-stabilizerness of the ground state wavefunctions obtained. Section 4.3 presents the comparison of the ground state energy and non-stabilizerness found using density matrix renormalization group (DMRG), neural quantum states (NQS), and a variational quantum eigensolver (VQE); this comparison focuses on the respective accuracies of different methods compared to exact diagonalization, the interplay between the energy and non-stabilizerness accuracies, and the fluctuations of their solutions with repeated runs. In Section 4.4 we discuss our findings and possible next steps in aligning classical and quantum variational methods.

4.2. METHODS

4.2.1. TRANSVERSE-FIELD ISING MODEL

This paper is focused on parameterized ansätze that approximate the ground state of the transverse-field Ising model (TFIM). The Hamiltonian of this model is defined as

$$H = J \sum \sigma_i^z \sigma_{i+1}^z - h \sum \sigma_i^x. \quad (4.1)$$

In this definition, σ^z and σ^x are the Pauli matrices, J is a constant that dictates the coupling between neighboring spins (we will consider $J < 0$ and thus neighboring spins being aligned is energetically favorable), and h is the transverse magnetic field strength; we are considering the case of periodic boundaries. The basis that will be used to represent the wavefunction will be the spin projections along the z -axis, comprised of either spin up or down relative to this axis. This is also known as the computational basis.

The TFIM begets a phase transition with a critical point in the vicinity of $|h/J| = 1$ [27]. To explore this phase diagram we will find solutions of the ground state with fixed $J = -1$ and varying h over the range of $[0 - 3]$.

4.2.2. PARAMETERIZED QUANTUM STATES

The energy spectrum, dynamics, and a plethora of other observables related to a quantum system are obtainable through the wavefunction, ψ . However, Nature does not grant one access to the wavefunction, nor would it be computationally feasible to store these data for a system larger than a few tens of qubits. The latter complication is due to the exponential increase in the number eigenstates with system size. In this work we employ three different parameterized quantum states that all circumvent these limitations.

Parameterized quantum states can offer two key features. Firstly, by representing the wavefunction as a parameterized function, ψ_{θ} , we can learn a representation of the true wavefunction by learning the parameters θ . Secondly, by restricting the representation such that the number of parameters grows polynomially (rather than exponentially) with the system size, we achieve an efficient representation that makes simulations feasible for larger systems.

4

NEURAL QUANTUM STATES

Beginning with the work of Carleo and Troyer, neural-network-based methods were introduced to act as physics-agnostic, parameterized quantum states known as neural quantum states (NQS) [8]. NQS have shown to be useful in a variety of problems, such as finding the ground state in different quantum systems [13, 28, 29], evolving quantum states through time [8, 30], and simulating quantum circuits [31]. There exist different architectures for the NQS [8–13], for the purpose of this paper, however, we restrict ourselves to a simple case of NQS, namely the restricted Boltzmann machine (RBM) depicted in Figure 4.1.

The RBM has the simple structure of two neural network layers with no intra-layer connections but full inter-layer connectivity: one visible layer consisting of N units and one hidden layer of M units. N must be equal to the number of qubits/particles in the system, whereas there is no formal restriction on M ; the ratio M/N , referred to as α , is often used to convey the size of an RBM. The number of parameters in the RBM is given by $N + \alpha N + \alpha N^2$, and thus for fixed α this scales polynomially with the system size; however, this does not guarantee that the desired state can be represented by this network, in which case the true ground state may still require a number of parameters larger than this. The wavefunction amplitude given by the RBM ansatz is

$$\psi_{\theta}(\mathbf{s}) = \sum_{\mathbf{h}} e^{\sum_j a_j \sigma_j + \sum_i b_i h_i + \sum_{ij} W_{ij} h_i \sigma_j}, \quad (4.2)$$

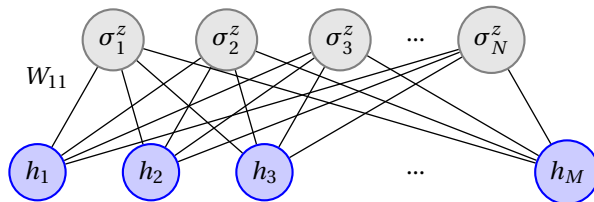


Figure 4.1: A pictorial representation of the restricted Boltzmann machine (RBM) with M hidden neurons and N visible neurons encoding the projection in the σ^z basis.

where $\mathbf{s} = (\sigma_1, \sigma_2, \dots, \sigma_N)$ such that $\sigma_i = \pm 1$ is the spin configuration in z basis; $\mathbf{h} = (h_1, h_2, \dots, h_M)$, with $h_i = \pm 1$, denotes the M hidden spin variables; and the parameters to be optimized are $\boldsymbol{\theta} = \{\mathbf{a}, \mathbf{b}, \mathbf{W}\}$. The full wavefunction can be constructed from

$$|\psi_{\boldsymbol{\theta}}\rangle = \sum_{\mathbf{s}} \psi_{\boldsymbol{\theta}}(\mathbf{s}) |\mathbf{s}\rangle. \quad (4.3)$$

With the specific form of the parameterized quantum state in-hand, what remains is to train this model such that the wavefunction that is represented captures the behavior of the ground state of the Hamiltonian being considered. To do this we will consider the expectation value of the Hamiltonian with respect to the NQS wavefunction, $\langle H \rangle_{\psi_{\boldsymbol{\theta}}} := \langle \psi_{\boldsymbol{\theta}} | H | \psi_{\boldsymbol{\theta}} \rangle$. In line with the variational principle [32], this quantity is bounded from below by the ground state energy and will equal that bound when the NQS represents the ground state wavefunction.

One of the benefits of a parameterized quantum state is that, for a fixed α , the number of free parameters that characterize the wavefunction in Equation (4.1) is polynomial with the number of qubits. This work would be undone if we required the full wavefunction or access to the entire Hilbert space to compute expectation values.

To maintain the efficient, computationally feasible computations of expectation values we use Monte Carlo (MC) sampling alongside so-called *local estimators*. The combination of MC sampling and a variational ansatz is known as variational Monte Carlo (VMC). An excellent outline of the computational efficiencies included in VMC is outlined in [33]. Following the conventions of that work, we can reduce the calculation of the expectation value from a sum over an exponentially large Hilbert space to a statistical expectation of local estimators. Thus reducing

$$\langle \hat{O} \rangle = \frac{\langle \psi_{\boldsymbol{\theta}} | \hat{O} | \psi_{\boldsymbol{\theta}} \rangle}{\langle \psi_{\boldsymbol{\theta}} | \psi_{\boldsymbol{\theta}} \rangle}, \quad (4.4)$$

to the more tractable sum of $\langle \hat{O} \rangle = \langle O_{\text{loc}} \rangle_P$. The local estimator and probability distribution are defined as

$$O_{\text{loc}}(\mathbf{s}) = \sum_{\mathbf{s}'} \langle \mathbf{s} | \hat{O} | \mathbf{s}' \rangle \frac{\langle \mathbf{s}' | \psi_{\boldsymbol{\theta}} \rangle}{\langle \mathbf{s} | \psi_{\boldsymbol{\theta}} \rangle}, \quad (4.5)$$

and

$$P(\mathbf{s}) = \frac{|\langle \psi_{\boldsymbol{\theta}} | \mathbf{s} \rangle|^2}{\sum_{\mathbf{s}'} |\langle \psi_{\boldsymbol{\theta}} | \mathbf{s}' \rangle|^2}, \quad (4.6)$$

respectively. The VMC procedure generates an ensemble of configurations distributed under $P(\mathbf{s})$.

The computation of Equation (4.5) is only efficient if each local estimator contains, at most, a polynomial number (relative to the total number of qubits in the system) of connected states, \mathbf{s}' : equivalent to only having a polynomial number of distinct matrix elements, $\langle \mathbf{s} | \hat{O} | \mathbf{s}' \rangle$. As can be seen from Equation (4.1), the Hamiltonian of the TFIM contains only terms that involve one or two qubits, and thus there are only two or four connected states for each term in the Hamiltonian, regardless of the system size. Therefore, the condition of only a polynomial number of neighboring states is met.

Using this efficient computation for expectation values, we can compute the energy of the NQS for a given set of parameters, $\langle H \rangle_{\psi_{\boldsymbol{\theta}}}$. As the NQS is a differentiable function,

we can also compute the gradient of this energy with respect to each of the network's parameters. As is the common paradigm for training neural networks, the cost function (in this case the energy) and its derivatives are used to tune the parameters until the cost function is minimized. And, as previously mentioned, this will occur when the NQS represents the ground state wavefunction. For this work we used the Python package NetKet [34, 35] which implements the efficient computations laid out here.

For small systems, the entire Hilbert space is not prohibitively large. Therefore, for comparison, we can compute the exact expectation value, $\langle H \rangle_{\psi_\theta}$, rather than having to rely on MC sampling. The effects of exact against MC sampling is mentioned in Appendix 4.8 alongside further details of the RBM architecture. Unless stated otherwise, all RBM data shown in this paper was generated from a network with $\alpha = 5$.

4

DENSITY MATRIX RENORMALIZATION GROUP (DMRG)

A well established, classical approach to finding the smallest eigenvalue of a given Hamiltonian was introduced by White in [36], and is known as DMRG. DMRG is an iterative process of solving smaller matrix inversion problems to eventually invert a larger matrix. If the inversion problem can be written in terms of matrix product states (MPS) and matrix product operators (MPO) then there is an efficient implementation of DMRG [6].

A generic tensor can be represented as an MPS or MPO. However, tensors representing low-entanglement wavefunctions, or local Hamiltonians, can be represented as low-rank MPSs and MPOs respectively. The rank of the MPS is called the bond dimension, D , and can be adjusted during the DMRG procedure to balance between computational efficiency (small D) and allowing for high entanglement (large D). It is common practice to limit the bond dimension to achieve a more efficient representation of the wavefunction [37]. For this work, however, we allowed the DMRG algorithm to grow the bond dimension to as large a value as 100 if there was a significant decrease in energy.

The parameters that get updated in the DMRG algorithm are the elements of the MPS at each node. The way that these parameters are optimized is as follows:

1. An initial, random, set of values is chosen for every element in the MPS $|\psi\rangle$.
2. The MPO representing the Hamiltonian is contracted from both sides by the MPS. This is equivalent to the equation $\langle \psi | H | \psi \rangle = E_0$.
3. A pair of neighboring nodes are chosen and are contracted into a larger tensor; the result is no longer an MPS (this is shown in Figure 4.2(b)). An iterative method is then performed in this subspace (subspace because it is still not the entire Hilbert space) to compute a new tensor that replaces the selected pair but lowering the eigenvalue of the MPS.
4. The altered tensor is then broken back into two tensors using singular value decomposition (SVD) to return $|\psi\rangle$ to an MPS whilst maintaining the lower eigenvalue achieved in step 3.
5. The next neighboring pair of links are chosen and steps 3 and 4 are repeated, systematically moving along the chain of the MPS, until a predefined convergence criterion is met.

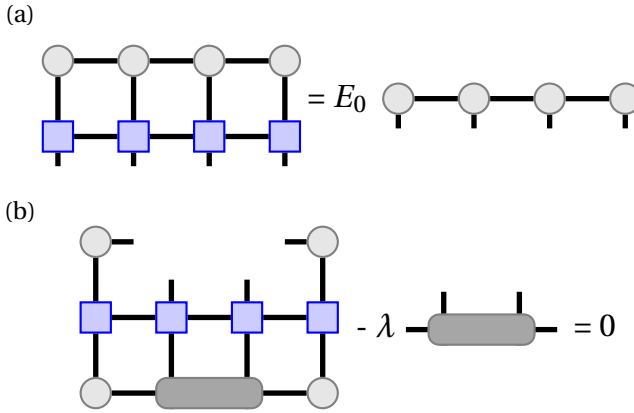


Figure 4.2: Tensor network representation of the eigenvalue equation $H|\psi\rangle = E_0|\psi\rangle$ shown in (a). The gray nodes represent the MPS version of the ground state wavefunction, and the blue nodes are the Hamiltonian converted into an MPO. Panel (b) shows an intermediate stage of the DMRG algorithm which poses a smaller inversion problem whereby a pair of nodes are discarded and only the dark gray node is optimized to minimize λ ; the dark node is created by contracting the two neighbouring nodes at the sites straddled by this dark gray node. The location of the node that is updated sweeps left and right along the chain until some convergence criterion is met.

Upon the termination of the DMRG algorithm, one is left with an MPS that represents the ground state wavefunction, and the ground state energy. For this work we used the implementation provided by ITensor [38, 39].

VARIATIONAL QUANTUM EIGENSOLVER

An alternate approach to classically approximating the wavefunction is to use a parameterized quantum circuit to prepare a trial wavefunction and then use classical optimization to vary the parameters until a desired wavefunction is reproduced. When this process is applied to finding the ground state wavefunction it is known as a variational quantum eigensolver (VQE) [40].

The formulation of VQE spearheaded the development of a rich field of variational quantum algorithms (VQAs) [14–17]. We will first outline the VQE algorithm and then explore some of the challenges related to its implementation.

One begins the VQE procedure with an easily prepared initial state wavefunction, $|\psi_{in}\rangle$, to which one applies a sequence of unitary operators, or *gates*, that comprise the parameterized quantum circuit. The output of the circuit will be a parameterized wavefunction $|\psi_{\theta}\rangle$. Thus, with the quantum circuit denoted by the unitary matrix $\mathcal{U}(\theta)$, the parameterized wavefunction generated by the quantum circuit reads

$$|\psi_{\theta}\rangle = \mathcal{U}(\theta) |\psi_{in}\rangle. \quad (4.7)$$

An example of a parameterized quantum circuit is depicted in Figure 4.3; the circuit used for this work is four contiguous layers of the circuit shown, repeated in series. The values of the parameterized gates are varied to find the minimum of the expectation value of the Hamiltonian, Equation (4.1), with respect to $|\psi_{\theta}\rangle$, denoted $\langle H \rangle_{\psi_{\theta}}$ as in Section 4.2.2.

For this work, given the system sizes simulated, a classical simulation of the quantum circuit was performed using PennyLane [41]. There are, however, implementations on quantum hardware [42–47].

Given that this work presents classical simulations of quantum circuits, access is granted to the full wavefunction rather than just projective measurements. This limits the size of the system that can be simulated but the effects of using the full wavefunction rather than projective measurements to estimate $\langle H \rangle_{\psi_{\theta}}$ is presented in Appendix 4.9.

Considering, still, the case of a classical simulation, free from hardware-related noise and imperfections, there exist fundamental limitations in the VQE algorithm. Firstly, common to all variational algorithms that require a predetermined ansatz, including those in this Section, is that there is no guarantee that the ansatz in question (the quantum circuit) is expressive enough to represent the function it hopes to capture (the wavefunction) using a polynomial number of parameters. This is especially true for strongly correlated quantum systems [48]. Broadly speaking there are two approaches to circuit design for VQEs: problem-specific ansätze and hardware-efficient ansätze (HEA). In the former regime, one constructs the ansatz from elements that one hopes captures known behaviors of the solution. The latter attempts to create a more general, easier to implement on quantum hardware, ansatz built from simple gates; this is where the ansatz for this work resides. Neither approach, however, is guaranteed to produce an ansatz that can represent the desired function, and thus the algorithm can converge on a sub-optimal solution. Secondly, VQAs have been shown to be especially prone to so-called *barren plateaus* [49–52]. The phenomenon of a barren plateau is when the gradient of the loss function with respect to the variational parameters vanishes exponentially with the number of qubits in the system. This means that training the variational parameters becomes exceptionally difficult for even modest sized systems - even with gradient-free optimizers [53] - as the true minimum becomes exponentially hard to find. Thirdly, and even affecting small systems, the loss landscape for VQEs often contains many local minima, and therefore even without vanishing gradients there can be inherent difficulties training these quantum circuits. The alleviation of these difficulties is ongoing, with a good survey available [54], the references therein, as well as [55–58].

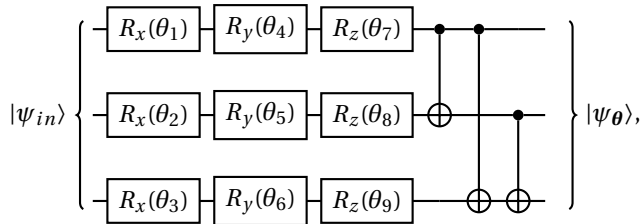


Figure 4.3: A single layer of the VQE ansatz that evolves an initial state, $|\psi_{in}\rangle$ to a parameterized state $|\psi_{\theta}\rangle = \mathcal{U}(\theta)|\psi_{in}\rangle$. The output state is then used as a trial for the ground state and the expectation value of the Hamiltonian is computed. The parameters, θ , which are angles of the rotation gates, are varied to minimize this expectation value. Diagram created using [59].

4.2.3. NON-STABILIZERNESS

The non-stabilizer, also commonly called magic, is known to be the resource for quantum computation [60]. It is known, from the Gottesman-Knill theorem [18], that Clifford circuits (that is, circuits comprised entirely of gates in the Clifford group) can be efficiently simulated on classical hardware. Therefore, in order to achieve a quantum advantage we need to go beyond the Clifford group, which means adding non-Clifford operations. Adding non-Clifford operations means increasing non-stabilizer. The non-stabilizer is measured by different methods, such as the robustness of magic [61–63], the min-relative entropy [64] and stabilizer entropies [20, 65].

For the purpose of this work, we use the 2-Renyi stabilizer entropy, M_2 , since it is easily calculable for small systems and it has been shown to be a magic monotone [66, 67]. The 2-Renyi stabilizer entropy for pure states is defined as

$$M_2(|\psi\rangle) = -\log \sum_{P \in \mathcal{P}_N} \frac{\langle \psi | P | \psi \rangle^4}{2^N}, \quad (4.8)$$

where \mathcal{P}_N is the set of all N -qubit Pauli strings and $|\psi\rangle$ can either be a parameterized representation of the quantum state, or the exact result found through exact diagonalization (ED).

Recent studies have also explored the non-stabilizer in random circuits [24, 68], and many-body quantum systems such as the transverse-field Ising model [21, 69–71], the Potts model [26, 72], chaotic models [73], and the class of models known as generalized Rokhsar-Kivelson systems [72]. It has also been shown that in special cases there can be a significant reduction of Equation (4.8) into a form that scales only polynomially in the system size [74].

We are motivated by the observation that classical simulatability from the Clifford group point of view does not enter generic formulation of quantum or classical variational problems. We use Equation (4.8) to evaluate the non-stabilizer of exact transverse-field Ising (TFI) ground states as well as its approximations determined using the methods described above, and compare the performance of these methods from the non-stabilizer perspective across the phase diagram.

4.3. RESULTS

4.3.1. QUANTUM AND CLASSICAL MODEL ACCURACY

The simplest comparison between the three aforementioned methods is to compare them each to the results obtained from exact diagonalisation (ED).

Figure 4.4 shows the energy and magic obtained from ED and all three variational approaches applied to an 8 qubit TFI system. Both the values themselves (top) and the accuracies with respect to the ED result (bottom) are shown. From the left-hand panels of this figure it is clear that there is a hierarchy in terms of energy accuracy: DMRG is more accurate than the RBM, which is in-turn more accurate than the VQE. From the right-hand panels, however, the magic accuracy does not quite follow this hierarchy; beyond $h = 1$ the accuracies follow that of the energy, but approaching criticality from below there are signs that although the DMRG and RBM converged on states with more accurate energy than the VQE, the magic accuracies of all three are similar. It should be

noted that in this region of the phase diagram the ground state of the TFIM is known to be degenerate (or near-degenerate, depending on finite system size effects and the specific value of h). The magic of the states within the degenerate eigenspace can differ greatly and thus the accuracy in energy does not constrain the state to have a similar magic to the ED result. One possible way to circumvent this would be to use ansätze that are aware of the symmetry that leads to this degeneracy. We will return to this in Section 4.3.2 as this highlights an important case of when energy accuracy alone is not sufficient for assessing the quality of the approximate ground state.

Figure 4.5 shows the energy and magic accuracy of the same methods for a 12 qubit system. Due to the increased computational cost of simulating a larger system, the h spacing is increased. Once again the accuracy in energy follows the ordering noted in Figure 4.4. Also in a similar fashion to the 8 qubit simulation, the accuracy of the magic does not follow this trend over the entire phase diagram.

From Figures 4.4 and 4.5 we can conclude that energy accuracy and magic accuracy appear strongly correlated for most of the phase diagram, we can also say that, for these implementations, DMRG outperforms RBM which outperforms VQE when it comes to energy accuracy. In Appendix 4.9 we present the energy and magic accuracy computed for a 4 qubit system. In this smaller setting the VQE and RBM perform similarly. Despite the smaller system size, the same pattern in energy and magic accuracies can be seen: they appear correlated except for the low h region.

For clarity of the figures in this Section, the statistical fluctuations of the data were not shown. In Section 4.3.3 will explore the statistical uncertainties to measure the robustness of these methods and further probe the correlations between the energy and magic of the ground state solutions found.

4.3.2. NON-STABILIZERNESS AND SYMMETRY

By and large, in the figures from Section 4.3.1, where we selected best performing hyperparameter configuration for MPS, VQE and RBM, the accuracy of the energy appears to be directly linked to the accuracy of the magic. One may expect that by minimizing the energy towards the ground state then one ends up nearby in the Hilbert space and thus the magic of the solution is likely similar. However, the exception of the degenerate ground states at low h was noted. This section will explore the interplay between the accuracy of energy and magic further, paying careful attention to the degeneracy of the solutions in the small h region.

The Hamiltonian of the TFIM exhibits a global \mathbb{Z}_2 symmetry, meaning that the energy of two configurations that differ by flipping every single spin is the same. The ground states of this Hamiltonian do not have to respect this symmetry to still achieve the smallest possible energy. This leads to a range of different, but energetically equivalent, variational ground states. Importantly, the magic of these degenerate states can differ greatly. To give an indication of this, consider the $h = 0$ case and any superposition of the all up and all down states (all of which have the same energy): an equal superposition has zero magic as it can be prepared using only Clifford operations acting on the all up state, however, for other unequal superpositions it is not guaranteed that one could prepare this state using only Clifford operations and thus it can have non-zero magic. To circumvent this, one can explicitly encode the global \mathbb{Z}_2 symmetry into the ansatz. We will explore

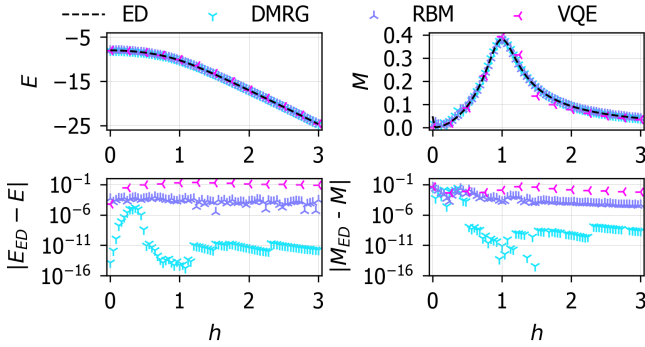


Figure 4.4: (top) The energy (left) and magic (right) of the ground state wavefunction for the 8 qubit transverse field Ising model at a range of transverse-field strengths, h . (bottom) The accuracy of the estimates of energy (left) and magic (right) from the three methods presented in Section 4.2.2 relative to the result from exact diagonalization (ED). Each datum for the RBM and VQE is the mean of 10 repeats and the statistical errors are omitted for clarity; see Figure 4.7 for error estimates.

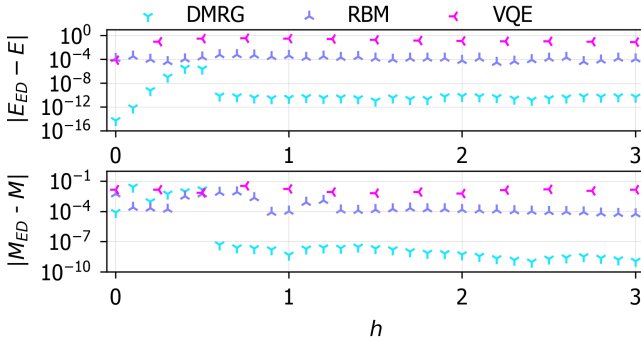


Figure 4.5: The accuracy of the estimates of energy (left) and magic (right) from the three methods presented in Section 4.2.2 relative to the result from exact diagonalization (ED). These results are for a 12 qubit system, shown at a range of transverse-field strengths, h . Each datum for the RBM and VQE is the mean of 10 repeats and the statistical errors are omitted for clarity; see Figure 4.7 for error estimates.

this in the context of the RBM.

For such a small, discrete symmetry group, one can make a symmetric (or \mathbb{Z}_2 -invariant) RBM simply by feeding both the configuration \mathbf{s} and $-\mathbf{s}$ through the RBM defined in Equation (4.2) and taking the mean of each amplitude as the amplitude of the configuration \mathbf{s} (and thus also of $-\mathbf{s}$). All other details of the training and RBM architecture are unchanged.

To explore the intuition that energy accuracy alone is a good probe of whether or not the approximate ground state is similar to the true ground state, we compare it with two other figures of merit. Firstly, as in the other sections of this work, we compare with the magic accuracy, but then we also show the infidelity of the approximate ground state with the ground state found through ED. We define the infidelity of the normalized approximate state $|\psi_\theta\rangle$ with the normalized ED result $|\psi_{\text{ED}}\rangle$ as

$$I = 1 - |\langle \psi_\theta | \psi_{\text{ED}} \rangle|^2. \quad (4.9)$$

Figure 4.6 shows the energy accuracy, magic accuracy, and infidelity of the RBM and symmetric RBM ground states with respect to the ED results. The data are shown for three sizes of RBM, denoted by $\alpha = 1, 3,$ and $5,$ to explore if the increase in the number of parameters allows the network to learn this symmetry without the need for the explicit construction of the symmetric RBM.

From Figure 4.6 it is clear that the energy accuracy of the RBM and the symmetric RBM is similar. However, the effect on the magic accuracy and infidelity in the $0 \leq h \leq 1$ range is stark: the symmetric RBM outperforms the conventional RBM by up to five orders of magnitude. There does not seem to be much change to the rest of the h -range considered. Importantly, though, is that this five orders of magnitude improvement, indicating a significantly better ground state solution, is completely imperceptible when considering the energy accuracy alone.

The effect of increasing the size of the RBM, through increasing $\alpha,$ is one of a mild increase in quality of all metrics, with the exception of the small h region for the conventional RBM. Interestingly, this is the area that is most plagued by the effect of the degenerate ground states, and thus the extra parameters do not account for the symmetry. This means that just using a larger neural network was not enough to overcome the fact that energy accuracy alone is insufficient for the ansatz to fully approximate the non-stabilizerness of the ground state.

4.3.3. FLUCTUATIONS IN QUANTUM AND CLASSICAL SOLUTIONS

One theme that this work aims to shed some light onto is the representativeness of a ground state found through energy minimization alone. Magic is used as a second axis to ascertain how well the approximate state represents the true ground state. In this section we will explore how similar in magic repeated energy minimizations are, probing the landscape around, what one hopes to be, the energy minimum containing the true ground state.

Figure 4.7 shows the statistical error from 10 repeated ground state searches, in energy (left) and magic (right), for 8 qubit (top) and 12 qubit (bottom) simulations. The comparison is shown only for the VQE and RBM methods. From this figure it can be seen that the fluctuations in energy are almost always smaller for the RBM compared to

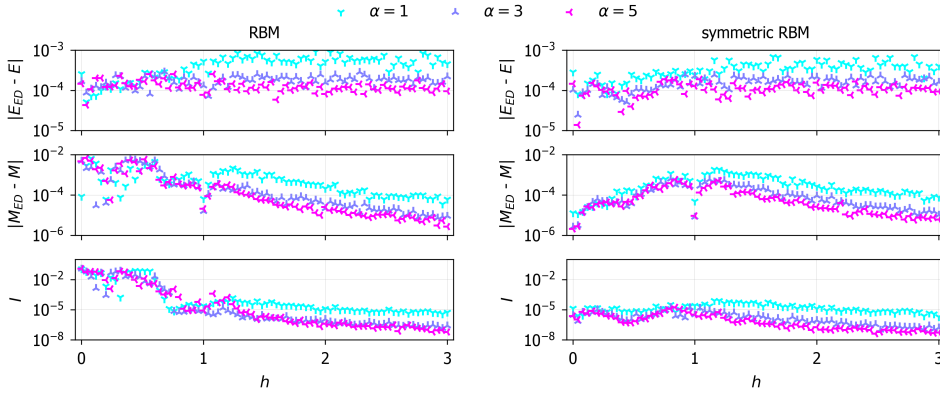


Figure 4.6: The energy accuracy (top), magic accuracy (middle), and infidelity (bottom) of the variational ground states compared to the ED results. The ansatz used for the NQS is either a conventional RBM defined in Equation (4.2) (left) or the symmetric RBM as described in Section 4.3.2 (right). These results are for an 8 qubit system, shown at a range of transverse-field strengths, h , with each datum being the average of 10 repeats with the statistical errors omitted for clarity.

the VQE. The exception to this is the $h = 0$ point; the ground state of the Hamiltonian here is, in fact, the initial state fed into the VQE and thus this is perhaps not surprising. The fact that the VQE can, in very high and low field, reach almost the level of consistency of the RBM yet it cannot minimize the energy as well suggests that perhaps this is a limitation of the expressivity of the ansatz.

In Section 4.3.2 we already noted the difficulties with an RBM that is not aware of the symmetries of the system. This is reflected here in the fluctuations of the magic; interestingly this is less pronounced in the 12 qubit simulation. Those data notwithstanding, the fact that the fluctuations of the magic are very small does suggest that each approximate ground state, when near to the minimum in energy, is also in a region with similar magic.

4.4. DISCUSSION AND CONCLUSIONS

In this work we set up the framework to reconcile classical simulatability notions of quantum resource theory with the formalism of classical variational techniques. We used non-stabilizerness, a quantity that measure how far is a given state from being classically simulatable in a sense of Gottesmann-Knill theorem, as a figure of merit for quality of classical variational approximation of a quantum state. Specifically, we assessed non-stabilizerness expressivity for three qualitatively different types of variational ansätze: tensor networks, neural networks and variational quantum circuits.

We found, that when comparing the best model (in terms of energy performance) for each method with exact diagonalization, on average, there is a general trend for better energy to correspond to better approximation in non-stabilizerness. This is an encouraging observation that suggests that the state reconstructed as a result of classical variational procedure has a complexity structure that represents the exact quantum solution

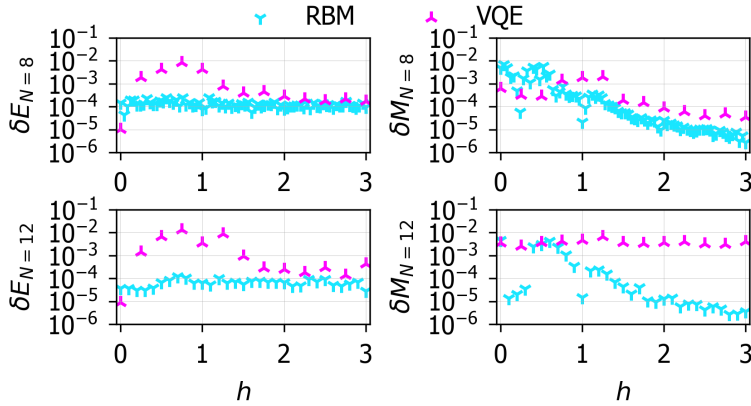


Figure 4.7: The statistical errors of the energy (left) and magic (right) against the transverse-field strength, h , across the 10 repeats of the ground state optimization procedure using an RBM and VQE. Data are shown for 8 (top) and 12 (bottom) qubits, with the corresponding mean values reported in Figures 4.4 and 4.5 respectively.

reasonably well. At the same time, we immediately noted that this correspondence is far from straightforward and universal. For example, an RBM constructed to share the symmetry of the Hamiltonian led to ground states with up to four orders of magnitude higher accuracy in non-stabilizerness than a conventional RBM, with no change in the energy accuracy.

We hope this work will be a stepping stone towards starting a closer dialogue between quantum computing and classical variational perspectives on solving the quantum many-body problem, and more specifically, on how the quality of the results is assessed. We set up a system of benchmarks for small system sizes ($N = 8, 12$) and noted a number of similarities and differences between accuracies in non-stabilizerness and in energy. The possible next steps include obtaining large scale benchmarks for each of the methods we tested here. The current limitation of system size is the calculation of the non-stabilizerness, however, the first impressive step towards this calculation at scale has already been taken in Ref. [22] for matrix product state representation of a wavefunction. It would be interesting to see how the smaller system observations translate into a large scale benchmark. Further ahead, one could think of how to embed non-stabilizerness optimization iterations into energy-based quantum and classical variational models.

4.5. DATA AND CODE AVAILABILITY

A GitLab repository containing this project is available at [75]. All the data and code to analyze them is available at [76].

4.6. AUTHOR CONTRIBUTIONS

EG designed the project with input from TS and AA. TS and AA jointly performed neural network and ED simulations. TS and BC performed the VQE simulations. TS performed

the tensor network simulations. AA provided the non-stabilizerness calculation. TS, AA, BC, and EG analyzed and interpreted the data. TS, EG, and AA co-wrote the manuscript. EG supervised the project.

4.7. ACKNOWLEDGMENTS

We are thankful for instructive discussions on DMRG with B. M. La Rivière, J. Soto Garcia, and P. S. Tarabunga. We also thank A. Valenti, J. Nys, and S. Khaleefah for fruitful conversations regarding NQS. This work is part of the project Engineered Topological Quantum Networks (Project No.VI.Veni.212.278) of the research program NWO Talent Programme Veni Science domain 2021 which is financed by the Dutch Research Council (NWO). This publication is also part of the project Optimal Digital-Analog Quantum Circuits with file number NGF.1582.22.026 of the research programme NGF-Quantum Delta NL 2022 which is (partly) financed by the Dutch Research Council (NWO) and the Dutch National Growth Fund initiative Quantum Delta NL.

4.8. APPENDIX-1: NQS ARCHITECTURE

There are a vast number of hyperparameters and architectural configurations that one can tweak to alter the training of the NQS. To arrive at the specific RBM presented in Figures 4.4 and 4.5 we explored: the size of the ansatz, using the entire Hilbert space for the computation of expectation values, and the inclusion of the stochastic reconfiguration (SR) preconditioner as part of the parameter optimization routine. Other avenues of exploration could include introducing a representation learning step to map the configurations from projective measurements to continuous vectors [11] or other neural network architectures [8–13], but these lie outside the scope of this work. This appendix will also cover the stopping criterion used to estimate when the ground state is approximately reached.

The effects of a larger RBM were shown in Figure 4.6, from this it can be seen that there is a mild improvement in all metrics with increased model size. The drawback, however, is in the time taken to train the larger model: more parameters leads to increased training time. Given that the improvement is larger from $\alpha = 1$ to $\alpha = 3$ than it is between $\alpha = 3$ and $\alpha = 5$, alongside the increased training time, we chose to stop at $\alpha = 5$.

In Section 4.2.2 we mentioned the approximations made as part of the VMC procedure, notably, as part of the computation of the expectation value, the reduction of the sum over the entire Hilbert space (Equation (4.4)) to the Monte Carlo estimate sampled from Equation (4.6). We tested the energy and magic accuracy for an 8 qubit system using both the full expectation value and the Monte Carlo estimate to train the RBMs. We found that, across the entire range of h , the fluctuations between repeated optimizations of the exact expectation solutions were lower than the Monte Carlo sampled counterparts, and the energy accuracies were smoother as a function of h for the exact expectation method, too. Both effects were, however, mild, and as the exact expectation is much more computationally expensive (it scales exponentially with the system size), we chose to remain with the Monte Carlo sampling.

Finally, for the configuration of the RBM, we tested the inclusion of the SR preconditioner.

tioner. Introduced to VMC in [77, 78], SR alters the gradient obtained from an optimizer in a way that accounts for the curvature of the optimization landscape that is caused only by the ansatz. This can be seen as an application of what is known as the natural gradient in the wider machine learning community [79, 80]. Put simply, the inclusion of SR lead to better energy and magic accuracies of the ground states found.

During the optimization of the RBM parameters one must establish a point at which to stop. For this work we considered the training to be done when the relative change in energy did not improve by more than 10^{-7} for 500 consecutive epochs. This can be easily implemented using the `callbacks.EarlyStopping` function from `NetKet`.

We used the ADAM [81] optimizer and 1,000 (5,000) samples for the MC estimates of expectation values for the 8 (12) qubit systems for all of the RBM results presented in this work.

4.9. APPENDIX-2: VQE ARCHITECTURE

Whilst, in theory, VQE is a Hamiltonian-agnostic and flexible algorithm, there are optimizations that can be made in its implementation. In a similar fashion to Appendix 4.8, this section will explore the choices made when exploring the implementation of the VQE: the number of layers in the ansatz, the method for computing the expectation value of the Hamiltonian, and the optimizer. It will also elucidate the stopping criteria used.

Figure 4.3 shows a single layer of the VQE ansatz used in this work. We explored using up to four layers of this as the ansatz and found that the energy and magic accuracies improved with more layers, however, interestingly the performance of one and two layers were similar, as were three and four layers. The training time increases with each added layer and therefore we chose not to go beyond four layers, using four layers as the final ansatz.

Given that this VQE implementation was performed using a classical simulation of a quantum circuit, we could compute the expectation value of the Hamiltonian two ways: either using projective measurements of the final state or by exact computation (exploiting the full wavefunction of the final state that is only easily accessible in classical simulations and not in real quantum experiments). We tested using both methods to compute the expectation value of the Hamiltonian during training and found no significant difference between the two sets of ground states found, neither in energy nor magic. However, the time taken for the ground state search when using measured expectations was up to three orders of magnitude longer than when using exact expectations (up from 10^2 to 10^5 seconds). This could be caused by several things, the two that seem most pertinent to mention are related to the gradient of the expectation of the Hamiltonian with respect to the circuit parameters. Firstly, as the projective measurement step of a quantum circuit is not differentiable, the gradient was estimated using the parameter-shift rule [82, 83] which requires multiple evaluations of the circuit; this is in contrast to the exact case which only required a single execution to compute the value and gradient of the expectation value. Secondly, as an estimation of the expectation value can only be as accurate, or less accurate, than the exact value, the estimations of the gradient of the expectation value with respect to the circuit angles can only be equal to, or less accurate, than the exact case. Given this, then, it is natural to assume that with likely many sub-

optimal estimations of the gradient, the optimization procedure would take longer and require more evaluations of the quantum circuit. Both of these factors will contribute to the increased runtime of the VQE procedure. Given the lack of clear improvement by either approach, and as this paper does not extend to system sizes beyond the range of what is classically simulatable, we chose to use the exact expectation value for the VQE procedure for significantly more efficient use of computational resources.

To assess the point at which we stop training the quantum circuit we implemented a two-step stopping criteria. Firstly, to consider a single instance of a ground state to have been found we require that three consecutive epochs give the same energy to within 10^{-6} , but then we also require that if the whole VQE is reinitialised then the next instance must not differ from the previous by more than a relative change of 10^{-4} in the energy. The training of the quantum circuit was less stable and led to larger fluctuations in energy than for the RBM, and thus the stopping criterion for the single instance is less strict, but the problem of local minima in the search space was more common here and thus the second part of the stopping criteria was added.

There is a large community interest in alleviating the problem of barren plateaus in quantum machine learning applications. Specifically to VQEs, the authors in [84] explored the effect of using three different optimizers: Broyden-Fletcher-Goldfarb-Shanno (BFGS) [85–88], ADAM [81], and the natural gradient [79, 80] to avoid the problem of local minima in the variational landscape. Here we consider the energy accuracy of an 8 qubit energy minimization of a VQE for four different optimizers: ADAM, BFGS, SPSA [89], and simulated annealing [90]. This is a mix of gradient- and non-gradient-based optimizers: BFGS and ADAM were chosen to cover those of interest for avoiding local minima, SPSA for its utility with applications on quantum hardware [44], and annealing as a second non-gradient based approach as this avoids the use of the parameter-shift rule. The ansatz chosen for these optimizations is the three-layer version of the ansatz depicted in Figure 4.3. The number of layers was reduced to three because the annealing optimizer consistently failed to converge for a four-layer ansatz. Figure 4.8 shows the energy accuracies achieved from 10 repeated energy minimizations of the TFI Hamiltonian for each of the chosen optimizers. From this we can see that both BFGS and ADAM

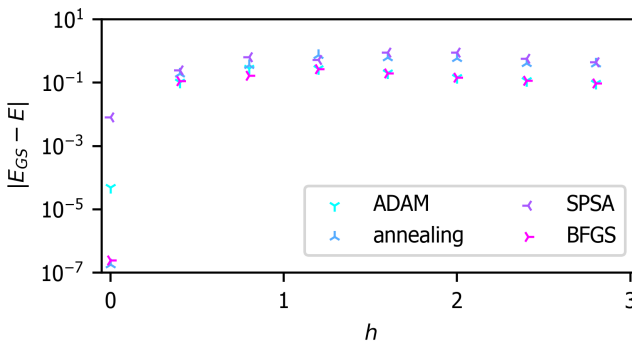


Figure 4.8: Energy accuracy against transverse-field strength for a three-layer VQE ansatz, shown for a range of optimizers used in the energy minimization procedure. All data are for an 8 qubit simulation.

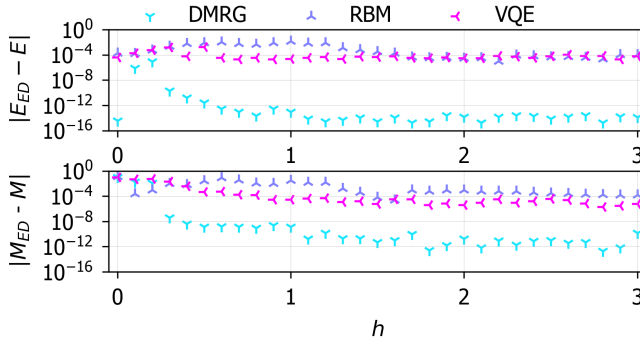


Figure 4.9: The energy accuracy (top) and magic accuracy (bottom) against transverse-field strength for a 4 qubit simulation. Each datum is the average over 10 minimizations.

4

perform the best but there is a very quick degradation of performance with increased transverse field strength, h . As concluded by the authors of Ref. [84], both ADAM and BFGS struggle to scale to systems with a large number of parameters; for the ansatz used here there are 72 free parameters, much larger than the upper limit of 42 that they propose. BFGS especially struggles to scale to larger systems. For this reason, all other VQE data shown in this work uses ADAM as the optimizer. As previously mentioned, reducing the number of layers in the ansatz led to worse energy accuracies, so we will now explore the other way to reduce the number of parameters: a smaller system size.

To explore a regime where the VQE optimization maintains a flexible and expressive ansatz, but with fewer variational parameters, we will consider a 4 qubit TFI system. Exactly as done in Section 4.3.1, Figure 4.9 shows the accuracies in energy and magic of the VQE, RBM, and DMRG algorithms. Unlike in Figures 4.4 and 4.5, however, the energy accuracy of the VQE is better than that of the RBM. This shows that the VQE is able to achieve accurate ground state energies, but Figures 4.4 and 4.5 show that this does not easily scale to larger systems with our current implementation. It should also be noted that in Figure 4.9 we can still see that the accuracy in energy does not always correlate with accuracy in magic.

BIBLIOGRAPHY

1. Jastrow, R. Many-Body Problem with Strong Forces. *Phys. Rev.* **98**, 1479–1484. <https://link.aps.org/doi/10.1103/PhysRev.98.1479> (5 June 1955).
2. Gutzwiller, M. C. Effect of Correlation on the Ferromagnetism of Transition Metals. *Phys. Rev. Lett.* **10**, 159–162. <https://link.aps.org/doi/10.1103/PhysRevLett.10.159> (5 Mar. 1963).
3. Gutzwiller, M. C. Effect of Correlation on the Ferromagnetism of Transition Metals. *Phys. Rev.* **134**, A923–A941. <https://link.aps.org/doi/10.1103/PhysRev.134.A923> (4A May 1964).
4. Gutzwiller, M. C. Correlation of Electrons in a Narrow s Band. *Phys. Rev.* **137**, A1726–A1735. <https://link.aps.org/doi/10.1103/PhysRev.137.A1726> (6A Mar. 1965).
5. Bardeen, J., Cooper, L. N. & Schrieffer, J. R. Theory of Superconductivity. *Phys. Rev.* **108**, 1175–1204. <https://link.aps.org/doi/10.1103/PhysRev.108.1175> (5 Dec. 1957).
6. Schollwöck, U. The density-matrix renormalization group in the age of matrix product states. *Annals of Physics* **326**. January 2011 Special Issue, 96–192. ISSN: 0003-4916. <https://www.sciencedirect.com/science/article/pii/S0003491610001752> (2011).
7. Perez-Garcia, D., Verstraete, F., Cirac, J. I. & Wolf, M. M. PEPS as unique ground states of local Hamiltonians. *arXiv preprint arXiv:0707.2260* (2007).
8. Carleo, G. & Troyer, M. Solving the quantum many-body problem with artificial neural networks. *Science* **355**, 602–606. eprint: <https://www.science.org/doi/pdf/10.1126/science.aag2302>. <https://www.science.org/doi/abs/10.1126/science.aag2302> (2017).
9. Choo, K., Neupert, T. & Carleo, G. Two-dimensional frustrated $J_1 - J_2$ model studied with neural network quantum states. *Phys. Rev. B* **100**, 125124. <https://link.aps.org/doi/10.1103/PhysRevB.100.125124> (12 Sept. 2019).
10. Hibat-Allah, M., Ganahl, M., Hayward, L. E., Melko, R. G. & Carrasquilla, J. Recurrent neural network wave functions. *Phys. Rev. Res.* **2**, 023358. <https://link.aps.org/doi/10.1103/PhysRevResearch.2.023358> (2 June 2020).
11. Viteritti, L. L., Rende, R. & Becca, F. Transformer Variational Wave Functions for Frustrated Quantum Spin Systems. *Phys. Rev. Lett.* **130**, 236401. arXiv: [2211.05504](https://arxiv.org/abs/2211.05504) [[cond-mat.dis-nn](https://arxiv.org/abs/2211.05504)] (2023).
12. Luo, D., Carleo, G., Clark, B. K. & Stokes, J. Gauge Equivariant Neural Networks for Quantum Lattice Gauge Theories. *Phys. Rev. Lett.* **127**, 276402. arXiv: [2012.05232](https://arxiv.org/abs/2012.05232) [[cond-mat.str-el](https://arxiv.org/abs/2012.05232)] (2021).

13. Roth, C. & MacDonald, A. H. *Group Convolutional Neural Networks Improve Quantum State Accuracy* 2021. arXiv: 2104.05085 [quant-ph].
14. Cerezo, M. *et al.* Variational quantum algorithms. *Nature Reviews Physics* **3**, 625–644 (2021).
15. Kremenetski, V., Hogg, T., Hadfield, S., Cotton, S. & Tubman, N. Quantum Alternating Operator Ansatz (QAOA) Phase Diagrams and Applications for Quantum Chemistry. arXiv 2021. *arXiv preprint arXiv:2108.13056*.
16. Moll, N. *et al.* Quantum optimization using variational algorithms on near-term quantum devices. *Quantum Science and Technology* **3**, 030503 (2018).
17. Yao, Y.-X. *et al.* Adaptive variational quantum dynamics simulations. *PRX Quantum* **2**, 030307 (2021).
18. Gottesman, D. The Heisenberg representation of quantum computers. *arXiv preprint quant-ph/9807006*. <https://www.osti.gov/biblio/319738> (June 1998).
19. Bravyi, S. & Kitaev, A. Universal quantum computation with ideal Clifford gates and noisy ancillas. *Phys. Rev. A* **71**, 022316. <https://link.aps.org/doi/10.1103/PhysRevA.71.022316> (2 Feb. 2005).
20. Haug, T., Lee, S. & Kim, M. S. Efficient stabilizer entropies for quantum computers. *arXiv 2305.19152* (2023).
21. Haug, T. & Piroli, L. Quantifying nonstabilizerness of matrix product states. *Phys. Rev. B* **107**, 035148. <https://link.aps.org/doi/10.1103/PhysRevB.107.035148> (3 Jan. 2023).
22. Tarabunga, P. S., Tirrito, E., Banuls, M. C. & Dalmonte, M. Nonstabilizerness via matrix product states in the Pauli basis. *arXiv:2401.16498*. <https://doi.org/10.48550/arXiv.2401.16498> (2024).
23. Lami, G. & Collura, M. Nonstabilizerness via Perfect Pauli Sampling of Matrix Product States. *Phys. Rev. Lett.* **131**, 180401. <https://link.aps.org/doi/10.1103/PhysRevLett.131.180401> (18 Oct. 2023).
24. Ahmadi, A. & Greplova, E. Quantifying non-stabilizerness via information scrambling. *SciPost Phys.* **16**, 043. <https://scipost.org/10.21468/SciPostPhys.16.2.043> (2024).
25. Frau, M., Tarabunga, P., Collura, M., Dalmonte, M. & Tirrito, E. Nonstabilizerness versus entanglement in matrix product states. *Physical Review B* **110**, 045101 (2024).
26. White, C. D., Cao, C. & Swingle, B. Conformal field theories are magical. *Physical Review B* **103**. ISSN: 2469-9969. <http://dx.doi.org/10.1103/PhysRevB.103.075145> (Feb. 2021).
27. Sachdev, S. *Quantum phases of matter* (Cambridge University Press, 2023).
28. Nomura, Y. & Imada, M. Dirac-Type Nodal Spin Liquid Revealed by Refined Quantum Many-Body Solver Using Neural-Network Wave Function, Correlation Ratio, and Level Spectroscopy. *Phys. Rev. X* **11**, 031034. <https://link.aps.org/doi/10.1103/PhysRevX.11.031034> (3 Aug. 2021).

29. Astrakhantsev, N. *et al.* Broken-Symmetry Ground States of the Heisenberg Model on the Pyrochlore Lattice. *Phys. Rev. X* **11**, 041021. <https://link.aps.org/doi/10.1103/PhysRevX.11.041021> (4 Oct. 2021).
30. Gutiérrez, I. L. & Mendl, C. B. Real time evolution with neural-network quantum states. *Quantum* **6**, 627. ISSN: 2521-327X. <https://doi.org/10.22331/q-2022-01-20-627> (Jan. 2022).
31. Medvidović, M. & Carleo, G. Classical variational simulation of the Quantum Approximate Optimization Algorithm. *npj Quantum Information* **7**. <https://doi.org/10.1038/s41534-021-00440-z> (June 2021).
32. Becca, F. & Sorella, S. *Quantum Monte Carlo Approaches for Correlated Systems* (Cambridge University Press, 2017).
33. Medvidović, M. & Moreno, J. R. Neural-network quantum states for many-body physics. arXiv: [2402.11014](https://arxiv.org/abs/2402.11014) [[cond-mat.dis-nn](https://arxiv.org/abs/2402.11014)] (Feb. 2024).
34. Carleo, G. *et al.* NetKet: A Machine Learning Toolkit for Many-Body Quantum Systems. *SoftwareX*, 100311. <http://www.sciencedirect.com/science/article/pii/S2352711019300974> (2019).
35. Vicentini, F. *et al.* NetKet 3: Machine Learning Toolbox for Many-Body Quantum Systems. *SciPost Phys. Codebases*, **7**. [https://scipost.org/10.21468/SciPostPhysCodeb.7\(2022\)](https://scipost.org/10.21468/SciPostPhysCodeb.7(2022)).
36. White, S. R. Density matrix formulation for quantum renormalization groups. *Phys. Rev. Lett.* **69**, 2863–2866 (1992).
37. Cirac, J. I., Pérez-García, D., Schuch, N. & Verstraete, F. Matrix product states and projected entangled pair states: Concepts, symmetries, theorems. *Rev. Mod. Phys.* **93**, 045003. <https://link.aps.org/doi/10.1103/RevModPhys.93.045003> (4 Dec. 2021).
38. Fishman, M., White, S. R. & Stoudenmire, E. M. The ITensor Software Library for Tensor Network Calculations. *SciPost Phys. Codebases*, **4**. [https://scipost.org/10.21468/SciPostPhysCodeb.4\(2022\)](https://scipost.org/10.21468/SciPostPhysCodeb.4(2022)).
39. Fishman, M., White, S. R. & Stoudenmire, E. M. Codebase release 0.3 for ITensor. *SciPost Phys. Codebases*, **4**–r0.3. <https://scipost.org/10.21468/SciPostPhysCodeb.4-r0.3> (2022).
40. McClean, J. R., Romero, J., Babbush, R. & Aspuru-Guzik, A. The theory of variational hybrid quantum-classical algorithms. *New Journal of Physics* **18**, 023023 (2016).
41. Bergholm, V. *et al.* PennyLane: Automatic differentiation of hybrid quantum-classical computations. arXiv: [1811.04968](https://arxiv.org/abs/1811.04968) [[quant-ph](https://arxiv.org/abs/1811.04968)] (Nov. 2018).
42. Peruzzo, A. *et al.* A variational eigenvalue solver on a photonic quantum processor. *Nature communications* **5**, 4213 (2014).
43. O'Malley, P. J. *et al.* Scalable quantum simulation of molecular energies. *Physical Review X* **6**, 031007 (2016).

44. Kandala, A. *et al.* Hardware-efficient variational quantum eigensolver for small molecules and quantum magnets. *nature* **549**, 242–246 (2017).
45. Bentellis, A., Matic-Flierl, A., Mendl, C. B. & Lorenz, J. M. *Benchmarking the Variational Quantum Eigensolver using different quantum hardware in 2023 IEEE International Conference on Quantum Computing and Engineering (QCE)* **01** (2023), 518–523.
46. Atas, Y. Y. *et al.* SU(2) hadrons on a quantum computer via a variational approach. *Nature Commun.* **12**, 6499. arXiv: [2102.08920](https://arxiv.org/abs/2102.08920) [quant-ph] (2021).
47. Zhang, J. *et al.* Simulating gauge theories with variational quantum eigensolvers in superconducting microwave cavities. *Quantum* **7**, 1148. arXiv: [2108.08248](https://arxiv.org/abs/2108.08248) [quant-ph] (2023).
48. Avella, A., Mancini, F., *et al.* *Strongly Correlated Systems* (Springer, 2012).
49. McClean, J. R., Boixo, S., Smelyanskiy, V. N., Babbush, R. & Neven, H. Barren plateaus in quantum neural network training landscapes. *Nature communications* **9**, 4812 (2018).
50. Wang, S. *et al.* Noise-induced barren plateaus in variational quantum algorithms. *Nature communications* **12**, 6961 (2021).
51. Cerezo, M., Verdon, G., Huang, H.-Y., Cincio, L. & Coles, P. J. Challenges and opportunities in quantum machine learning. *Nature Computational Science* **2**, 567–576 (2022).
52. Holmes, Z., Sharma, K., Cerezo, M. & Coles, P. J. Connecting Ansatz Expressibility to Gradient Magnitudes and Barren Plateaus. *PRX Quantum* **3**, 010313. <https://link.aps.org/doi/10.1103/PRXQuantum.3.010313> (1 Jan. 2022).
53. Arrasmith, A., Cerezo, M., Czarnecki, P., Cincio, L. & Coles, P. J. Effect of barren plateaus on gradient-free optimization. *Quantum* **5**, 558 (2021).
54. Fedorov, D. A., Peng, B., Govind, N. & Alexeev, Y. VQE method: a short survey and recent developments. *Materials Theory* **6**, 2 (2022).
55. You, X., Chakrabarti, S. & Wu, X. A convergence theory for over-parameterized variational quantum eigensolvers. *arXiv preprint arXiv:2205.12481* (2022).
56. Tang, H. L. *et al.* Qubit-ADAPT-VQE: An Adaptive Algorithm for Constructing Hardware-Efficient Ansätze on a Quantum Processor. *PRX Quantum* **2**, 020310. <https://link.aps.org/doi/10.1103/PRXQuantum.2.020310> (2 Apr. 2021).
57. Matsuo, A., Suzuki, Y., Hamamura, I. & Yamashita, S. Enhancing VQE Convergence for Optimization Problems with Problem-Specific Parameterized Quantum Circuits. *IEICE TRANSACTIONS on Information and Systems* **106**, 1772–1782 (2023).
58. Anastasiou, P. G., Chen, Y., Mayhall, N. J., Barnes, E. & Economou, S. E. TETRIS-ADAPT-VQE: An adaptive algorithm that yields shallower, denser circuit Ansätze. *Phys. Rev. Res.* **6**, 013254. <https://link.aps.org/doi/10.1103/PhysRevResearch.6.013254> (1 Mar. 2024).
59. Kay, A. *Tutorial on the Quantikz Package* 2023. arXiv: [1809.03842](https://arxiv.org/abs/1809.03842) [quant-ph].

60. Chitambar, E. & Gour, G. Quantum resource theories. *Reviews of Modern Physics* **91**. ISSN: 1539-0756. <http://dx.doi.org/10.1103/RevModPhys.91.025001> (Apr. 2019).
61. Veitch, V., Mousavian, S. A. H., Gottesman, D. & Emerson, J. The resource theory of stabilizer quantum computation. *New Journal of Physics* **16**, 013009 (2014).
62. Howard, M. & Campbell, E. Application of a Resource Theory for Magic States to Fault-Tolerant Quantum Computing. *Physical Review Letters* **118**. <https://doi.org/10.1103/PhysRevLett.118.090501> (Mar. 2017).
63. Hamaguchi, H., Hamada, K. & Yoshioka, N. Handbook for Efficiently Quantifying Robustness of Magic. *arXiv 2311.01362* (2023).
64. Liu, Z.-W. & Winter, A. Many-Body Quantum Magic. *PRX Quantum* **3**, 020333. <https://link.aps.org/doi/10.1103/PRXQuantum.3.020333> (2 May 2022).
65. Leone, L., Oliviero, S. F. & Hamma, A. Stabilizer Rényi Entropy. *Physical Review Letters* **128**. <https://doi.org/10.1103/PhysRevLett.128.050402> (Feb. 2022).
66. Haug, T. & Piroli, L. Stabilizer entropies and nonstabilizerness monotones. *Quantum* **7**, 1092. ISSN: 2521-327X. <https://doi.org/10.22331/q-2023-08-28-1092> (Aug. 2023).
67. Leone, L. & Bittel, L. Stabilizer entropies are monotones for magic-state resource theory. *arXiv:2404.11652*. <https://arxiv.org/abs/2404.11652> (2024).
68. Ahmadi, A., Helsen, J., Karaca, C. & Greplova, E. Mutual information fluctuations and non-stabilizerness in random circuits. *arXiv:2408.03831* (2024).
69. Oliviero, S. F. E., Leone, L. & Hamma, A. Magic-state resource theory for the ground state of the transverse-field Ising model. *Phys. Rev. A* **106**, 042426. <https://link.aps.org/doi/10.1103/PhysRevA.106.042426> (4 Oct. 2022).
70. Odavić, J. *et al.* Complexity of frustration: A new source of non-local non-stabilizerness. *SciPost Phys.* **15**, 131. <https://scipost.org/10.21468/SciPostPhys.15.4.131> (2023).
71. Tarabunga, P. S., Tirrito, E., Chanda, T. & Dalmonte, M. Many-Body Magic Via Pauli-Markov Chains—From Criticality to Gauge Theories. *PRX Quantum* **4**, 040317. <https://link.aps.org/doi/10.1103/PRXQuantum.4.040317> (4 Oct. 2023).
72. Tarabunga, P. S. & Castelnovo, C. Magic in generalized Rokhsar-Kivelson wavefunctions. *Quantum* **8**, 1347. ISSN: 2521-327X. <http://dx.doi.org/10.22331/q-2024-05-14-1347> (May 2024).
73. Passarelli, G., Lucignano, P., Rossini, D. & Russomanno, A. *Chaos and magic in the dissipative quantum kicked top 2024*. arXiv: 2406.16585 [quant-ph]. <https://arxiv.org/abs/2406.16585>.
74. Passarelli, G., Fazio, R. & Lucignano, P. Nonstabilizerness of permutationally invariant systems. *Phys. Rev. A* **110**, 022436. <https://link.aps.org/doi/10.1103/PhysRevA.110.022436> (2 Aug. 2024).

75. Spriggs, T., Ahmadi, A., Chen, B. & Greplova, E. *Quantum resources of quantum and classical variational methods*<https://gitlab.com/QMAI/papers/quantumresources>
76. Spriggs, T., Ahmadi, A., Chen, B. & Greplova, E. *Quantum resources of quantum and classical variational methods*<https://doi.org/10.5281/zenodo.13759651>.
77. Sorella, S. Green Function Monte Carlo with Stochastic Reconfiguration. *Phys. Rev. Lett.* **80**, 4558–4561. <https://link.aps.org/doi/10.1103/PhysRevLett.80.4558> (20 May 1998).
78. Sorella, S. Wave function optimization in the variational Monte Carlo method. *Phys. Rev. B* **71**, 241103. <https://link.aps.org/doi/10.1103/PhysRevB.71.241103> (24 June 2005).
79. Amari, S.-i. Natural Gradient Works Efficiently in Learning. *Neural Computation* **10**, 251–276. ISSN: 0899-7667. eprint:<https://direct.mit.edu/neco/article-pdf/10/2/251/813415/089976698300017746.pdf>. <https://doi.org/10.1162/089976698300017746> (Feb. 1998).
80. Stokes, J., Izaac, J., Killoran, N. & Carleo, G. Quantum Natural Gradient. *Quantum* **4**, 269. ISSN: 2521-327X. <https://doi.org/10.22331/q-2020-05-25-269> (May 2020).
81. Kingma, D. P. & Ba, J. *Adam: A Method for Stochastic Optimization* in (Dec. 2014). arXiv: [1412.6980](https://arxiv.org/abs/1412.6980) [cs.LG].
82. Mitarai, K., Negoro, M., Kitagawa, M. & Fujii, K. Quantum circuit learning. *Phys. Rev. A* **98**, 032309. <https://link.aps.org/doi/10.1103/PhysRevA.98.032309> (3 Sept. 2018).
83. Schuld, M., Bergholm, V., Gogolin, C., Izaac, J. & Killoran, N. Evaluating analytic gradients on quantum hardware. *Phys. Rev. A* **99**, 032331. <https://link.aps.org/doi/10.1103/PhysRevA.99.032331> (3 Mar. 2019).
84. Wierichs, D., Gogolin, C. & Kastoryano, M. Avoiding local minima in variational quantum eigensolvers with the natural gradient optimizer. *Phys. Rev. Res.* **2**, 043246. <https://link.aps.org/doi/10.1103/PhysRevResearch.2.043246> (4 Nov. 2020).
85. BROYDEN, C. G. The Convergence of a Class of Double-rank Minimization Algorithms 1. General Considerations. *IMA Journal of Applied Mathematics* **6**, 76–90. ISSN: 0272-4960. eprint: <https://academic.oup.com/imamat/article-pdf/6/1/76/2233756/6-1-76.pdf>. <https://doi.org/10.1093/imamat/6.1.76> (Mar. 1970).
86. Fletcher, R. A new approach to variable metric algorithms. *The Computer Journal* **13**, 317–322. ISSN: 0010-4620. eprint: <https://academic.oup.com/comjnl/article-pdf/13/3/317/988678/130317.pdf>. <https://doi.org/10.1093/comjnl/13.3.317> (Jan. 1970).
87. Goldfarb, D. A family of variable-metric methods derived by variational means. *Mathematics of computation* **24**, 23–26 (1970).
88. Shanno, D. F. Conditioning of quasi-Newton methods for function minimization. *Mathematics of computation* **24**, 647–656 (1970).

89. Spall, J. C. Multivariate stochastic approximation using a simultaneous perturbation gradient approximation. *IEEE transactions on automatic control* **37**, 332–341 (1992).
90. Xiang, Y., Sun, D., Fan, W. & Gong, X. Generalized simulated annealing algorithm and its application to the Thomson model. *Physics Letters A* **233**, 216–220 (1997).

5

CONCLUSION

In this thesis, we explored a fundamental relation between two concepts from quantum science. The first one, non-stabilizerness, borrowed from the quantum computing community, and the second one from quantum information theory, information scrambling. We established there is a fundamental relationship between these two concepts in different ways.

In chapter 2, we formulated a fundamental relation between Out-of-Time Ordered Correlators (OTOC) and non-stabilizerness. We saw that in the qutrit case, the fluctuations of OTOC, the standard deviation of the measured instances of OTOC, have a linear relation to the magic monotone, mana, in the random t -doped circuits.

Further, we investigated the same relation of the fluctuations of OTOC and the Stabilizer 2-Renyi Entropy, and we found a deep general relation. We found that there exists a log dependency between the fluctuations of OTOC and the Stabilizer 2-Renyi entropy of the corresponding Choi state. We proposed a general framework for measuring the OTOC instances for a general unitary dynamic $U(t)$ where from the quantum computation resource perspective is favourable. Also, this general method proposed in this research seems to be heuristically efficient since the number of OTOC seems to be constant for any number of qubits in the system. For a larger scale, this effect has been observed experimentally for +50 qubits [1]. However, the formal proof of efficiency remains a direction for future research.

In chapter 3, we explored the same relation between non-stabilizerness and information scrambling measures, this time via entropic-based measures. We showed, both numerically and analytically, that the log of the fluctuations of mutual information also has a linear dependency on the non-stabilizerness in t -doped random circuits. Given the fact that mutual information is also a standard measure for detecting entanglement phase transition in measurement-induced random circuits, we also explored the effect of non-stabilizerness in this setup. With no surprise, we observed that fluctuations of mutual information also show decremental behaviour with the injection of non-stabilizerness in these systems.

In chapter 4, we benchmarked the energy accuracy and the non-stabilizerness ac-

curacy in variational state approximation for the ground state search problem, thus relating quantum computing and classical variational perspectives on the ground state search. We checked this effect for both classical variational models, namely neural-network quantum states and matrix product states, and quantum variational models, known as variational quantum eigensolvers. We observed that between different models, the model that achieves better accuracy in the ground state energy can have better accuracy in non-stabilizerness as well. However, having better accuracy in energy is essential but not sufficient to obtain better accuracy in non-stabilizerness. We showed this by considering a symmetric version of the neural-network quantum state model and checking that it has more accurate energy while the accuracy in non-stabilizerness does have a considerable change.

The results of this thesis established a fundamental and unique relationship between information scrambling and non-stabilizerness and a potentially more scalable way for quantifying non-stabilizerness. This thesis also includes a benchmark for the accuracy of variational models in capturing non-stabilizerness and raises questions about whether only considering one parameter, here ground state energy, to optimise a variational model would be sufficient to study every aspect of the system or not.

The new connection between the fluctuations of OTOC and non-stabilizerness allows us to explore the non-stabilizerness in quantum systems that are not feasible to study using conventional classical methods. An example that I am excited about is the role of non-stabilizerness in chemical systems. It is already shown that a chemical reaction can be as good as a black hole in scrambling the information [2]. With an intimate relation between information scrambling and non-stabilizerness we can study the non-stabilizerness in such systems.

We can also employ the power of neural networks in approximating the non-stabilizerness that is currently unexplored so we can possibly go beyond the MPS in the approximation methods of Stabilizer Renyi entropies on classical computers.

BIBLIOGRAPHY

1. Mi, X. *et al.* Information scrambling in quantum circuits. *Science* **374**, 1479–1483. eprint: <https://www.science.org/doi/pdf/10.1126/science.abg5029>. <https://www.science.org/doi/abs/10.1126/science.abg5029> (2021).
2. Zhang, C., Kundu, S., Makri, N., Gruebele, M. & Wolynes, P. G. Quantum Information Scrambling and chemical reactions. *Proceedings of the National Academy of Sciences* **121**. <https://www.pnas.org/doi/10.1073/pnas.2321668121> (Apr. 2024).

ACKNOWLEDGEMENTS

Completing this PhD has been an incredible journey, and I am deeply grateful to those who have supported and guided me along the way.

First and foremost, I would like to express my heartfelt gratitude to my supervisor, **Eliska**. Her unwavering support, invaluable guidance, and constant encouragement have played a crucial role in shaping my research and academic growth. I am especially thankful for the opportunity she provided me to join her research group and pursue my PhD under her mentorship. Her insightful advice and inspiring leadership have been instrumental in my development as a researcher.

I would also like to extend my sincere appreciation to my promoter, **Simon**, whose support has gone beyond academic guidance. Their encouragement and assistance in helping me apply for a grant to embark on a startup venture have been truly transformative. Their belief in my potential and the opportunities they have helped create for me will always be deeply appreciated.

A special thank you to my mentor, **Gary**, who played a crucial role in my first year of the PhD. Navigating the challenges of the beginning was not easy, and their guidance, patience, and encouragement helped me find my footing during a period of uncertainty and learning. Their support in those early days made a significant impact on my academic journey, and I will always be grateful for their kindness and wisdom.

I am also incredibly thankful to my colleagues and friends who have been part of this journey. A special thanks to **Jin**, with whom I started this PhD adventure, and **Vini**, who joined us a few months later. Sharing this experience with you both has made the process so much more meaningful, and I deeply appreciate your support, discussions, and the many moments we've shared along the way. I am also grateful to **Tom**, **Ana**, **Aram**, **Dima**, **Rouven**, and **Valentina** for their collaboration, encouragement, and the friendships that made this journey both productive and enjoyable.

I would also like to express my gratitude to **Ali**, my master's thesis supervisor, for the constructive scientific discussions that we had during my PhD helped shape my research perspective. The knowledge and critical thinking skills I developed during that time were invaluable in preparing me for this PhD journey.

A very special thank you to **Leila**, my girlfriend, for her unwavering love, patience, and encouragement throughout this entire process. Her support has been a constant source of strength, helping me navigate both the challenges and successes of this journey. I am deeply grateful for her presence, understanding, and the motivation she has given me to keep pushing forward.

I am also deeply thankful for the supportive friendship of **Sirous**, **Artemis**, **Masoud** and **Reza**. Their kindness, encouragement, and companionship have been invaluable throughout this journey. Whether through thoughtful conversations, moments of laughter, or simply being there during tough times, their friendship has made a meaningful difference in my life.

A huge thanks to my dear friends **Reza, Ali, Meiti**, and **Mammad** for their friendship and for all the unforgettable boys' nights we shared. The laughter, the late-night conversations, and the countless memories we created together have been a cherished part of this journey. Your support, humour, and camaraderie have made even the most stressful moments easier to navigate, and I am grateful to have such an amazing group of friends.

Additionally, I would like to thank my old friends, **Habib, Peyman, Elyas**, and **Mammad**, for their continued friendship over the years. Even as life took us on different paths, your presence and support have always been meaningful to me. The shared experiences, deep conversations, and good times we've had together are memories I will always treasure.

Lastly, I want to extend my gratitude to my family for their unwavering support, patience, and encouragement throughout this endeavor. Their belief in me has been a constant source of strength.

Finally, I acknowledge the funding agencies and institutions that have supported my research, making this work possible.

This thesis is a testament to the collective effort and generosity of many, and I am truly grateful to all who have contributed to my academic and professional journey.

CURRICULUM VITÆ

Arash AHMADI

19-12-1995 Born in Hamedan, Iran.

EDUCATION

2014–2020 **M.Sc. Physics**
Institute for Advanced Studies in Basic Sciences, Zanjan, Iran
Thesis: Topological properties of a Non-Hermitian mechanical metamaterials
Supervisor: Dr. Ali G. Moghaddam

2021–2025 **Ph.D. Physics**
Delft University of Technology, the Netherlands
Thesis: Magic of fluctuations: from the quantum information's measure fluctuations to magic resource
Supervisor: Dr. Eliska Greplova
Promotor: Prof. dr. Simon Groblacher

AWARDS

2023 Casimir Ph.D. Travel Grant

LIST OF PUBLICATIONS

1. **A. Ahmadi** and E. Greplova, *Quantifying non-stabilizerness via information scrambling*, *Sci-Post Physics* **16**, 043 (2024).
2. **A. Ahmadi**, J. Helsen, C. Karaca, and E. Greplova, *Mutual information fluctuations and non-stabilizerness in random circuits*, [arXiv: 2408.03831](https://arxiv.org/abs/2408.03831) (2024).
3. T. Spriggs*, **A. Ahmadi***, Bokai Chen, and E. Greplova, *Quantum resources of quantum and classical machine learning ansätze*, [arXiv: 2409.13008](https://arxiv.org/abs/2409.13008) (2024).

* indicates equal contribution